Controlled Polymerization for Ocular Drug Delivery

Controlled Polymerization for Ocular Drug Delivery

By: Graeme Prosperi-Porta, BSc Eng.

A Thesis
Submitted to the School of Graduate Studies
In Partial Fulfilment of the Requirements
For the Degree Master of Applied Science

Master of Applied Science (2015) McMaster University
School of Biomedical Engineering Hamilton, Ontario

TITLE: Controlled Polymerization for Ocular Drug Delivery

AUTHOR: Graeme Prosperi-Porta, BSc. Eng. (University of Alberta)
SUPERVISOR: Dr. Heather Sheardown
NUMBER OF PAGES: xii,96

ABSTRACT

Effective drug delivery to ocular tissues is an unmet challenge that has significant potential to improve the treatment of ocular diseases. Whether the intended drug delivery target is the anterior or posterior segment, the eye's efficient natural protection mechanisms prevent effective and sustained drug delivery. Anatomical and physiological barriers including the rapid tear turnover that effectively washes away topically applied drugs, the impermeable characteristics of the cornea, conjunctiva, and sclera, and the tight junctions in the blood-ocular barriers make conventional drug delivery methods ineffective. New materials that are able to overcome these barriers are essential to improving the sustained delivery of ophthalmic therapeutics to the intended targets within the eye. This thesis will explore two polymeric drug delivery systems that have the potential to improve therapeutic delivery to ocular tissues. Chapter 1 will discuss the anatomical and physiological barriers to ophthalmic drug delivery and overview current research in this area. Chapter 2 will discuss the synthesis of N-isopropylacrylamide-based copolymers with adjustable gelation temperatures based on composition and molecular weight. Chapter 3 will discuss further development of these copolymers into an injectable, thermoresponsive, and resorbable polymeric drug delivery system intended for the treatment of diseases in the posterior segment. Chapter 4 will discuss the development of mucoadhesive polymeric micelle nanoparticles based on phenylboronic acid intended for topical administration of ophthalmic therapeutics. Finally, Chapter 5 will provide an overview of potential future work on these materials that could further develop and broaden their therapeutic use.

ACKNOWLEDGMENTS

I would first like to thank my supervisor Dr. Heather Sheardown for her continuous support and guidance. Her encouragement and trust in my research ideas allowed me to pursue research that I was truly passionate about. Although my ideas often did not work, these opportunities helped me to grow my knowledge, skills, and experience beyond what I could have ever imagined. Thank you for everything!

I next want to thank Stephanie Kedzior, my amazing girlfriend, who has always supported me in both research and life. You helped me to take a break from work and gave me someone to cook for that almost never complained. Your ongoing support over the past two years and your impulse decision to buy our wonderful kitten Oreo have contributed to my success. Oreo gave us endless entertainment, lots of laughter, and many early mornings. Without the two of you the past two years would not have been nearly as wonderful.

To the entire Sheardown group: thanks for making each day in the lab more fun and listening to all of my stories about Oreo. He heard just as many stories about all of you! This experience would not have been the same without you all. I appreciate the friendships that have made this experience memorable.

Lastly, I would like to thank my parents Marina and Frank, my brother Matthew, and my grandparents Trudy and Ed for their love and support over the past 24 years. Your encouragement and support to pursue my interests have allowed me to maximize my potential and achieve my goals. To my grandparents who always kept me well fed during the holidays, I would have been homesick without our frequent visits. I am so grateful to have such a supportive family that will continue to encourage me to pursue my goals.

TABLE OF CONTENTS

LIST OF FIGURES

Chapter 1

Chapter 2

Chapter 3

Chapter 4

LIST OF TABLES

Chapter 1

Chapter 2

Chapter 3

Chapter 4

LIST OF ABBREVIATION AND SYMBOLS

AA	Acrylic Acid
AAm	Acrylamide
AIBN	Azobisisobutyronitrile
BAB	Blood-aqueous barrier
BRB	Blood-retinal barrier
BT	Brimonidine Tartrate
CalAM	Calcein AM
CMC	Critical micelle concentration
CycA	Cyclosporine A
DBA	(r)-α-acryloyloxy-β,β-dimethyl-γ-butyrolactone
DDMAT	2-(Dodecylthiocarbonothioylthio)-2-methylpropionic acid
DED	Dry eye disease
Dex	Dexamethasone
DND	Did not dissolve
DR	Diabetic retinopathy
DSC	Differential scanning calorimetry
EthD	Ethidium homodimer-1
EWC	Equilibrium water content
FR	Free radical
FTIR	Fourier transform infrared spectroscopy
GE	Gelation equilibrium
GPC	Gel permeation chromatography
HCEC	Human corneal epithelial cells
IVI	Intravitreal injection
LCST	Lower critical solution temperature
KSFM	Keratinocyte serum-free media
LiBr	Lithium bromide
LMP	Poly(L-lactide)-b-poly(methacrylic acid-co-phenylboronic acid)
MAA	Methacrylic acid
NAS	Acrylic acid N-hydroxysuccinimide ester
NIPAAm	N-isopropylacrylamide
NMR	Nuclear magnetic resonance
PBA	Phenylboronic acid
PBS	Phosphate buffered saline
PEG	Poly(ethylene glycol)
pLA	Poly(L-lactide)
pNAND	Poly(NIPAAm-AAm-NAS-DBA)
PPO	Poly(propylene oxide)
RAFT	Reversible addition-fragmentation chain-transfer

DECLARATION OF ACADEMIC ACHIEVEMENT

Chapter 1: The literature review was organized, prepared, and written solely by Graeme Prosperi-Porta. Stephanie Kedzior assisted with proof-reading and editing the final draft.

Chapter 2: This work entitled "Tuning the LCST of N-isopropylacrylamide copolymers through composition and molecular weight changes" describes the synthesis and characterization of a series of N-isopropylacrylamide copolymers. This work was used to create a library of materials that was used to select material properties based on composition and molecular weight. All work including copolymer synthesis, LCST characterization, and data analysis was performed solely by Graeme Prosperi-Porta.

Chapter 3: The manuscript entitled "Tunable release of ophthalmic therapeutics from injectable, resorbable, thermoresponsive copolymer scaffolds" was written solely by Graeme Prosperi-Porta with proof-reading and editing of the final draft by Stephanie Kedzior. All work performed in this manuscript including copolymer synthesis, characterization (equilibrium water content, gelation equilibrium, degradation, ^{1}H NMR, FTIR, and drug release was performed by Graeme Prosperi-Porta. Benjamin Muirhead guided, advised, and taught cell culture techniques.

Chapter 4: In the manuscript entitled "Phenylboronic acid nanoparticles for mucoadhesive drug delivery to the ocular surface" Graeme Prosperi-Porta was responsible for copolymer synthesis, micelle formation, NanoSight, critical micelle concentration, drug release, and cell viability. Stephanie Kedzior performed Zeta Potential measurement, and mucoadhesion measurements with surface plasmon resonance. Marion Jamard and Lina Liu performed transmission electron microscopy. The manuscript was prepared solely by Graeme Prosperi-Porta with assistance editing the final draft by Stephanie Kedzior.

1. Chapter 1: Literature review

1.1. Anatomical and physiological barriers

The eye is a small organ responsible for sight. It is a globe structure that can be divided into anterior and posterior segments. Shown in Figure 1-1, the anterior segment is coated in a thin lubricating layer of tears and is primarily composed of the cornea, iris, lens, and ciliary body while the posterior segment is primarily composed of the sclera, choroid, and retina. The eye can also be divided into a series of three concentric layers that each perform a vital role in the function and protection of the eye. In order to effectively deliver therapeutics to the eye these layers must be circumvented.

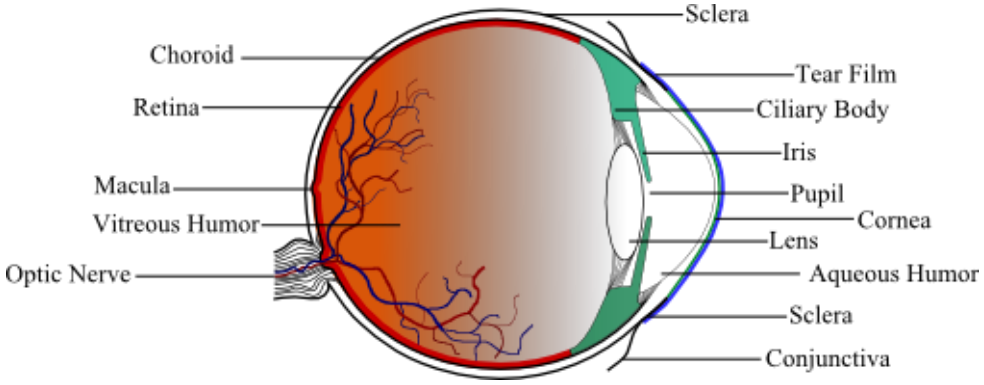

Figure 1- 1. Basic ocular anatomy showing major components.

1.1.1. Tear film

The tear film is a multi-layered liquid that coats the surface of the anterior eye to protect it from irritants, pathogens, and harmful substances. This tear film is the first barrier against drug delivery due to its structure, composition, and its rapid turnover and drainage into the systemic circulation. Figure 1-2 shows the general structure of the tear film. It is composed of three layers including the external lipid layer, the middle aqueous layer, and an inner immobilized mucin layer [1]. The tear film has an approximate thickness of 3 μm and a normal volume of approximately 6-8 μL, but it can hold up to 30 μL in the cul de sac transiently [2]. Its most prominent role in

preventing efficient drug delivery is the rapid tear drainage that washes away drug through the lacrimal duct onto the nasal mucosa, which can then enter systemic circulation.

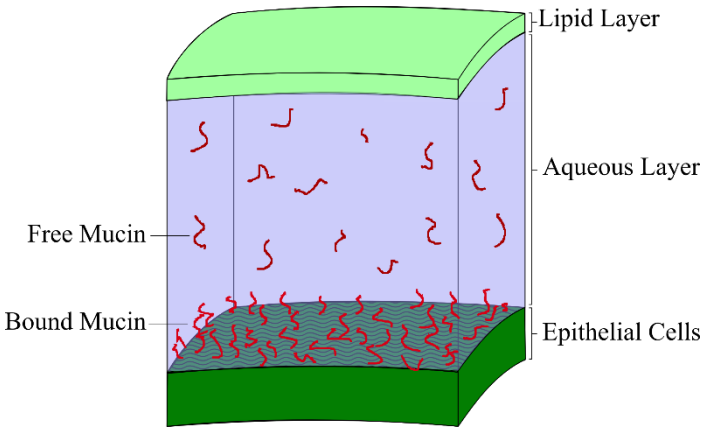

Figure 1- 2. Basic tear film structure showing three distinct layers: the outer lipid layer, the middle aqueous layer, and the inner mucin layer.

Although not extensively studied, the mucin layer has also been shown to act as a permeation barrier to the diffusion of macromolecules. Mucins are large negatively charged glycoproteins with high water content due to sialic acid carbohydrate residues [1]. The hydrophilic negatively charged mucins may act to repel negatively charged or hydrophobic molecules. Arueso et al. showed a reduced cellular uptake of negatively charged rose bengal dye in stratified corneal epithelial cells with higher mucin expression [3]. This suggests that it can act as a barrier to drug delivery. The tear film is an effective first line of defense that prevents the infiltration of foreign substances including drugs into the ocular tissues, and must be overcome to achieve effective topical drug delivery.

1.1.2. External fibrous layer

The external fibrous layer is composed of three components: the cornea, conjunctiva, and sclera. The cornea is an approximately 500 μm thick transparent window in the anterior segment of the eye composed of three cellular layers (epithelium, stroma, endothelium) and two interfaces (Bowman and Descemet membranes) and a newly discovered Dua's layer [4,5]. Compared to the

cellular layers, the Bowman and Descemet membranes do not have a significant effect on drug transport and the contribution of the Dua's layer is still unknown. The outermost epithelium is composed of multiple epithelial cell layers that possess intercellular tight junctions, which produce a hydrophobic barrier to drug transport [6]. The middle layer, called the stroma, provides between 80-85% of the corneal thickness. This layer is composed of mainly water, highly organized collagen fibrils and few cells, which are mainly keratocytes that maintain the extracellular environment [6]. The innermost layer is composed of non-mitotically active endothelial cells that contain numerous intercellular tight junctions similar to the epithelial cell layer [4]. The alternating hydrophobic-hydrophilic sandwich that is formed by the five corneal layers provides an effective barrier to the transport of drugs across the cornea.

The conjunctiva is a thin transparent mucous membrane composed of epithelial cells that prevents foreign substances from entering the eye [7]. The conjunctiva also contains goblet cells, which are involved in secreting mucin, a component of tear fluid that lubricates and nourishes the cornea [8]. The sclera is an opaque outer ocular layer covering approximately 80% of the ocular surface [6]. This smooth connective tissue is involved in maintaining the shape of the eye and acts as a barrier to foreign substances. It is avascular and mainly composed of collagen, elastin fibers, and proteoglycans.

The non-corneal route (conjunctival-scleral) is favored for hydrophilic drugs while hydrophobic drugs are more readily absorbed through the corneal route. For example, hydrophobic hydrocortisone was absorbed 70 times more through the corneal route [9] while large hydrophilic substances such as inulin were show to primarily absorb through the non-corneal route [10]. Molecular size is another parameter that affects the permeation of molecules through anterior tissues. PEG oligomers ranging from approximately 200 to 1000 Da were found to penetrate all

three anterior tissues more readily at smaller molecular weights [11]. Interestingly, corneal permeation significantly decreased with increasing PEG molecular weight while conjunctival permeation was highest for all PEG molecular weights. The drug dependent permeation rates though different tissues are important factors that can be used to design biomaterial delivery vehicles that utilize these properties. Unfortunately, even if a drug successfully penetrates the cornea or conjunctiva and sclera, aqueous humor drainage and underlying vasculature present further barriers to the successful delivery of therapeutics to their target tissue.

1.1.3. Vascular uveal layer

The middle uveal layer of the eye is composed of mainly the choroid, iris, and ciliary body. The choroid is a vascular laminate layer between the sclera and retina that accounts for approximately 85% of ocular blood flow and it supplies the retina with nutrients [12]. This large percentage of blood flow makes the choroid a significant factor in both systemic drug delivery to the eye and drug removal from the eye. Systemic drug penetration from the inner choriocapillaris that nourish RPE cells is not significantly impeded due to numerous fenestrations in the choriocapillaris [13]. However, these fenestrations can also uptake drug that penetrates through the sclera causing it to enter the systemic circulation, which prevents it from reaching the retinal tissues. Even if drug successfully penetrates the choroid layer, it must still pass the blood-retinal barrier (BRB) in the inner neural layer before reaching its final target in the posterior segment.

The iris plays a relatively passive role in drug delivery. It is a highly pigmented muscular ring that adjusts the amount of light that enters the eye. Due to its heavy pigmentation, the iris can act as a reservoir for hydrophobic drugs that can be absorbed in the pigment granules [6]. This can improve drug release kinetics by acting as a slow releasing reservoir for prolonged release, but it can also give the metabolic enzymes more time to detoxify drugs. Das et al. found that drug

metabolizing enzymes aryl hydrocarbon hydroxylase, UDP glucuronyl transferase, and gamma-glutamyl transpeptidase were highest in the ciliary body followed by the RPE and finally the iris [14]. Nakanot al. also showed P450 drug metabolizing enzymes that are abundantly present in the liver are also involved in metabolism in the iris and ciliary body [15]. The presence of these metabolic enzymes in the ciliary body is one reason that it plays a more active role as a drug barrier. The ciliary body is a muscular ring containing an extensive capillary network and is responsible for the shape of the lens and production of the aqueous humor. The inner of its two layers that faces the vitreous is composed of non-pigmented epithelial cells while the outer layer contains numerous pigment granules and is continuous with the RPE [6]. There are no tight junctions on the vessels of the ciliary body itself so drug penetration from this vasculature occurs readily, but before drug can enter the aqueous humor it must pass the blood-aqueous barrier (BAB)

The BAB is a more significant barrier to drug permeation in the iris and ciliary body. It is composed of the tight junctions in the vascular endothelial cells of the iris and tight junctions in the non-pigmented epithelial cells of the ciliary body [16]. These act as effective barriers against the paracellular transport of drugs into the anterior chamber. Unfortunately, even if the drug successfully enters the aqueous humor its concentration can be further reduced by aqueous humor turnover, as will be discussed in section 1.2.1

1.1.4. Inner neural layer

The neural retina has the sole purpose of transforming light into electrical signals for processing by the brain into final images. As shown in Figure 1-3, the neural retinal is a laminate structure which contains highly effective barriers against the transport of therapeutics from systemic circulation and non-corneal diffusion to target sites in the retina [6].

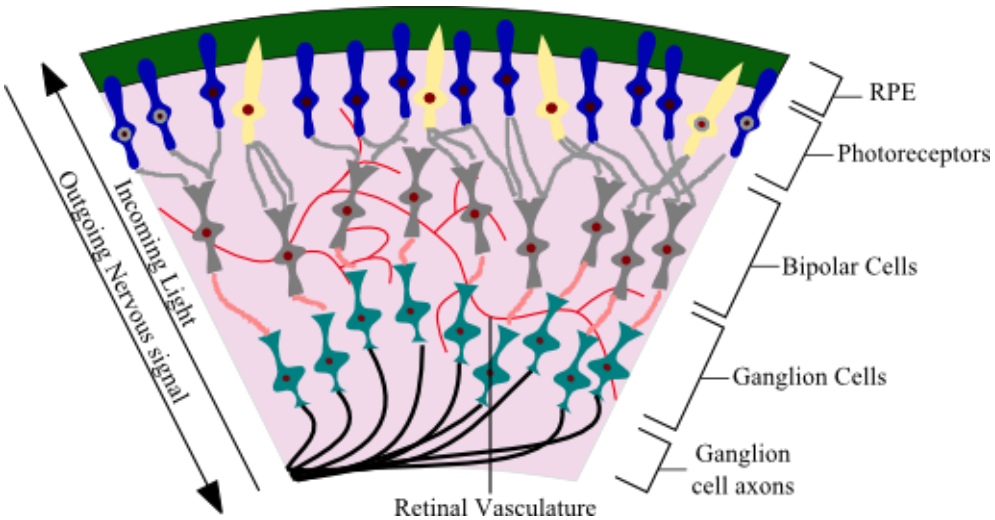

Figure 1- 3. Schematic of the neural retina. Adapted from [17]**.**

Together, the retinal pigment epithelium and the retinal vasculature make up the BRB that prevents effective treatment of posterior segment diseases such as age related macular degeneration, and diabetic retinopathy. The retinal vessels that exist throughout the neural retina are lined with endothelial cells that form belt-like tight junctions between cells limiting paracellular transport of water soluble molecules [18]. Unfortunately this natural protective mechanism also prevents the passage of therapeutic drugs that are seen as foreign.

The retinal pigment epithelial (RPE) cell layer is a monolayer of highly pigmented cells that act to absorb stray light and control fluid, nutrient, and waste flow to and from the photoreceptors. The RPE has also been shown to contain multiple enzymes used for maintenance of the BRB, which may be also involved in drug detoxification [19]. Similar to retinal vascular endothelial cells, the RPE cells are connected by tight junctions that prevent paracellular transport of substances into the neural retina. Together the inner and outer BRBs effectively prevent drug penetration from systemic circulation and topically administered non-corneal penetration into the posterior ocular tissues.

1.2. Traditional ophthalmic drug delivery

Traditional drug delivery to the eye including topical, oral or systemic, periocular, and intravitreal injections, shown in Figure 1-4, all suffer from a similar fault. These methods of drug delivery require frequent administration due to the fast and effective clearance mechanisms of the eye.

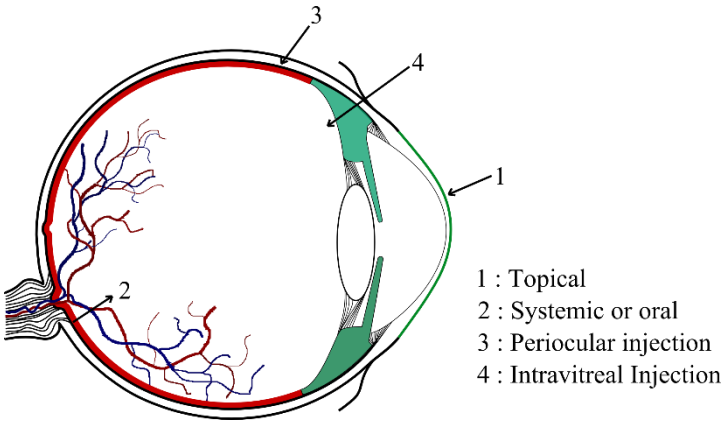

Figure 1- 4. Common drug delivery routes for the eye.

Rapid clearance mechanisms cause cyclic drug concentrations within the ocular tissues and high systemic exposure, depicted in Figure 1-5. High dosages are required to reach therapeutic drug levels in posterior tissues of the eye, but these can quickly reach toxic levels that quickly drop off below therapeutic levels, and they can cause side effects in systemic tissues. In terms of the therapeutic effect on the target tissues, this cyclic concentration is not ideal because it does not provide a constant therapeutic dose for extended periods of time. Therefore, the ideal drug delivery system is capable of targeting the specific tissue of interest at a therapeutic concentration for an extended period of time.

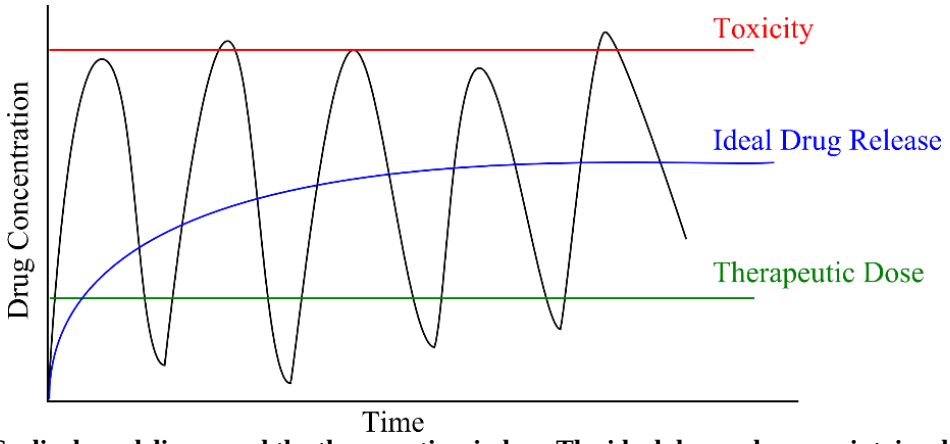

Figure 1- 5. Cyclic drug delivery and the therapeutic window. The ideal drug release maintains drug concentration in the targeted tissue within the therapeutic window, and does not exceed the toxicity in any tissues.

1.2.1. Topical administration

Eye drops are the most common method of drug dosage due it their relative ease of application, low physician involvement, and low cost. Unfortunately precorneal clearance mechanisms such as rapid tear turnover and nasolacrimal drainage result in extremely low bioavailability. Upon topical administration of drug solution the normal lacrimal turnover rate of approximately 16 % min^{-1} is greatly increased to restore the normal tear volume within 2-3 minutes [2,20,21]. This rapid drainage of lacrimal fluid enters systemic circulation through the lacrimal duct that empties on the nasal mucosa resulting in less than 5% ocular bioavailability [22]. Upon entering systemic circulation, unintended exposure to drug targets in other tissues can cause side effects and toxicity [23,24]. For example, Bowman et al. found that 0.2% brimonidine eye drops caused local irritation, fatigue, and fainting in children [25]. Similarly, timolol eye drops have been shown to have significant systemic exposure causing changes to heart rate and arterial blood pressure [26,27]. Even if drugs do successfully enter the aqueous humor, they face clearance through the trabecular meshwork down the Schlemm's canal into circulation that occurs at roughly 3 μL min^{-1} [28]. Hydrophobic drugs are particularly susceptible to clearance by penetration across the hydrophobic endothelial walls of the uveal blood vessels, which can be in the range of 20-30

μL min^{-1}. Combined, the half-life of drug in the anterior chamber is on the order or approximately one hour, which makes traditional topical drug administration extremely ineffective [28]. One method to improve topical drug delivery is to increase bioavailability on the ocular surface to increase penetration and reduce systemic drug exposure.

1.2.2. Systemic and oral administration

Systemic and oral administration are infrequent methods for drug delivery to the eye. As previously explained, tight junctions in the blood-ocular barriers prevent efficient drug delivery from systemic circulation form entering ocular tissues. Oral administration is further inhibited by digestion and drug metabolism in the liver before reaching circulation. Due to these effective barriers, drug delivery to the eye generally requires large doses that can lead to systemic complications and toxicity [22,29]. Therefore, systemic and oral administration of ophthalmic drugs are generally regarded as ineffective.

1.2.3. Periocular injections

Periocular drug delivery involves the injection of drug against the exterior of the sclera for subsequent penetration into the posterior tissues. These can include retrobulbar, peribulbar, subtenon, and conjunctival routes, but these will be all be considered as similar in context of periocular injections [30]. The periocular space is located behind the conjunctiva and outside of the sclera. Periocular drug delivery allows therapeutics to bypass the conjunctiva and avoid precorneal clearance mechanisms to directly access the scleral delivery route. However, as previously discussed, the drug must still penetrate the sclera, choroid, and neural retina, which present multiple barriers. Although the sclera does not pose a significant barrier to drug delivery, the choroidal vasculature can effectively absorb drug into systemic circulation, and the outer BRB in the RPE will prevent penetration of drug into the vitreous and retina. Compared to eye drops,

periocular delivery significantly improves drug bioavailability in the retinal tissues [31]. It is also much less invasive compared to intravitreal injections that require penetration of the globe to deliver drugs directly into the vitreous. Unfortunately, much of the drug is lost within the periocular space to conjunctival lymphatics and blood flow before it can diffuse across the sclera, choroid, and neural retina [32]. In order to improve periocular drug delivery, a longer residence time on the scleral surface is needed to increase the time available for diffusion.

1.2.4. Intravitreal injections and inserts

Intravitreal injections (IVIs) are the most targeted drug delivery method of solutions, particles, or implants for posterior segment diseases [29,33]. They physically penetrate most of the ocular barriers to deposit the drug formulation directly into the vitreous body where it can act on target tissues. However, once drugs are deposited in the vitreous, concentrations can still be reduced by aqueous humor drainage through the trabecular meshwork and by diffusion across the BRB into circulation. Smaller molecules with molecular weights less than 500 Da need more frequent administration due to faster clearance from the vitreous [30]. This suggests that larger drugs or drug-polymer combinations may increase vitreal retention. The biggest advantage of IVIs is their ability to achieve high therapeutic drug concentrations in the vitreous, but unfortunately this method has a long list of complications due to its invasive nature. These can include retinal detachment, hemorrhage, endophthalmitis, increased IOP, and cataracts [29,34]. Stefano et al. showed that the risk of complications caused by IVIs was reduced by using larger gauge needles that limited tissue damage at the injection site [35]. The development of smart biomaterial delivery systems that are capable of sustained release upon injection from a large gauge needle would be extremely beneficial to reduce the number of complications associated with IVIs. This trend of

reducing invasiveness and injection frequency can be seen in the progression of FDA approved inserts in the following section, but there is still progress to be made in the future.

1.2.4.1. Current FDA approved IVIs

There are currently four FDA approved IVIs and ocular insets: Vitrasert®, Retisert®, Ozurdex®, and Iluvien®. Table 1-1 summarizes the properties of these intravitreal inserts along with some of their important positive and negative attributes that have demonstrated important goals in designing the next generation of intravitreal drug releasing implants. Some of the goals that have been identified from these products are:

- Reduce surgical invasiveness of implant installation or replacement by injection from a needle.
- Introduce biodegradability or bioresportion to reduce vision obstruction, eliminate implant removal, and reduce anterior implant migration.
- Maintain a sustained release of drug for at least 6 months to compete with the currently marketed materials.
- Further reduce invasiveness by injecting implants through a ≥30G needle.

Table 1- 1. Summary of FDA approved intravitreal implants.

	FDA Approval	Description	Pros and cons
Vitrasert®	1996	- Non-biodegradable polymer implant for the treatment of cytomegalovirus retinitis [36]. - Release up to 8 months containing 4.5 mg ganciclovir [37].	- Highly invasive due to suturing to the pars plana region of the sclera. - Removal or replacement results in continued invasiveness and higher risks for complication. - Common complications include endophthalmitis, cataracts, IOP elevation, and retinal detachment [38].
Retisert®	2005	- Non-biodegradable silicone and polyvinyl alcohol coated fluocinolone acetonide tablet for chronic posterior uveitis [39]. - Release of fluocinolone acetonide up to 2.5 years at 0.6 μg day^{-1} [40].	- Highly invasive due to incision and suturing to the sclera. - Removal or replacement results in continued invasiveness and higher risk for complications. - Common complications include increased IOP, cataracts, and retinal detachment [41].
Ozurdex®	2009	- Biodegradable poly(lactide-co-glycolide) vitreous implant containing dexamethasone for treatment of macular edema [42]. - Release up to 6 months containing 700 μg dexamethasone [30].	- Injection through a 22G needle and biodegradability reduces invasiveness. - Numerous cases of implant migration into the anterior segment causing visual obstruction and invasive surgical intervention [43,44].
Iluvien®	2014	- Non-biodegradable polyimide and PVA implant containing fluocinonide acetonide for the treatment of diabetic macular edema [37]. - Release up to 3 years.	- Injection through a 25G needle reduces invasiveness - Available in high dose (0.5 μg day^{-1}) or low dose (0.2 μg day^{-1}) [40]. - Continued use results in numerous non-biodegradable residual implants. - Implant migration into the anterior segment causing complications.

The numerous anatomical, physiological, and metabolic barriers present in the eye make effective drug delivery extremely challenging. These barriers result in off-target systemic drug exposure and low ocular drug bioavailability. Increasing the bioavailability of ophthalmic therapeutics to reduce administration frequency, dosage, side effects, and complications is the main aim of this research. The ideology behind the development of two biomaterial drug delivery systems aimed at improving the bioavailability of ocular therapeutics will be discussed below. The first is a thermoresponsive, resorbable, injectable copolymer scaffold for the sustained release of dexamethasone to the posterior segment, and the second is a mucoadhesive nanoparticle micelle for the sustained topical delivery of cyclosporine A to the anterior segment.

1.3. Temperature responsive drug delivery systems

Temperature responsive materials have been extensively explored for biomedical applications such as drug delivery and tissue engineering. These materials are desirable due to their solution to gel phase transformation that occurs above the lower critical solution temperature (LCST), depicted in Figure 1-6.

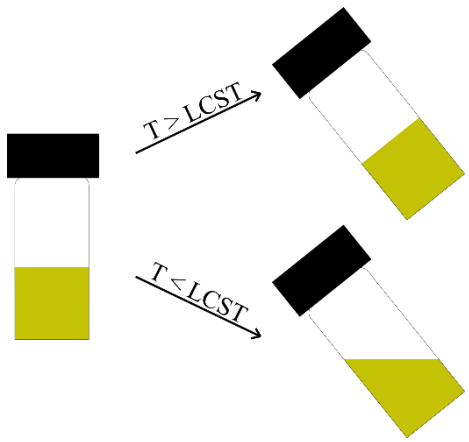

Figure 1- 6. Depiction of temperature responsive materials above and below their LCST.

The phase transition is caused by a shift from hydrophilic to hydrophobic interactions between polymer chains. These polymers generally have both hydrophilic and hydrophobic groups. At low temperatures the hydrophilic groups form hydrogen bonds with water molecules

resulting in polymer solubility. As the temperature is increased, hydrogen bonding decreases, and intermolecular hydrophobic interactions increase. Once the temperature is raised above the LCST, the increased hydrophobic intermolecular interactions reach a critical point resulting in the collapse of the polymer network into an insoluble hydrogel. Temperature responsive polymers can be classified as positive- or negative-temperature sensitive systems. Negative systems have an LCST while positive systems have an upper critical solution temperature (UCST), which is the temperature at which a gel phase transitions to a solution phase. While most natural polymers transition from solution to gel at low temperatures, some natural polymers have been modified to induce LCST properties [45]. Synthetic polymers however can be designed more easily to possess the hydrophilic-hydrophobic balance that is needed to drive these temperature sensitive properties. Some of these natural and synthetic polymers will be discussed below.

1.4.Natural thermoresponsive polymers

1.4.1. Cellulose derivatives

Cellulose is a linear naturally occurring water insoluble polysaccharide. Upon modification of the natural polymer's hydroxyl groups with more hydrophobic molecules, temperature responsive properties can be introduced. This etherification introduces water solubility and provides thermoresponsive properties due to the interactions discussed above. Figure 1-7 shows the structure of cellulose and some of its thermoresponsive derivatives.

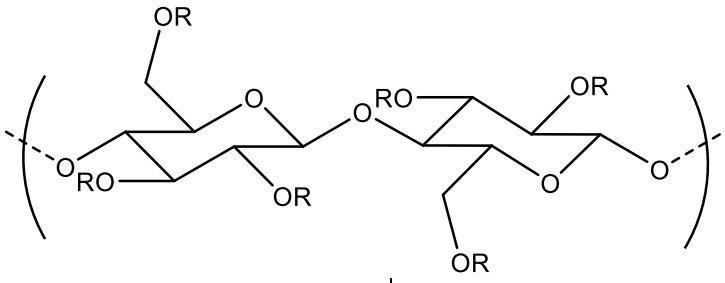

Cellulose derivative	R group
Cellulose	-H
Methyl cellulose	-H, $-CH_3$
Hydroxypropyl cellulose	-H, $-CH_2CHOH-CH_3$
Hydroxypropylmethyl cellulose	-H, $-CH_3$, $-CH_2CHOH-CH_3$
Ethylhydroxyethyl cellulose	-H, $-CH_2CH_3$, $-CH_2CH_2OH$

Figure 1- 7. Cellulose derivatives with LCSTs.

The LCST of these cellulose derivatives varies greatly, but is generally well above physiological temperatures, which limits their usefulness in temperature responsive drug delivery applications. Table 1-2 summarizes the LCST of these cellulose derivatives. Without further chemical or physical modification the usefulness of these polymers as temperature sensitive drug delivery systems are limited.

Table 1- 2. LCST values of cellulose derivatives.

Cellulose Derivative	LCST	Reference
Methyl cellulose	~60-80°C	[46,47]
Hydroxypropyl cellulose	~40-50°C	[48,49]
Hydroxypropylmethyl cellulose	~75-90	[49]
Ethylhydroxyethyl cellulose	~65°C	[50]

Temperature responsive cellulose derivatives have been used for ophthalmic applications. El-Kamel et al. used methyl cellulose and hydroxypropylmethyl cellulose in conjunction with poloxomer F127 to increase the bioavailability of timolol maleate eye drops [51]. Blends of hyaluronic acid and methyl cellulose have also been explored for use as in situ gelling cell delivery scaffolds [52]. The usefulness of cellulose derivatives in thermoresponsive applications on their own is limited, but their biocompatibility and degradability make them excellent candidates for use in composite systems.

1.4.2. Xyloglucan

Xyloglucan is a branched polysacharide with a chemically identical backbone to cellulose with xylose and xylose/galactose side chains [53]. In its native form, xyloglucan is not thermoresponsive, but upon partial degalactosylation temperature responsive properties can be introduced. Depending on the percent of degalactosylation, LCST temperatures ranging from 17-55°C have been achieved [54,55]. Although xyloglucan has had relatively limited application in ocular drug delivery, Miyazaki et al. used 1.5 % w/w xyloglucan to improve the sustained release of topically applied pilocarpine hydrochloride [56]. These studies showed a significant reduction in cumulative release rate that was comparable to a 25 % w/w pluronic F127 hydrogel. The ability of xyloglucan to form temperature sensitive hydrogels at low concentrations of 1.5 % w/w is a significant advantage over other polymeric systems.

1.4.3. Chemically thermoresponsive systems

Thermoresponsive systems can also be produced by combining natural polymers with gelation agents or in situ crosslinking agents. For example, chitosan, a linear polysacharide derived by the partial deacetylation of chitin, can become thermoresponsive when heated in the presence of polyol compounds such as glycerophosphate [57] or tripolyphosphate [58]. Chitosan, although not thermoresponsive itself, undergoes strong interactions with the polyol compounds at high temperatures to form chemically cross-linked gels. However, these chemically induced thermoresponsive chitosan polymers may have limited use due to the significant inflammatory response that they produce [59]. Crompton et al. found that chitosan-glycerphosphate gels injected into the brain were engulfed by macrophages within 7 days, which may limit their usefulness for sustained drug delivery [60].

1.5. Synthetic thermoresponsive polymers

Synthetic thermoresponsive polymer systems are significantly more common due to the simple alteration of hydrophilic and hydrophobic monomeric functional groups. Two main types of synthetic thermoresponsive polymers exist: homopolymers and multi-block copolymers. A brief list of homopolymers and multi-block copolymers are shown in Table 1-3. It can be seen in both classes of synthetic thermoresponsive polymers large variations in LCST can be achieved by varying the monomeric functional groups, composition, or molecular weight.

Table 1- 3. Examples of synthetic thermoresponsive polymers and their corresponding LCST.

Homopolymers	**LCST**	**Reference**
Poly(N-isopropylacrylamide)	31°C	[61]
Poly(N,N-diethacrylamide)	33°C	[62]
Poly(N-ethylacrylamide)	73°C	[63]
Poly(2-dimethylamino)ethyl methacrylate)	50°C	[64]
Poly(2-cyclopropyl-2-oxazoline)	28°C	[65]
Poly(2-ethyl-2-oxazoline)	91°C	[65]
Multi-block copolymers	**LCST**	**Reference**
Poly(ethylene oxide)-poly(propylene oxide)-poly(ethylene oxide) (PEO-PPO-PEO)		
$PEO_{12}PPO_{67}PEO_{12}$	19°C	[66]
$PEO_{13}PPO_{30}PEO_{13}$	58°C	[66]
$PEO_{17}PPO_{60}PEO_{17}$	86°C	[66]

For drug delivery applications, homopolymers are generally copolymerized with other monomers to alter the LCST or introduce functional monomers. For example, Cho et al. showed that copolymerizing 2-dimethylaminoethyl methacrylate with 6 mol. % acrylamide led to a reduction in the LCST from 50°C to below 30°C due to hydrogen bond formation between the amide and dimethylamino groups [64]. Although this study showed a reduction in LCST from copolymerization with acrylamide, generally hydrophilic monomers cause an increase in LCST. For example, Kratz et al. showed the increase in LCST of poly(N-isopropylacrylamide-co-acrylic acid) microgels with increasing acrylic acid [67]. Control over the composition of synthetic

temperature responsive hydrogels provides an effective method to tune the LCST to suit a particular application.

1.5.1. N-isopropylacrylamide polymers in ocular drug delivery

N-isopropylacrylamide (NIPAAm) is the most extensively studied synthetic thermoresponsive polymer, and has been explored for its application to the eye [68–70]. These NIPAAm based materials have been studied for their use as both injectable and topical drug delivery devices. Hsiue et al. developed topical mixtures of linear NIPAAm and cross-linked NIPAAm nanoparticles for the delivery of epinephrine for glaucoma treatment, but IOP-lowering was only achieved for less than 32 hours post administration [71]. This is likely due to the rapid clearance mechanisms of the front of the eye as previously discussed. Fedorchak et al. explored one way to improve the ocular bioavailability using a poly(NIPAAm-co-PEG diacrylate) copolymer that housed brimonidine tartrate (BT) loaded poly(lactide-co-glycolide) microparticles [72]. These polymer composites that were instilled and gelled within the fornix and were shown to be equivalent to administration of twice daily BT drops. While this device shows effective release, it requires significant patient dexterity to apply the drops into the fornix and position the gelled material, which may not be possible for all patients, reducing compliance and efficacy especially in elderly and disabled patients. Ideally, topical drug delivery would not require any post application adjustment or patient interaction.

NIPAAm based hydrogels have also been explored for their use as injectable, targeted, sustained drug releasing implants. Common to these materials is the combination or copolymerization with a hydrophilic molecule such as PEG diacrylate [69], acrylic acid [73] and gelatin [74] to adjust the LCST, drug release, and biocompatibility. Derwent et al. developed NIPAAm cross-linked with PEG diacrylate for the intravitreal injection and release of protein

therapeutics, which showed sustained release over approximately 3 weeks [69]. Increased crosslinking was found to slow protein release, but also made it more difficult to inject from large gauge needles that would reduce invasiveness. Unfortunately, these NIPAAm based drug delivery devices all suffer from the non-degradability of NIPAAm, which over the course of numerous treatments will result in the build-up of residual polymers in the target tissue. Fitzpatrick et al. developed a series of drug releasing NIPAAm copolymers containing (R)-α-acryloyloxy-β,β-dimethyl-γ-butyrolactone, which was shown to undergo ring opening hydrolysis to raise the LCST above physiological temperature for clearance from the vitreous [75]. These copolymers showed excellent sustained release of less than 20% dexamethasone after 25 days, but the copolymer properties and subsequent release rates were not readily adjustable. Fitzpatrick et al. also developed NIPAAm copolymers containing acrylic acid N-hydroxysuccinimide ester (NAS), an amine reactive monomer, used to graft RGDS peptide sequences, modified hyaluronic acid, and collagen for cell delivery [76,77]. The ideal injectable drug delivery scaffold would be fully degradable or resorbable to prevent device accumulation, and have the ability to control drug release properties such as release rate and total release time to meet the demands of different diseases and treatment regimes.

1.5.1.1. Tuning the LCST of N-isopropylacrylamide

Two common methods have been explored to adjust the LCST of synthetic thermoresponsive polymers such as poly(NIPAAm). These include copolymerization with hydrophilic or hydrophobic monomers to increase or decrease the LCST respectively, and changing the molecular weight to adjust the LCST. Adjusting the hydrophilic/hydrophobic balance in the final polymer also affects other properties such as water content and diffusion, which are important factors in drug delivery. For example, Feil et al. showed that the hydrophobic butyl

methacrylate linearly decreased LCST while hydrophilic acrylic acid, (diethylamino)ethyl methacrylate, and acrylamide linearly increased the copolymer LCST to varying degrees based on monomer hydrophilicity [78]. This study also showed that hydrogel water content increased as the proportion of hydrophilic monomer increased, which may be beneficial in altering drug release profiles. In another study poly(N-isopropylacrylamide-co-acrylic acid) hydrogels with higher acrylic acid were shown to release diltiazem hydrochloride faster [79]. Another method used to adjust the LCST of poly(NIPAAm) hydrogels is to change the molecular weight. Using atom transfer radical polymerization to produce various narrowly distributed molecular weights of poly(NIPAAm), Xia et al. showed that the LCST was decreased from approximately 43°C for 3.3 kDa to approximately 33°C for 32.5 kDa polymers [80]. Other drug releasing systems have shown that molecular weight can have a significant affect over drug release rates. Mittal et al. showed that estradiol release from PLGA nanoparticles was slower for copolymers with the same composition but higher molecular weight [81]. The changes in physical properties of polymeric hydrogels by altering composition and molecular weight show significant potential to adjust and control the drug release rates.

1.6.Polymerization techniques

1.6.1. Free radical polymerization

Free radical (FR) polymerization is the most common form of polymer synthesis due to its relative ease, versatility, and general robustness. It requires the formation of a free radical produced during the decomposition of a reactive initiator under an externally applied stimulus such as increased temperature or UV irradiation. This free radical then reacts with reactive alkene bonds to polymerize the polymer backbone. The FR mechanism, shown in Figure 1-8, results in termination by combination and disproportionation which results in a large uncontrollable range

of molecular weights [82]. This limits the usefulness of FR polymerization when attempting to develop highly controlled polymeric systems with tunable chemical and physical properties.

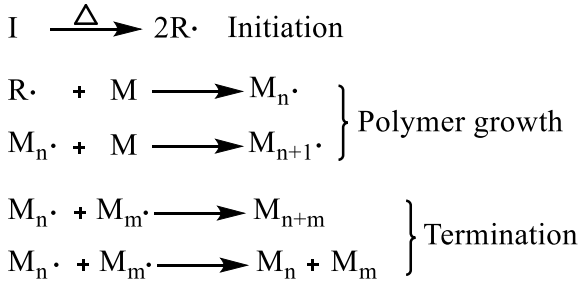

Figure 1- 8. Free radical polymerization mechanism. Adapted from [82]**.**

1.6.2. Reversible addition-fragmentation chain-transfer polymerization

Reversible addition-fragmentation chain-transfer polymerization (RAFT) is a common method used to produce polymers with high control over architecture, polydispersity (PDI), and composition. First published by Cheifari et al. in 1998, this polymerization method is advantageous over other controlled polymerization methods because of its ability to polymerize a range of monomer types under different reaction conditions while still producing a very low polydispersity [83]. The RAFT mechanism, shown in Figure 1-9, is achieved through the use of a di- or trithiocarbonyl reversible chain transfer agent along with a conventional free radical initiator. Living polymerization is achieved because the chain transfer agent allows for an equilibrium between the dormant polymer and propagating radical. RAFT polymerization can be used to synthesize complex polymer architectures such as surface grafted polymers [84], block copolymers [85], and star polymers [86]. These structures can be used to alter interfacial biomaterial properties, or synthesize micelles or polymerisomes. The versatility of RAFT to develop complex polymer architectures gives biomaterial scientists the ability to develop new smart drug delivery systems. A major advantage of RAFT compared to conventional FR polymerization in the development of bulk hydrogels is the ability to select a desired molecular

weight based on the monomer to RAFT agent ratio. This can be used to tailor molecular weight dependent properties to suit a particular application.

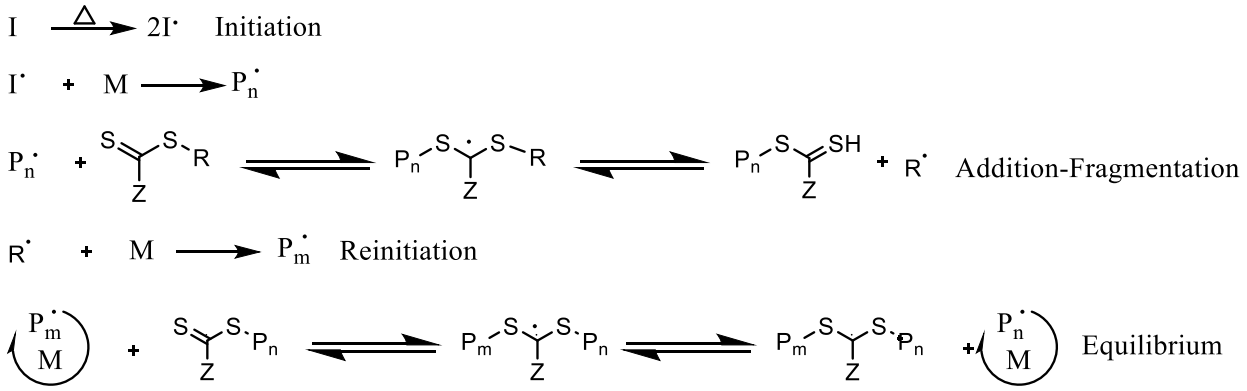

Figure 1- 9. RAFT polymerization mechanism. Adapted from [82]**.**

1.7.Drug release from polymer scaffolds

Drug releasing polymeric scaffolds can be classified as degradable or non-degradable. Degradable and non-degradable release mechanisms are depicted in Figure 1-10. Drug release from non-degradable polymer scaffolds occurs by diffusion from the polymer matrix. Drug release is diffusion controlled, which depends on the concentration gradient, diffusion distance, and drug diffusivity [87]. Release from non-degradable scaffolds is generally non-linear due to a changing concentration gradient and diffusion distance with time.

Drug release from degradable scaffolds can occur by diffusion, surface erosion, bulk erosion, or a combination of these three. In surface erosion, polymer backbone scission occurs at the surface releasing oligomers, monomers, and drug. In bulk degradation, polymer scission occurs throughout the material altering material properties such as water content, which can change the drug's diffusivity in the matrix. Water is an extremely important factor in the degradation process, which dictates the degradation rate and the ratio between surface and bulk erosion [87]. As hydrogel water content is increased, the interior polymeric chains are more susceptible to hydrolysis leading to a higher rate of bulk degradation. Lower water content

causes the majority of hydrolysis to occur at the surface where water contact is high. Tailoring the water content of hydrogels gives biomaterial scientists a way to control the rate and mechanism of degradation, which can be used to alter the drug release properties.

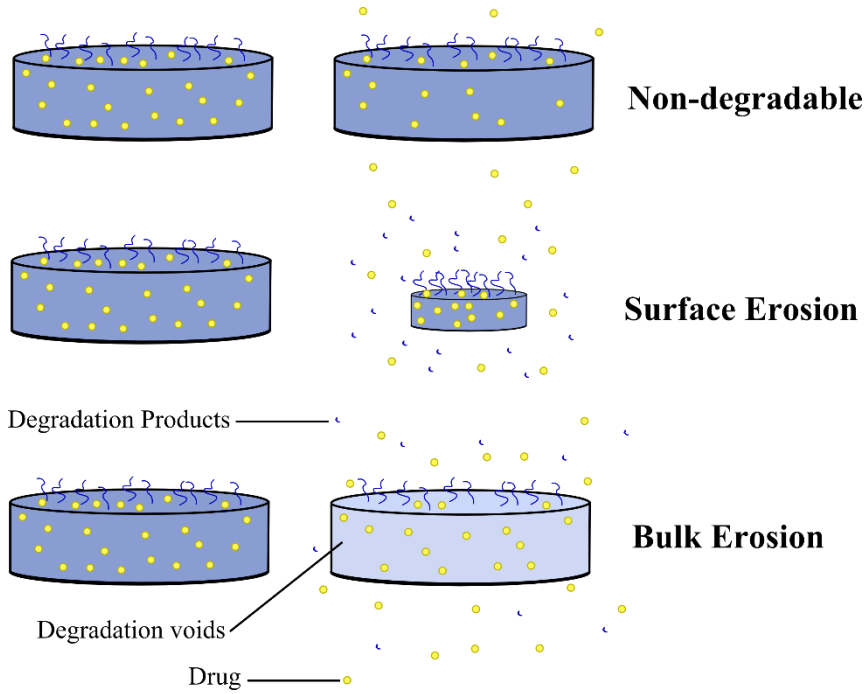

Figure 1- 10. Drug release mechanisms from degradable and non-degradable polymeric hydrogels.

Resorbable polymers have a slightly different release mechanism compared to degradable polymer scaffolds. In resorbable systems the backbone of individual polymers do not undergo hydrolysis, but rather the polymer chains re-dissolve for clearance from the implant. Similar to degradable systems, this can occur by surface or bulk erosion although surface erosion is more common due to the extremely low diffusivities of large polymer chains. The rate at which surface erosion occurs is also dependent on the polymer molecular weight, which governs the disentanglement of polymers at the interface [88]. The subsequent rate of drug release is dependent on two factors: diffusion out of the polymer matrix and the re-dissolution of polymers at the interface [89]. Manjkow et al. found that increased molecular weight and decreased polydispersity slowed slower surface dissolution [90]. This can be explained by higher polymer chain

entanglement, which prevents the re-dissolution of polymer chains, which is depicted in Figure 1-11. This suggests that controlling molecular weight and polydispersity can be used to alter the rate of polymer dissolution, which can be used to control the drug release rate.

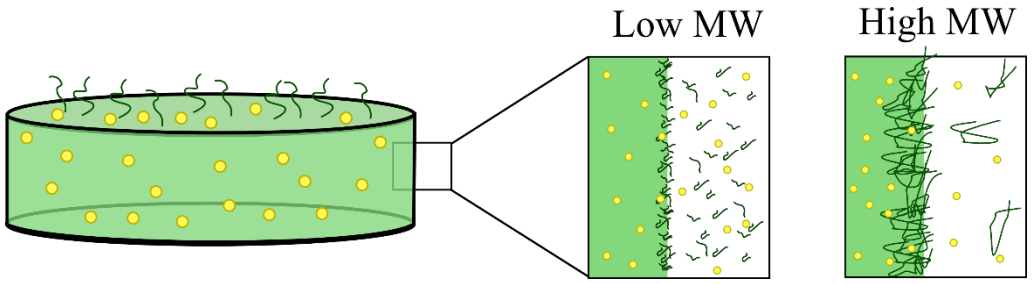

Figure 1- 11. Drug release mechanism from resorbable polymeric hydrogels. Adapted from [90]**.**

1.8.Mucoadhesive materials

The major problem with conventional topical drug delivery to the eye is the short residence time that prevents adequate penetration into the ocular tissues. One method to increase ocular drug bioavailability is to use mucoadhesive materials that interact with ocular mucin. This essentially entraps the drug on the ocular surface to increase the bioavailability of the drug and reduce losses due to lacrimal drainage.

The exact mechanism of mucoadhesion is not well understood, but a number of theories depending on the material have been proposed to describe the process [91]. These theories are summarized below in Table 1-4.

Table 1- 4. Theories describing mucoadhesion [91,92]**.**

Theory	Description
Wetting	- Applies to liquid systems. - Governing force for mucoadhesion is surface tension. - Liquids that reduce the surface energy between mucin and air/solution will be mucoadhesive.
Diffusion	- Interpenetration of polymer and mucin chains to form an entangled network. - Increased inter-polymer diffusion results in increased mucoadhesion. - 0.2-0.5 μm penetration depth required to produce an effective bioadhesive. - Diffusion depends on polymer diffusivity, chain flexibility, and contact time.
Fracture	- Analyzes the forces required to separate two surfaces after adhesion. - Suitable for non-mobile polymeric materials.
Electronic	- Electron transfer between mucin and mucoadhesive material based on differences in electronic structures. - Electron transfer between mucin and material results in the formation of a double later of electric charges. This double layer results in attractive forces.
Adsorption	- Mucoadhesion is due to primary bonding (ionic, covalent, and metallic), and secondary bonding (van der Waals, hydrophobic interactions and hydrogen bonding). - Secondary bonding is generally weaker and non-permanent, but more prominent than other mucoadhesion theories.

There are numerous natural polymers as well as synthetic materials that have been found to be mucoadhesive to different degrees. These can be grouped as non-ionic, anionic, cationic, thiol, and phenylboronic acid polymers. Non-ionic polymers such as methyl cellulose, hydroxypropyl cellulose, hydroxypropylmethyl cellulose, and hyaluronic acid are typically less mucoadhesive compared to ionic polymers [93]. Anionic polymers such as poly(acrylic acid), poly(methacrylic acid), carboxymethyl cellulose, and sodium alginate to name a few were found to be more mucoadhesive at low pH [94]. This suggests that the carboxylic acid groups provide substantial mucoadhesion in their acid form, which may be explained by increased hydrogen bonding with the mucins. Cationic polymers such as chitosan show excellent mucoadhesion due to the positive charge that can interact electrostatically with the negatively charged sialic acid on the mucin as well as hydrogen bonding [95]. Thiomers are a hybrid class of mucoadhesive polymers that often modify a non-ionic, or charged polymer discussed above to graft thiol functional groups along the polymer. Examples of these include chitosan-thioglycolic acid [96],

poly(acrylic acid)-cysteamine [97], and alginate-cystein [98]. Thiomers have significantly enhanced mucoadhesion compared to their non-thiolated base materials because of disulfide bonds that form with cysteine amino acids of mucin [93]. One significant disadvantage when working with thiolated polymers is the instability of thiols towards oxidation that may prevent long term storage.

Phenylboronic acid (PBA) is a relatively new class of synthetic mucoadhesive polymers that have been studied due to their interactions with 1,2-cis-diols [99]. PBA has a pKa of approximately 8.8. Shown in Figure 1-8, the equilibrium between the trigonal/tetragonal boronic acid/boronic acid esters is pH depended. As pH of a solution containing diol is increased the proportion of tetragonal boronic esters increases and the proportion of trigonal boronic acid decreases. The proportion of tetragonal boronic acid and trigonal boronate ester remains small and relatively unchanged. At pH 7.4 the proportion of tetragonal boronate ester was found to be approximately 50%, which is important for biomedical applications because it suggests that these materials can be substantially mucoadhesive at physiological pH.

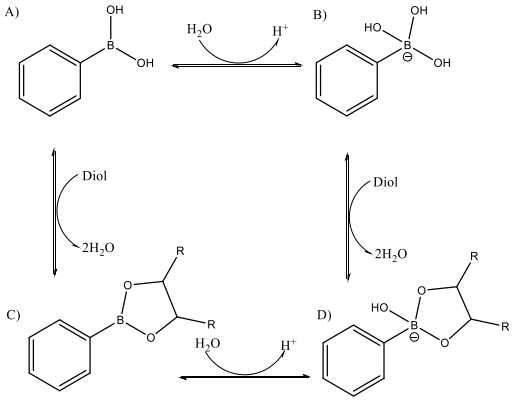

Figure 1- 12. Boronic acid acid-base equilibrium with diols. A) trigonal boronic acid, B) tetragonal boronic acid, C) trigonal boronic acid ester, D) tetragonal boronic acid ester. Adapted from [99]**.**

Interestingly, the optimal pH for binding between a boronic acid and its diol has been found to be approximately the average between the pKa of the acid and diol [100]. Therefore, sialic acid

with a pKa of approximately 2.6 [101] will have an optimal PBA binding at approximately pH 5.7. The affinity between PBA and diols can be represented by an equilibrium shown in equation 1-1:

$$K_{eq} = \frac{Boronate\ ester}{[Boronic\ acid][Diol]} \qquad (1\text{-}1)$$

This equilibrium constant varies for different diol compounds. For example, at pH 7.4 D-fructose has a K_{eq} of 160 M^{-1}, sucrose 0.67 M^{-1}, and sialic acid 21 M^{-1} [99]. These considerably high affinities for carbohydrates have been the basis on which the majority of PBA drug delivery devices have been developed.

1.9.Phenylboronic acid in drug delivery

To date, most biomaterials utilizing PBA have been investigated primarily for use in carbohydrate sensors and carbohydrate-mediated drug delivery devices, but recently there has been a growing trend for mucoadhesive drug delivery. Most PBA carbohydrate mediated drug delivery devices are based on glucose responsive insulin delivery. Nano- and microgels based on NIPAAm containing PBA have been explored for their glucose sensitive release of insulin [102,103]. These gels have shown changes in swelling and NIPAAm's LCST caused by PBA-glucose interactions, which change the physical properties of the gel. These changes in physical properties are extremely useful for glucose mediated drug release. Poly(NIPAAm-PBA) microgels have also be used for the temperature controlled release of diol compounds such as glucose during the microgel's temperature induced phase transition [104]. This utilized NIPAAm's temperature induced transition to force water and glucose out of the polymer matrix. Improvements to these nano- and microgels have been made by introducing degradable crosslinkers such as pentaerythritol tetra(3-mercaptopropionate) [105] and N,N'-bis(acryloyl)cystamine [106]. These gels were used for the glucose sensitive release of pre-loaded insulin that responded to clinically relevant glucose concentrations.

Unfortunately, rapid blood clearance of nano- and microparticles limit the usefulness of these materials for sustained insulin delivery. Amphiphillic block copolymers have been developed with outer poly(ethylene glycol) coronas for prolonged circulation and increased drug loading. Wang et al. developed a series of poly(ethylene glycol)-b-poly(acrylic acid-co-acrylamidophenylboronic acid) for the controlled release of insulin [107]. These block copolymers self-assembled into micelle structures and were able to disassemble when glucose-PBA complexes formed to release insulin. These nanosized micelles show stability against aggregation due to their hydrophillic shell and fast glucose release due to their nanosized diameter.

Phenylboronic acid has also been specifically targeted for drug delivery to mucous membranes. Li et al. developed silver nanoparticles coated in phenylboronic acid for the delivery of interferon to the vaginal mucosa [108]. In vitro, these nanoparticles were shown to have a release rate that depended on the mucin concentration in solution, which suggests that release would be dependent on interaction with the mucosal tissues. PBA based nanoparticles have also been developed for nasal drug delivery. In one study PBA was copolymerized with N-maleated glucosamine to produce nanoparticles for the nasal delivery of insulin [109]. They achieved insulin entrapment efficiencies greater than 60% and improved blood glucose reduction after nasal delivery compared to controls. Similarly Cheng et al. developed self-assembling PBA and poly(2-lactobionamidoethyl methacrylate) nanoparticles for nasal insulin delivery. These nanoparticles were able improve to insulin delivery to reduce blood glucose levels across the nasal mucosa, which shows that PBA interactions with mucin can improve drug delivery.

Phenylboronic acid has also been incorporated for mucoadhesive ocular drug delivery. Liu et al. developed poly(D,L-lactide)-b-dextran-g-PBA for the delivery of cyclosporine A (CycA) [110]. These polymers self-assembled in water to form micelles that were shown to be

mucoadhesive and able to release CycA for up to 5 days in vitro. Due to dextran's poor solubility in organic solvents, these micelles were formed by the drop method from dimethylsulfoxide (DMSO) into water. The only way to remove the DMSO is by dialysis, which also remove non-entrapped CycA. The DMSO/water mixture is likely why they were only able to achieve an 11.9% entrapment and rapid 5 day release. These micelles were only slightly negatively charged at physiological pH, which may not be enough to overcome PBA's highly hydrophobic phenyl ring from eventually forming micelle agglomerates. This would reduce their long-term shelf life and therefore ease of application for patients. It would be beneficial to develop a system whereby any organic solvents used to form stable drug loaded micelles could be removed without any drug loss.

1.10. Thesis objectives and scope

As outlined in this introduction the effective delivery of therapeutics to ocular tissues is a challenging due to the segmented structure and numerous clearance mechanisms of the eye. This has led to the development of biomaterial based drug delivery strategies to improve the efficacy of therapeutic delivery to ocular tissues. In the following chapters of this thesis, the development of two synthetic biomaterials using RAFT polymerization that have the potential to provide improved therapeutic delivery to the eye will be discussed.

The first biomaterial, covered in Chapters 2 and 3, is a NIPAAm based copolymer intended to prolong the release of intravitreal injections targeted at diseases of the posterior segment. The hypothesis was that by altering the compositional ratios of hydrophilic and hydrophobic functional monomers involved in degradability and LCST adjustment, and the molecular weight of the copolymer, we could develop a system with controllable degradation properties and drug release characteristics. This research covered the initial biomaterial development, and testing of its chemical, physical, and minor biological properties. We examined the effect of properties such as

composition, molecular weight, LCST, water content, gelation efficiency, and degradation time on drug release properties to develop a series of copolymers with tunable release profiles. The varying chemical and physical properties gave mechanistic insights into the predictable variation in dexamethasone release profiles between different materials. These NIPAAm based copolymers showed significant potential to act as minimally invasive injectable drug depots for the sustained release of posterior ophthalmic therapeutics.

The second biomaterial, discussed in Chapter 4, is a mucoadhesive block copolymer nanoparticle micelle based on phenylboronic acid for drug delivery to the front of the eye. The main focus of this project was initial material synthesis, chemical, physical, and minor biological testing. We hypothesized that by forming polymeric micelle nanoparticles with an outer phenylboronic acid shell we could improve the drug bioavailability on the ocular surface. We studied the effect of increasing the ratio of phenylboronic acid in the outer hydrophilic shell of the micelle on physical properties such as size, surface charge, mucoadhesion and drug release properties. Based on this research, these micelles show the potential to provide mucoadhesive sustained delivery of ophthalmic therapeutics to the anterior segment of the eye.

Overall, these research projects demonstrate two biomaterials that have the potential overcome the natural anatomical and physiological barriers of the eye to improve the efficacy of drug delivery to ocular tissues. These studies have laid the groundwork for further development of these materials as clinically applicable ocular drug delivery vehicles.

1.11. References

[1] H.J. Davidson, V.J. Kuonen, The tear film and ocular mucins, Vet. Ophthalmol. 7 (2004) 71–77.

[2] R. Gaudana, H.K. Ananthula, A. Parenky, A.K. Mitra, Ocular drug delivery., AAPS J. 12 (2010) 348–60.

[3] P. Argüeso, A. Tisdale, S. Spurr-Michaud, M. Sumiyoshi, I.K. Gipson, Mucin characteristics of human corneal-limbal epithelial cells that exclude the rose bengal anionic dye, Investig. Ophthalmol. Vis. Sci. 47 (2006) 113–119.

[4] D.W. DelMonte, T. Kim, S.T. Kitai, D.W. DelMonte, T. Kim, Anatomy and physiology of the cornea, J. Cataract Refract. Surg. 37 (2011) 588–598.

[5] H.S. Dua, L. a. Faraj, D.G. Said, T. Gray, J. Lowe, Human corneal anatomy redefined: A novel pre-descemet's layer (Dua's Layer), Ophthalmology. 120 (2013) 1778–1785.

[6] G.J. Thassu, Deepak and Chader, Eye anatomy, physiology, and occular barriers: basic considerations for drug delivery, in: Ocul. Drug Deliv. Syst. Barriers Appl. Nanoparticulate Syst., CRC Press Taylor & Francis Group, 2013: pp. 17–40.

[7] K. Hosoya, V.H.L. Lee, K.-J. Kim, Roles of the conjunctiva in ocular drug delivery: a review of conjunctival transport mechanisms and their regulation, Eur. J. Pharm. Biopharm. 60 (2005) 227–240.

[8] K.S. Kunert, A.S. Tisdale, I.K. Gipson, Goblet cell numbers and epithelial proliferation in the conjunctiva of patients with dry eye syndrome treated with cyclosporine., Arch. Ophthalmol. 120 (2002) 330–337.

[9] M.G. Doane, A.D. Jensen, C.H. Dohlman, Penetration Routes of Topically Applied Eye Medications, Am. J. Ophthalmol. 85 (1978) 383–386.

[10] I. Ahmed, T.F. Patton, Disposition of timolol and inulin in the rabbit eye following corneal versus non-corneal absorption, Int. J. Pharm. 38 (1987) 9–21.

[11] K.M. Hämäläinen, K. Kananen, S. Auriola, K. Kontturi, A. Urtti, Characterization of paracellular and aqueous penetration routes in cornea, conjunctiva, and sclera, Investig. Ophthalmol. Vis. Sci. 38 (1997) 627–634.

[12] J. Flammer, S. Orgül, V.P. Costa, N. Orzalesi, G.K. Krieglstein, L.M. Serra, et al., The impact of ocular blood flow in glaucoma, Prog. Retin. Eye Res. 21 (2002) 359–393.

[13] G.A. Lutty, T. Hasegawa, T. Baba, R. Grebe, I. Bhutto, D.S. McLeod, Development of the human choriocapillaris, Eye. 24 (2010) 408–415.

[14] N.D. Das, H. Shichi, Enzymes of mercapturate synthesis and other drug-metabolizing reactions-specific localization in the eye, Exp. Eye Res. 33 (1981) 525–533.

[15] M. Nakano, C.M. Lockhart, E.J. Kelly, A.E. Rettie, Ocular cytochrome P450s and transporters: roles in disease and endobiotic and xenobiotic disposition., Drug Metab. Rev. 2532 (2014) 1–14.

[16] T.F. Freddo, A contemporary concept of the blood-aqueous barrier, Prog. Retin. Eye Res. 32 (2013) 181–195.

[17] B.J. Kirkwood, Anatomy of the retina., Webvision Organ. Retin. Vis. Syst. 37 (2012) 5–8.

[18] E.A. Runkle, D. Antonetti, The Blood-Retinal Barrier: Structure and Functional Significance, in: S. Nag (Ed.), Blood-Brain Other Neural Barriers SE - 5, Humana Press, 2011: pp. 133–148.

[19] M.L. Schwartzman, J. Masferrer, M.W. Dunn, J.C. McGiff, N.G. Abraham, Cytochrome P450, drug metabolizing enzymes and arachidonic acid metabolism in bovine ocular tissues., Curr. Eye Res. 6 (1987) 623–630.
[20] J.W. Shell, Pharmacokinetics of topically applied ophthalmic drugs, Surv. Ophthalmol. 26 (1982) 207–218.
[21] S. Mishima, A. Gasset, S.D.J. Klyce, J.L. Baum, Determination of tear volume and tear flow., Invest. Ophthalmol. 5 (1966) 264–276.
[22] P.M. Hughes, O. Olejnik, J.-E. Chang-Lin, C.G. Wilson, B. Barrier, R.V. Leakage, et al., Topical and systemic drug delivery to the posterior segments, Adv. Drug Deliv. Rev. 57 (2005) 2010–2032.
[23] M. Ruponen, A. Urtti, Undefined role of mucus as a barrier in ocular drug delivery, Eur. J. Pharm. Biopharm. (2015) In press.
[24] A. Urtti, L. Salminen, Minimizing systemic absorption of topically administered ophthalmic drugs, Surv. Ophthalmol. 37 (1993) 435–456.
[25] R.J.C. Bowman, J. Cope, K.K. Nischal, Ocular and systemic side effects of brimonidine 0.2% eye drops (Alphagan) in children., Eye (Lond). 18 (2004) 24–26.
[26] J.-M. Korte, T. Kaila, M. Saari, Systemic bioavailability and cardiopulmonary effects of 0.5% timolol eyedrops, Graefe's Arch. Clin. Exp. Ophthalmol. 240 (2002) 430–435.
[27] H. Uusitalo, J. Niño, K. Tahvanainen, V. Turjanmaa, A. Ropo, J. Touminen, et al., Efficacy and systemic side-effects of topical 0.5% timolol aqueous solution and 0.1% timolol hydrogel, Acta Ophthalmol. Scand. 83 (2005) 723–728.
[28] A. Urtti, Challenges and obstacles of ocular pharmacokinetics and drug delivery, Adv. Drug Deliv. Rev. 58 (2006) 1131–1135.
[29] D.H. Geroski, H.F. Edelhauser, Drug delivery for posterior segment eye disease., Invest. Ophthalmol. Vis. Sci. 41 (2000) 961–964.
[30] T.R. Thrimawithana, S. Young, C.R. Bunt, C. Green, R.G. Alany, Drug delivery to the posterior segment of the eye., Drug Discov. Today. 16 (2011) 270–7.
[31] V.-P. Ranta, E. Mannermaa, K. Lummepuro, A. Subrizi, A. Laukkanen, M. Antopolsky, et al., Barrier analysis of periocular drug delivery to the posterior segment., J. Control. Release. 148 (2010) 42–8.
[32] J.E. Chan, T. a. Pridgen, K.G. Csaky, Episcleral clearance of sodium fluorescein from a bioerodible sub-tenon's implant in the rat, Exp. Eye Res. 90 (2010) 501–506.
[33] G.A. Peyman, E.M. Lad, D.M. Moshfeghi, Intravitreal injection of therapeutic agents., Retina. 29 (2009) 875–912.
[34] K.M. Sampat, S.J. Garg, Complications of intravitreal injections., Curr. Opin. Ophthalmol. 21 (2010) 178–183.
[35] V.S. De Stefano, J.J.K. Abechain, L.F.S. de Almeida, D.M. Verginassi, E.B. Rodrigues, E. Freymuller, et al., Experimental investigation of needles, syringes and techniques for intravitreal injections, Clin. Experiment. Ophthalmol. 39 (2011) 236–242.
[36] M. Naveed Yasin, D. Svirskis, A. Seyfoddin, I.D. Rupenthal, Implants for drug delivery to the posterior segment of the eye: A focus on stimuli-responsive and tunable release systems., J. Control. Release. 196 (2014) 208–221.
[37] N. Kuno, S. Fujii, Biodegradable Intraocular Therapies for Retinal Disorders, Drugs Aging. 27 (2010) 117–134.
[38] J.I. Lim, R. a. Wolitz, A.H. Dowling, H.R. Bloom, A.R. Irvine, D.M. Schwartz, Visual and anatomic outcomes associated with posterior segment complications after ganciclovir

implant procedures in patients with AIDS and cytomegalovirus retinitis, Am. J. Ophthalmol. 127 (1999) 288–293.
[39] G.J. Jaffe, D. Martin, D. Callanan, P.A. Pearson, B. Levy, T. Comstock, Fluocinolone Acetonide Implant (Retisert) for Noninfectious Posterior Uveitis: Thirty-Four–Week Results of a Multicenter Randomized Clinical Study, Ophthalmology. 113 (2006) 1020–1027.
[40] F.E. Kane, J. Burdan, A. Cutino, K.E. Green, Iluvien: a new sustained delivery technology for posterior eye disease., Expert Opin. Drug Deliv. 5 (2008) 1039–46.
[41] D.A. Mohammad, B. V Sweet, S.G. Elner, Retisert: Is the New Advance in Treatment of Uveitis a Good One?, Ann. Pharmacother. . 41 (2007) 449–455.
[42] E. Pacella, A.R. Vestri, R. Muscella, M.R. Carbotti, M. Castellucci, L. Coi, et al., Preliminary results of an intravitreal dexamethasone implant (Ozurdex®) in patients with persistent diabetic macular edema, Clin. Ophthalmol. 7 (2013) 1423–1428.
[43] D. Pardo-López, E. Francés-Muñoz, R. Gallego-Pinazo, M. Díaz-Llopis, Anterior chamber migration of dexametasone intravitreal implant (Ozurdex®), Graefe's Arch. Clin. Exp. Ophthalmol. 250 (2012) 1703–1704.
[44] R. Bansal, P. Bansal, P. Kulkarni, V. Gupta, A. Sharma, A. Gupta, Wandering Ozurdex® implant, J. Ophthalmic Inflamm. Infect. 2 (2012) 1–5.
[45] S. Jain, P.S. Sandhu, R. Malvi, B. Gupta, Cellulose derivatives as thermoresponsive polymer: An overview, J. Appl. Pharm. Sci. 3 (2013) 139–144.
[46] L. Li, H. Shan, C.Y. Yue, Y.C. Lam, K.C. Tam, X. Hu, Thermally Induced Association and Dissociation of Methylcellulose in Aqueous Solutions, Langmuir. 18 (2002) 7291–7298.
[47] M. Takahashi, M. Shimazaki, J. Yamamoto, Thermoreversible gelation and phase separation in aqueous methyl cellulose solutions, J. Polym. Sci. Part B Polym. Phys. 39 (2001) 91–100.
[48] J. Gao, G. Haidar, X. Lu, Z. Hu, Self-association of hydroxypropylcellulose in water, Macromolecules. 34 (2001) 2242–2247.
[49] N. Sarkar, Thermal Gelation Properties of Methyl and Hydroxypropyl Methylcellulose., J Appl Polym Sci. 24 (1979) 1073–1087.
[50] J. Persson, H.O. Johansson, I. Galaev, B. Mattiasson, F. Tjerneld, Aqueous polymer two-phase systems formed by new thermoseparating polymers, Bioseparation. 9 (2000) 105–116.
[51] a. H. El-Kamel, In vitro and in vivo evaluation of Pluronic F127-based ocular delivery system for timolol maleate, Int. J. Pharm. 241 (2002) 47–55.
[52] M.J. Caicco, T. Zahir, A.J. Mothe, B.G. Ballios, A.J. Kihm, C.H. Tator, et al., Characterization of hyaluronan-methylcellulose hydrogels for cell delivery to the injured spinal cord, J. Biomed. Mater. Res. - Part A. 101 A (2013) 1472–1477.
[53] Fry Stephen C, The Structure and Functions of Xyloglucan, J. Exp. Bot. 40 (1989) 1–11.
[54] a. K. a S. Brun-Graeppi, C. Richard, M. Bessodes, D. Scherman, T. Narita, G. Ducouret, et al., Study on the sol-gel transition of xyloglucan hydrogels, Carbohydr. Polym. 80 (2010) 556–563.
[55] D.R. Nisbet, K.E. Crompton, S.D. Hamilton, S. Shirakawa, R.J. Prankerd, D.I. Finkelstein, et al., Morphology and gelation of thermosensitive xyloglucan hydrogels, Biophys. Chem. 121 (2006) 14–20.

[56] S. Miyazaki, S. Suzuki, N. Kawasaki, K. Endo, a. Takahashi, D. Attwood, In situ gelling xyloglucan formulations for sustained release ocular delivery of pilocarpine hydrochloride, Int. J. Pharm. 229 (2001) 29–36.
[57] Q.X. Ji, X.G. Chen, Q.S. Zhao, C.S. Liu, X.J. Cheng, L.C. Wang, Injectable thermosensitive hydrogel based on chitosan and quaternized chitosan and the biomedical properties., J. Mater. Sci. Mater. Med. 20 (2009) 1603–10.
[58] T. Ur-Rehman, S. Tavelin, G. Gröbner, Chitosan in situ gelation for improved drug loading and retention in poloxamer 407 gels, Int. J. Pharm. 409 (2011) 19–29.
[59] J. Sun, G. Jiang, T. Qiu, Y. Wang, K. Zhang, F. Ding, Injectable chitosan-based hydrogel for implantable drug delivery: Body response and induced variations of structure and composition, J. Biomed. Mater. Res. - Part A. 95 (2010) 1019–1027.
[60] K.E. Crompton, D. Tomas, D.I. Finkelstein, M. Marr, J.S. Forsythe, M.K. Horne, Inflammatory response on injection of chitosan/GP to the brain, J. Mater. Sci. Mater. Med. 17 (2006) 633–639.
[61] M. Heskins, J.E. Guillet, Solution Properties of Poly(N-isopropylacrylamide), J. Macromol. Sci. Part A - Chem. 2 (1968) 1441–1455.
[62] I. Idziak, D. Avoce, D. Lessard, D. Gravel, X.X. Zhu, Thermosensitivity of Aqueous Solutions of Poly(N,N -diethylacrylamide), Macromolecules. 32 (1999) 1260–1263.
[63] W. Cai, R.B. Gupta, Poly(N-ethylacrylamide) Hydrogels for Lignin Separation, Ind. Eng. Chem. Res. 40 (2001) 3406–3412.
[64] S.U.N.H. Cho, M.U.S. Jhon, S.H. Yuk, H. a I.B. Lee, Temperature-Induced Phase Transition of Poly (N , N- dimethylaminoethyl methacrylate-co-acrylamide), J. Polym. Sci. Part B Polym. Phys. 35 (1997) 595–598.
[65] M. Glassner, K. Lava, V.R. de la Rosa, R. Hoogenboom, Tuning the LCST of poly(2-cyclopropyl-2-oxazoline) via gradient copolymerization with 2-ethyl-2-oxazoline, J. Polym. Sci. Part A Polym. Chem. 52 (2014) 3118–3122.
[66] L.E. Bromberg, E.S. Ron, Temperature-responsive gels and thermogelling polymer matrices for protein and peptide delivery, Adv. Drug Deliv. Rev. 31 (1998) 197–221.
[67] K. Kratz, T. Hellweg, W. Eimer, Influence of charge density on the swelling of colloidal poly(N-isopropylacrylamide-co-acrylic acid) microgels, Colloids Surfaces A Physicochem. Eng. Asp. 170 (2000) 137–149.
[68] Y. Cao, C. Zhang, W. Shen, Z. Cheng, L. (Lucy) Yu, Q. Ping, Poly(N-isopropylacrylamide)-chitosan as thermosensitive in situ gel-forming system for ocular drug delivery, J. Control. Release. 120 (2007) 186–194.
[69] J.J. Kang Derwent, W.F. Mieler, Thermoresponsive hydrogels as a new ocular drug delivery platform to the posterior segment of the eye., Trans. Am. Ophthalmol. Soc. 106 (2008) 206–213; discussion 213–214.
[70] A. Famili, M.Y. Kahook, D. Park, A Combined Micelle and Poly(Serinol Hexamethylene Urea)- *Co* -Poly(*N* -Isopropylacrylamide) Reverse Thermal Gel as an Injectable Ocular Drug Delivery System, Macromol. Biosci. 14 (2014) 1719–1729.
[71] G.H. Hsiue, S.H. Hsu, C.C. Yang, S.H. Lee, I.K. Yang, Preparation of controlled release ophthalmic drops, for glaucoma therapy using thermosensitive poly-N-isopropylacrylamide, Biomaterials. 23 (2002) 457–462.
[72] M. V FEDORCHAK, S.R. Little, J.S. Schuman, A. CUGINI, Thermoresponsive hydrogel containing polymer microparticles for noninvasive ocular drug delivery, (2014).

[73] A. Prasannan, H.-C. Tsai, Y.-S. Chen, G.-H. Hsiue, A thermally triggered in situ hydrogel from poly(acrylic acid-co-N-isopropylacrylamide) for controlled release of anti-glaucoma drugs, J. Mater. Chem. B. 2 (2014) 1988.
[74] J.-Y. Lai, A.-C. Hsieh, A gelatin-g-poly(N-isopropylacrylamide) biodegradable in situ gelling delivery system for the intracameral administration of pilocarpine., Biomaterials. 33 (2012) 2372–87.
[75] S.D. Fitzpatrick, M. a Jafar Mazumder, B. Muirhead, H. Sheardown, Development of injectable, resorbable drug-releasing copolymer scaffolds for minimally invasive sustained ophthalmic therapeutics., Acta Biomater. 8 (2012) 2517–28.
[76] S.D. Fitzpatrick, M. a Jafar Mazumder, F. Lasowski, L.E. Fitzpatrick, H. Sheardown, PNIPAAm-grafted-collagen as an injectable, in situ gelling, bioactive cell delivery scaffold., Biomacromolecules. 11 (2010) 2261–7.
[77] M. a J. Mazumder, S.D. Fitzpatrick, B. Muirhead, H. Sheardown, Cell-adhesive thermogelling PNIPAAm/hyaluronic acid cell delivery hydrogels for potential application as minimally invasive retinal therapeutics., J. Biomed. Mater. Res. A. 100 (2012) 1877–87.
[78] H. Feil, Y.H. Bae, J. Feijen, S.W. Kim, Effect of comonomer hydrophilicity and ionization on the lower critical solution temperature of N-isopropylacrylamide copolymers, Macromolecules. 26 (1993) 2496–2500.
[79] E. Díez-Peña, P. Frutos, G. Frutos, I. Quijada-Garrido, J.M. Barrales-Rienda, The influence of the copolymer composition on the diltiazem hydrochloride release from a series of pH-sensitive poly[(N-isopropylacrylamide)-co-(methacrylic acid)] hydrogels., AAPS PharmSciTech. 5 (2004) 69–76.
[80] Y. Xia, X. Yin, N.A.D. Burke, H.D.H. Sto, H.D.H. Stöver, Thermal Response of Narrow-Disperse Poly(N-isopropylacrylamide) Prepared by Atom Transfer Radical Polymerization, Macromolecules. 38 (2005) 5937–5943.
[81] G. Mittal, D.K. Sahana, V. Bhardwaj, M.N. V Ravi Kumar, Estradiol loaded PLGA nanoparticles for oral administration: effect of polymer molecular weight and copolymer composition on release behavior in vitro and in vivo., J. Control. Release. 119 (2007) 77–85.
[82] G. Odian, Principles of polymerization, 4th Editio, John Wiley & Sons, Inc., 2004.
[83] J. Chiefari, Y.K.B. (Bill) Chong, F. Ercole, J. Krstina, J. Jeffery, T.P.T. Le, et al., Living Free-Radical Polymerization by Reversible Addition−Fragmentation Chain Transfer: The RAFT Process, Macromolecules. 31 (1998) 5559–5562.
[84] K. Ohno, Y. Ma, Y. Huang, C. Mori, Y. Yahata, Y. Tsujii, et al., Surface-initiated reversible addition-fragmentation chain transfer (RAFT) polymerization from fine particles functionalized with trithiocarbonates, Macromolecules. 44 (2011) 8944–8953.
[85] D.J. Keddie, A guide to the synthesis of block copolymers using reversible-addition fragmentation chain transfer (RAFT) polymerization., Chem. Soc. Rev. 43 (2013) 496–505.
[86] J. Liu, H. Duong, M.R. Whittaker, T.P. Davis, C. Boyer, Synthesis of functional core, star polymers via RAFT polymerization for drug delivery applications, Macromol. Rapid Commun. 33 (2013) 760–766.
[87] J. Fu, Yao and Kao, Drug release kinetic and transport mechanisms of non-degradable and degradable polymeric delivery systems, Expert O. 7 (2010) 429–444.
[88] B. Narasimhan, Mathematical models describing polymer dissolution: consequences for drug delivery, Adv. Drug Deliv. Rev. 48 (2001) 195–210.

[89] B. a. Miller-Chou, J.L. Koenig, A review of polymer dissolution, Prog. Polym. Sci. 28 (2003) 1223–1270.
[90] J. Manjkow, Influence of Processing and Molecular Parameters on the Dissolution Rate of Poly-(Methyl Methacrylate) Thin Films, J. Electrochem. Soc. 134 (1987) 2003.
[91] B.M. Boddupalli, Z.N.K. Mohammed, R.A. Nath, D. Banji, Mucoadhesive drug delivery system: An overview, J. Adv. Pharm. Technol. Res. 1 (2010) 381–387.
[92] R. Shaikh, T.R. Raj Singh, M.J. Garland, A.D. Woolfson, R.F. Donnelly, Mucoadhesive drug delivery systems, J. Pharm. Bioallied Sci. 3 (2011) 89–100.
[93] V. V Khutoryanskiy, Advances in mucoadhesion and mucoadhesive polymers., Macromol. Biosci. 11 (2011) 748–64.
[94] P. Haesun, R.R. Joseph, Mechanism of Mucoadhesion of Poly(Acrylic Acid) Hydrogels, Pharm. Res. 4 (1987) 457–464.
[95] R. Qaqish, M. Amiji, Synthesis of a fluorescent chitosan derivative and its application for the study of chitosan–mucin interactions, Carbohydr. Polym. 38 (1999) 99–107.
[96] C.E. Kast, W. Frick, U. Losert, A. Bernkop-Schnürch, Chitosan-thioglycolic acid conjugate: A new scaffold material for tissue engineering?, Int. J. Pharm. 256 (2003) 183–189.
[97] J. Hombach, T.F. Palmberger, A. Bernkop-Schnürch, M.J. Taylor, S. Tanna, T. Sahota, Development and in vitro evaluation of a mucoadhesive vaginal delivery system for nystatin, J. Pharm. Sci. 98 (2009) 555–564.
[98] A. Bernkop-Schnürch, C.E. Kast, M.F. Richter, Improvement in the mucoadhesive properties of alginate by the covalent attachment of cysteine, J. Control. Release. 71 (2001) 277–285.
[99] G. Springsteen, B. Wang, A detailed examination of boronic acid-diol complexation, Tetrahedron. 58 (2002) 5291–5300.
[100] J. Yan, G. Springsteen, S. Deeter, B. Wang, The relationship among pK a, pH, and binding constants in the interactions between boronic acids and diols - It is not as simple as it appears, Tetrahedron. 60 (2004) 11205–11209.
[101] E.R. Vimr, K. a Kalivoda, E.L. Deszo, S.M. Steenbergen, Diversity of microbial sialic acid metabolism., Microbiol. Mol. Biol. Rev. 68 (2004) 132–153.
[102] Z. Wu, X. Zhang, H. Guo, C. Li, D. Yu, An injectable and glucose-sensitive nanogel for controlled insulin release, J. Mater. Chem. 22 (2012) 22788–22796.
[103] T. Hoare, R. Pelton, Engineering glucose swelling responses in poly(N-isopropylacrylamide)-based microgels, Macromolecules. 40 (2007) 670–678.
[104] H. Ge, Y. Ding, C. Ma, G. Zhang, Temperature-controlled release of diols from N-isopropylacrylamide-co- acrylamidophenylboronic acid microgels, J. Phys. Chem. B. 110 (2006) 20635–20639.
[105] L. Zhao, C. Xiao, J. Ding, P. He, Z. Tang, X. Pang, et al., Facile one-pot synthesis of glucose-sensitive nanogel via thiol-ene click chemistry for self-regulated drug delivery, Acta Biomater. 9 (2013) 6535–6543.
[106] X. Zhang, S. Lü, C. Gao, C. Chen, X. Zhang, M. Liu, Highly stable and degradable multifunctional microgel for self-regulated insulin delivery under physiological conditions., Nanoscale. 5 (2013) 6498–506.
[107] B. Wang, R. Ma, G. Liu, Y. Li, X. Liu, Y. An, et al., Glucose-responsive micelles from self-assembly of poly(ethylene glycol)-a-poly(acrylic acid-co-acrylamidophenylboronic acid) and the controlled release of insulin, Langmuir. 25 (2009) 12522–12528.

[108] C. Li, Z. Liu, X. Yan, W. Lu, Y. Liu, Mucin-controlled drug release from mucoadhesive phenylboronic acid-rich nanoparticles, Int. J. Pharm. 479 (2015) 261–264.
[109] X. Zhang, Y. Wang, C. Zheng, C. Li, Phenylboronic acid-functionalized glycopolymeric nanoparticles for biomacromolecules delivery across nasal respiratory, Eur. J. Pharm. Biopharm. 82 (2012) 76–84.
[110] S. Liu, L. Jones, F.X. Gu, Development of mucoadhesive drug delivery system using phenylboronic acid functionalized poly(D,L-lactide)-b-dextran nanoparticles., Macromol. Biosci. 12 (2012) 1622–1626.

2. CHAPTER 2: Tuning the LCST of N-isopropylacrylamide copolymers through composition and molecular weight changes.

Objectives: To determine the effect of changing composition and molecular weight on the LCST of N-isopropylacrylamide copolymers for subsequent drug delivery studies.

Main Scientific Contributions:

- Showed that the LCST of poly(N-isopropylacrylamide) copolymers is dependent on the hydrophilic/hydrophobic copolymer ratio.
- Showed that increasing the molecular weight of poly(N-isopropylacrylamide) copolymers increases the LCST.

2.1. Materials and Methods

2.1.1. Materials

Unless otherwise stated, all materials were purchased from Sigma Aldrich (Oakville, ON, Canada). N-isopropylacrylamide was purified by recrystallization from 40:60 toluene:hexane before use. AIBN was recrystallized in methanol before use. All solvents were purchased from Caledon Laboratories (Caledon, ON). $(CD_3)_2SO$ was purchased from Cambridge Isotope Laboratories Inc. (Andover, MA, USA). Phosphate buffered saline (PBS) was purchased from BioShop (Burlington, ON, Canada).

2.1.2. Poly(NIPAAm-AAm-NAS-DBA) copolymer synthesis

Poly(NIPAAm-AAm-NAS-DBA) (pNAND) copolymers were synthesize by RAFT polymerization. In a typical reaction procedure (69:14:5:12:2 molar feed ratio of NIPAAm:AAm:NAS:DBA:DDMAT), NIPAAm (658.4 mg, 5.82 mmol), AAm (83.9 mg, 1.18 mmol), NAS (71.3 mg, 0.43 mmol), DBA (165.7 mg, 0.90 mmol), DDMAT (0.186 g, 0.17 mmol), and AIBN (1.4 mg, 0.008 mmol) were dissolved in 4 mL of 1,4-dioxane and added to a 10 mL round bottom flask. The solution was degassed by performing three freeze-pump-thaw cycles followed by replacement of the atmosphere with nitrogen. The flask was then heated to 70°C for 24 hours while stirring. This copolymer, denoted 14/12-5 (AAm/DBA-MW) was isolated and purified by precipitation into 10 times excess of cold anhydrous diethyl ether three times. pNAND polymers were synthesized with AAm compositions varying from 0 to 21 mol. % and DBA compositions from 0 to 18 mol. %. The copolymer was dried under vacuum at 50°C for 48 hours. Higher molecular weight copolymers were produced by reducing the amount of DDMAT relative to the monomers added.

2.1.3. pNAND Characterization

Proton nuclear magnetic resonance (^{1}H NMR, Bruker Avance 600 MHz $(CD_3)_2SO$) was used to determine monomer conversion after 24 hours of reaction. Gel permeation chromatography (GPC) was used to determine copolymer molecular weight with a Waters system composed of a 590 HPLC pump, three Styragel columns (HR2, HR3, HR4), and a 410 refractive index detector. Samples were eluted in N,N-dimethylformamide containing 50 mM LiBr at a flow rate of 0.5 mL min^{-1}, and the system was calibrated using narrow dispersed polyethylene glycol (PEG) standards.

2.1.3.1. Lower critical solution temperature characterization

Differential scanning calorimetry (DSC, TA Instruments Q20) was used to determine the copolymer LCST. For DSC, 15 μL of copolymer dissolved in PBS at 20 wt. % was heated from 0 to 50°C at a rate of 2°C min^{-1} in aluminum hermetic pans. The minimum value of the endothermic peak in the DSC curve was considered to be the copolymer LCST.

2.2. Results and Discussion

2.2.1. Copolymer Characterization

^{1}H NMR of pNAND copolymers was completed to determine the conversion after 24 hours. All copolymers showed ≥ 95% conversion for all monomers. The ^{1}H NMR of pNAND-14/6-5 reaction product after 24 hours is shown in Figure 2-1. Alkene monomer peaks (5.4 to 6.4 ppm) were compared to polymer peaks (DBA: 4.1 ppm, NIPAAm: 3.9 ppm, NAS: 2.8 ppm) to determine conversion. GPC was used to determine the copolymer molecular weight and PDI. Table 2-1 shows the molecular weight and PDI of select copolymers that were soluble in PBS at 4 °C. All copolymers showed low polydispersity, which is characteristic of RAFT polymerization. Although molecular weight is approximately 60 % lower than theoretical values, this is due to using PEG standards for calibration.

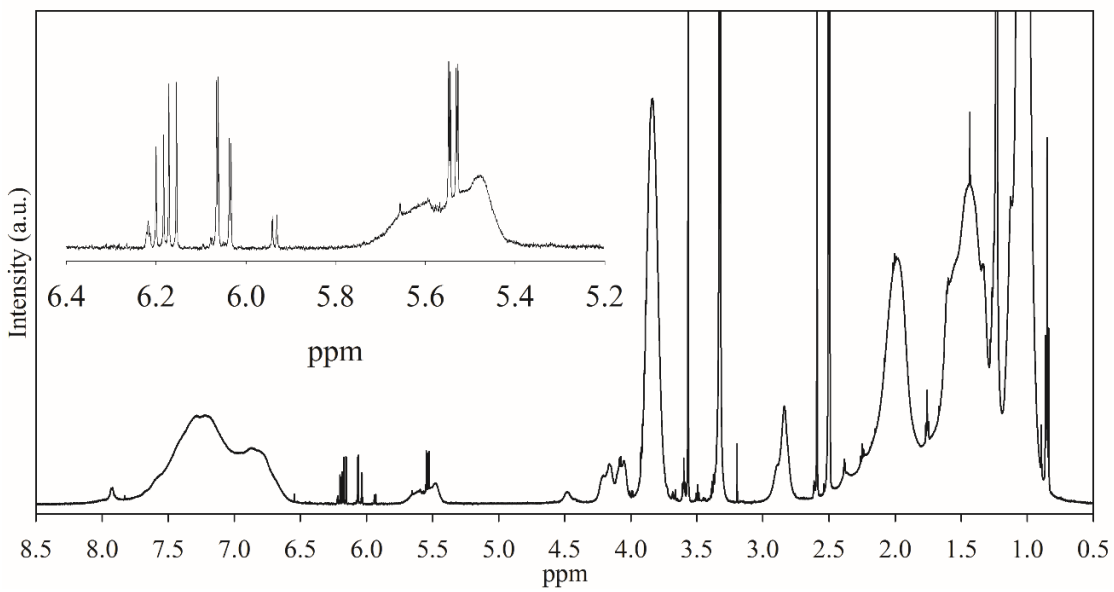

Figure 2 - 1. ^{1}H NMR of pNAND-14/6-5 showing high monomer conversion.

Using differential scanning calorimetry, the LCST of pNAND copolymers was determined. Table 2-1 contains the copolymer LCST of 5.5 kDa copolymers. The LCST of some copolymer formulations could not be measured because they did not dissolve (DND) in PBS at 4°C. This likely suggests that their LCST is below 4°C.

Table 2 - 1. pNAND copolymer molecular weight, polydispersity, and LCST. Only polymers that dissolved in PBS were measured using GPC. DND = did not dissolve.

Copolymer	Mn (g mol^{-1})[a]	PDI[a]	LCST ± SD (°C)[b]
pNAND-0/0-5	3061	1.13	24.0 ± 0.9
pNAND-0/6-5	3334	1.10	15.1 ± 1.0
pNAND-0/12-5	-	-	DND
pNAND-0/18-5	-	-	DND
pNAND-7/0-5	2938	1.12	27.7 ± 0.5
pNAND-7/6-5	3084	1.13	18.9 ± 0.2
pNAND-7/12-5	-	-	DND
pNAND-7/18-5	-	-	DND
pNAND-14/0-5	3182	1.11	33.2 ± 0.2
pNAND-14/6-5	3379	1.09	23.6 ± 0.2
pNAND-14/12-5	2942	1.11	11.05 ± 0.3
pNAND-14/18-5	-	-	DND
pNAND-21/0-5	3284	1.12	39.1 ± 0.3
pNAND-21/6-5	3351	1.10	27.8 ± 0.7
pNAND-21/12-5	3453	1.12	15.78 ± 1.5
pNAND-21/18-5	-	-	DND

[a] determine using DMF GPC
[b] determined using ^{1}H NMR

Using the LCST values from the 10 materials that dissolved in PBS at 4°C, a multiple linear regression was used to determine the effect of AAm and DBA composition on LCST. Equation 2-1 shows the result of the multiple linear regression where AAm and DBA variables are in mol. % and LCST is in °C. The R^2 value was determined to be 0.988, which shows excellent fit between the liner regression and experimental data.

$$LCST(5\ kDa) = 24.6 + 0.65\ AAm - 1.81\ DBA \qquad \text{(Eq. 2-1)}$$

Figure 2-2 shows the contour figure of 5 kDa pNAND copolymers, which depicts the linear relationship between LCST, AAm, and DBA.

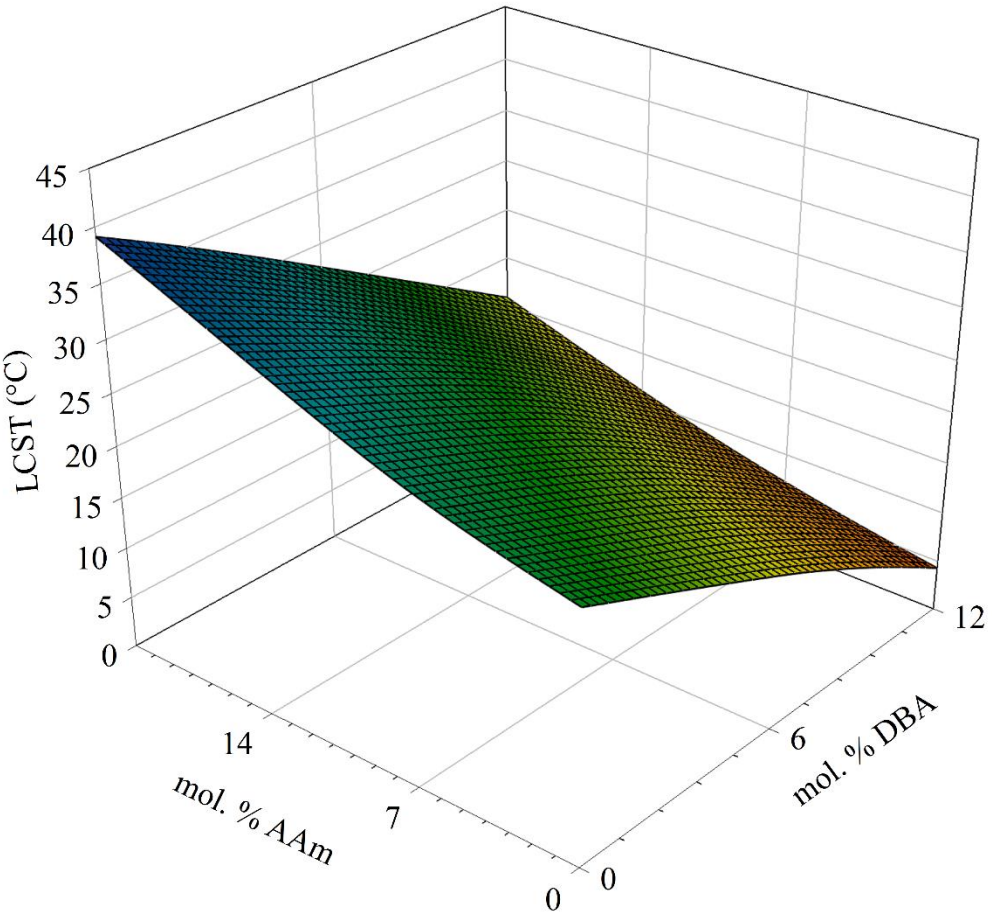

Figure 2 - 2. LCST contour map of 5 kDa pNAND copolymers showing the effect of AAm and DBA.

Using the LCST linear regression, three additional materials were synthesized. The LCST of these pNAND-13/8-5, 17/6-5, and 21/4-5 polymers in PBS was determined using DSC and compared to the theoretical values, which are shown in Table 2-2. It can be seen that the LCST values determined from DSC were similar, but slightly higher than the theoretical LCSTs.

Table 2 - 2. LCST of 5kDa pNAND copolymers compared to the theoretical model.

Copolymer	LCST ± SD (DSC, PBS pH 7.4)	Theoretical LCST
pNAND-13/8-5	22.1 ± 0.4 °C	18.6 °C
pNAND-17/6-5	26.0 ± 0.3 °C	24.8 °C
pNAND-21/4-5	32.1 ± 0.6 °C	31.0 °C

Next, we synthesized pNAND copolymers with the same composition, but with target molecular weights of 30 kDa. The LCST of these copolymers are shown in Table 2-3. Surprisingly, the LCST of these materials were similar to the LCST of copolymers with 2 mol. % less DBA and 4 mol. % more acrylamide. Further explanation and statistical analysis is shown in Chapter 3. The 5 and 30 kDa copolymers were then used for subsequent characterization and drug release studies shown in Chapter 3.

Table 2 - 3. LCST of 30 kDa pNAND copolymers.

Copolymer	LCST ± SD (DSC, PBS pH 7.4)
pNAND-13/8-30	27.2 ± 0.1 °C
pNAND-17/6-30	32.5 ± 0.6 °C
pNAND-21/4-30	37.2 ± 0.8 °C

2.3. Conclusions

We were able to synthesize a series of pNAND copolymers with molecular weights of approximately 5.5 kDa and 30 kDa. Based on the LCST determined using DSC we were able to construct a linear regression that predicted the LCST of 5 kDa copolymers with varying AAm and DBA compositions. It was also found that LCST increased proportionally with increased molecular weight. This data was then used for subsequent characterization and drug release studies discussed in Chapter 3.

3. Chapter 3: Tunable release of ophthalmic therapeutics from injectable, resorbable, thermoresponsive copolymer scaffolds

Authors: Graeme Prosperi-Porta, Benjamin Muirhead, Heather Sheardown
Publication Information: In review for publication in the Journal of Biomedical Materials Research: Part B

Objectives: To develop injectable, resorbable, and thermoresponsive copolymer scaffolds that are capable of prolonging the release of dexamethasone intravitreal injections to reduce the required frequency of therapeutic application.

Main Scientific Contributions:

- Developed a highly controlled method to polymerize NIPAAm, AAm, NAS, DBA copolymers
- Showed that LCST, WC and GE could be altered by copolymer composition and molecular weight
- Developed variable release rates of Dexamethasone based on composition and molecular weight

Abstract

The sustained release of ophthalmic therapeutics to the posterior segment of the eye is a challenge. Injectable polymer materials have the potential to reduce injection frequency by providing long term therapeutic delivery. Copolymers with varying N-isopropylacrylamide, acrylamide (AAm), acrylic acid N-hydroxysuccinimide (NAS), and (r)-α-acryloyloxy-β,β-dimethyl-γ-butyrolactone (DBA) were synthesized by RAFT polymerization to develop injectable, resorbable, and thermoresponsive copolymer scaffolds. Upon injection into physiological conditions, these copolymers undergo a temperature induced gelation to form a drug releasing scaffold. Modification of the copolymer's AAm/DBA ratio and molecular weight afforded significant and precise control over the scaffold's physical properties and subsequent drug release profile. Hydrolytic DBA ring-opening enables re-dissolution of the copolymers for clearance from the body. Precise control over the drug release profile from these copolymer scaffolds by simple alteration of composition and molecular weight provides an efficient method to customize the minimally invasive delivery of therapeutics to the posterior segment of the eye.

3.1. Introduction

The sustained delivery of ophthalmic therapeutics to the posterior segment of the eye remains one of the most unmet challenges in ophthalmology. It has been previously targeted by systemic, topical, periocular, and intravitreal routes, but each method has its unique limitations [1]. Systemic delivery is inefficient due to the blood-aqueous and blood-retinal barriers that separate ocular tissues from circulation [1–3]. Typically only 1-2% of the dose reaches the ocular tissues, requiring large and frequent doses, that can result in systemic toxicity and side effects [4,5]. Effective precorneal clearance mechanisms including blinking, rapid tear turnover [6], and nasolacrimal drainage result in less than 5% of topically administered drug reaching the anterior ocular tissues and even less reaching the posterior segment [1,3,7]. Periocular delivery is hindered by diffusion across the sclera, choroid, and retinal pigment epithelium, lymphatic flow in the conjunctiva and episclera [8], and circulation in the conjunctiva and choroid [9,10]. Intravitreal injections (IVI) are a highly effective means to deliver therapeutics targeted at the vitreous and retinal tissues, which minimize unintended systemic exposure [1]. Unfortunately, traditional IVIs require frequent injections to maintain therapeutic levels, which reduce patient compliance and increase the risk of complications such as retinal detachment, endophalmitis, lens opacification, and intraocular pressure elevation [11,12].

Currently four ocular implants are FDA approved to provide sustained release over months to years. Vitrasert® [1,13] and Retisert® [14,15], both non-biodegradable polymer implants, release ganciclovir for up to eight months and fluocinolone acetonide for up to 2.5 years respectively. Unfortunately, these implants are highly invasive as they are sutured to the sclera and require surgical insertion and removal or replacement [16]. Ozurdex® [17,18], a biodegradable implant releasing dexamethasone (Dex) for up to six months, and Iluvien® [18,19], a non-biodegradable implant

releasing fluocinolone acetonide for up to three years are injectable through 22- and 25-gauge needles respectively. Although these injectable vitreal implants offer a reduction in invasiveness, Stefano et al. showed increasing needle gauge can reduce ocular damage that causes IVI complications [20]. Therefore, the optimal IVI is a resorbable material capable of injection through a $\geq$ 30 gauge needle to provide sustained therapeutic release [21,22].

Diabetic retinopathy (DB), a retinal vascular disease, is a leading cause of blindness in the United States [23]. Vision loss can be caused by neovascularization leading to vitreal hemorrhage, retinal detachment, and macular edema. Corticosteroids, such as Dex and triamcinolone acetonide (TA), are believed to combat DB by reducing inflammation and inhibiting the release of angiogenic growth factors such as vascular endothelial growth factor from macrophages [24]. Dex has been shown to be less toxic than TA to retinal and lens epithelial cell culture, which may be beneficial in applications where prolonged exposure is required [25,26].

To meet the demand of improved IVIs the Sheardown group has previously developed poly(N-isopropylacrylamide) (pNIPAAm) based copolymers capable of in situ gelation upon injection into the vitreous for the sustained release of Dex [27]. pNIPAAm is a thermoresponsive polymer that undergoes a rapid transition from liquid to hydrogel phase upon heating above its lower critical solution temperature (LCST) of ~32°C [28,29]. Previous work developing NIPAAm copolymers achieved sustained delivery of Dex, but the release characteristics were not controllable. NIPAAm copolymerization with other functional monomers has been previously shown to introduce degradability, biological functionality, and modification of the LCST. Copolymerization of NIPAAm with (r)-α-Acryloyloxy-β,β-dimethyl-γ-butyrolactone (DBA) has been shown to introduce resorbable properties through hydrolytic ring opening of DBA, which raises the LCST above physiological temperature allowing the polymer to re-dissolve and be

cleared from the body through [30]. Acrylic acid N-hydroxysuccinimide ester (NAS), a functional monomer capable of conjugating amine functional groups, was utilized to increase the versatility of these copolymers. Although not discussed, NAS allows for the downstream conjugation of biological moieties such as cells and/or drugs for increased versatility of therapeutic delivery. Fitzpatrick et al. used NAS grafted RGDS peptide sequences to promote cell adhesion in NIPAAm copolymers [31].

Reversible addition-fragmentation chain-transfer (RAFT) polymerization is a versatile method used to copolymerize a wide range of monomer types while retaining high control over molecular weight and polydispersity index (PDI) [32]. Trithiocarbonyl chain transfer agents such as 2-(dodecylthiocarbonothioylthio)-2-methylpropionic acid (DDMAT) are used to obtain control over the polymerization. Control over molecular weight by adjusting the monomer to chain transfer ratio gives an additional parameter that can be exploited to control the properties of these copolymer scaffolds.

3.2. Materials and Methods

3.2.1. Materials

Unless otherwise stated, all materials were purchased from Sigma Aldrich (Oakville, ON, Canada). N-isopropylacrylamide was purified by recrystallization from 40:60 toluene:hexane before use. AIBN was recrystallized in methanol before use. All solvents were purchased from Caledon Laboratories (Caledon, ON). $(CD_3)_2SO$ was purchased from Cambridge Isotope Laboratories Inc. (Andover, MA, USA). 1.0 M sodium hydroxide was purchased from LabChem Inc. (Pittsburgh, PA, USA) and diluted with purified water. Purified water with a resistivity of 18.2 MΩ cm was prepared using a Milli-pore Barnstead water purification system (Graham, NC, USA). Phosphate buffered saline (PBS) was purchased from BioShop (Burlington, ON, Canada).

Cellulose dialysis membranes with a molecular weight cut-off (MWCO) value of 3.5 kDa was purchased from Spectrum Laboratories Inc. (Rancho Dominguez, CA, USA). 3-[4,5-dimethylthiazol-2-yl]-2,5-diphenyl-tetrazolium bromide (MTT), calcein AM, and ethidium homodimer-1 were purchased from Life Technologies (Carlsbad, CA, USA).

3.2.2. Synthesis of poly(NIPAAm-AAm-NAS-DBA) copolymers

Poly(NIPAAm-AAm-NAS-DBA) (pNAND) copolymers were synthesize by RAFT polymerization. In a typical reaction procedure (72:17:5:6:2 molar feed ratio of NIPAAm:AAm:NAS:DBA:DDMAT), NIPAAm (2.095 g, 18.51 mmol), AAm (0.311 g, 4.37 mmol), NAS (0.218 g, 1.29 mmol), DBA (0.284 g, 1.54 mmol), DDMAT (0.186 g, 0.53 mmol), and AIBN (4.1 mg, 0.025 mmol) were dissolved in 12 mL of 1,4-dioxane and added to a 25 mL round bottom flask. The solution was degassed by performing three freeze-pump-thaw cycles followed by replacement of the atmosphere with nitrogen. The flask was then heated at 70°C for 24 hours while stirring. This copolymer, denoted 17/6-5 (AAm/DBA-MW) was isolated and purified by precipitation into 10 times excess of cold anhydrous diethyl ether three times. The copolymer was dried under vacuum at 50°C for 48 hours. Higher molecular weight copolymers were produced by reducing the amount of DDMAT relative to the monomers added.

3.2.3. Material Characterization

Proton nuclear magnetic resonance (^{1}H NMR, Bruker AV 600) was used to determine copolymer composition, structure, and molecular weight based on monomer conversion. Fourier transform infrared spectrometry (FT-IR, Thermo Fisher Nicolet 6700) was used to determine pNAND copolymer composition and structure. Gel permeation chromatography (GPC) was used to determine copolymer molecular weight and polydispersity using a Waters system composed of a 590 HPLC pump, three Styragel columns (HR2, HR3, HR4), and a 410 refractive index detector.

10 mg mL^{-1} samples were eluted in N,N-dimethylformamide containing 50 mM LiBr at a flow rate of 0.5 mL min^{-1}, and the system was calibrated using narrow dispersed polyethylene glycol (PEG) standards.

3.2.4. Lower Critical Solution Temperature

Differential scanning calorimetry (DSC, TA Instruments Q20) and UV-visible spectrophotometry (UV-Vis, Cary Bio 100) were used to determine the copolymer LCST. For DSC, 15 μL of copolymer dissolved in 0.1 M PBS at 20 wt.% was heated from 0 to 50°C at a rate of 2°C min^{-1} in aluminum hermetic pans. The minimum value of the endothermic peak in the DSC curve was considered to be the copolymer LCST. For UV-Vis, copolymers were dissolved in 0.1 M PBS at 5 wt.%, 2 mL was placed in polystyrene cuvettes, and heated from 5 to 50°C at a rate of 2°C min^{-1}. The transmittance was measured at 500 nm in 30 second intervals.

3.2.5. Equilibrium Water Content and Gelation Equilibrium

pNAND copolymer equilibrium water content (EWC) and gelation equilibrium (GE) were determined gravimetrically. Briefly, 100 mg of copolymer was dissolved in 0.1 M PBS at 20 wt.% in glass vials and incubated at 37°C for 6 hours to drive scaffold formation. The supernatant surrounding the hydrogel was then discarded, and the gels were gently dabbed dry to remove any non-gelled polymer solution. The mass of the hydrated hydrogel (m_w) was determined prior to drying at 70°C to determine the dry hydrogel mass (m_d). EWC and GE were calculated by Equation 1 and 2 respectively. The GE represents the percent of copolymer that formed a gel scaffold upon gelation.

$$EWC = \frac{m_w - m_d}{m_d} \cdot 100\% \quad (1)$$

$$GE = \frac{m_d}{m_i} \cdot 100\% \quad (2)$$

Where m_w, m_d and m_i are the masses of the wet, dry, and initial copolymer respectively.

3.2.6. Accelerated Copolymer Degradation

To elucidate the degradation process in a timely manner, accelerated hydrolysis was performed in basic medium at elevated temperature. Briefly, 600 mg of copolymer was dissolved at 20 wt.% in purified water, the pH was adjusted to 10.0 using 1M NaOH, and then heated to 70°C (Fisher Isotemp 200 Series). The pH was adjusted daily to 10.0 using either 1.0 M or 0.1 M NaOH. Samples were removed at days 2, 7, and 14 or when the pH had stabilized at 10.0 for 3 days, whichever occurred first. The partially and fully degraded copolymers were dialysed against purified water and freeze dried before further characterization or use.

3.2.7. Copolymer Degradation in PBS

Real time copolymer degradation was assessed gravimetrically. 100 mg of copolymer was dissolved in 0.1 M PBS at 20 wt.% and incubated at 37°C. After 10, 30, 60, and 120 days the non-gelled solution was aspirated, the copolymers were dabbed to remove any residual copolymer solution and were dried in a 70°C oven to determine the dry mass (m_d). The % mass remaining was determined using Equation 3:

$$\% \text{ Mass Remaining} = \frac{m_d}{m_i} \bullet 100\% \qquad (3)$$

3.2.8. Drug Entrapment and Release

High performance liquid chromatography (HPLC) was used to measure Dex release from copolymer scaffolds following a previously defined method [27]. Briefly, 100 mg of copolymer was dissolved at 20 wt.% in a 0.1 mg mL^{-1} Dex solution in 0.1 M PBS overnight at 4°C. After two hours of incubation at 37°C, the non-gelled solution was removed to determine % entrapment efficiency (EE) and replaced with 2 mL of fresh 37°C 0.1 M PBS. At specified time points, 0.5 mL samples were removed and replaced with 0.5 mL of fresh 37°C 0.1 M PBS. Samples were analyzed using a Waters HPLC consisting of a 2707 auto sampler, 2489 UV spectrophotometer,

and 1525 binary HPLC pump. A 1 mL min^{-1} isocratic flow rate of 60:40 (v/v) acetonitrile:water, a 10 µL sample injection volume, and a 254 nm detection wavelength were used for analysis. Sample concentrations were determined based on a standard calibration curve of Dex in 60:40 (v/v) acetonitrile:water.

3.2.9. In Vitro Cell Viability

To eliminate sources of contamination, copolymers were dialysed (3.5 kDa MWCO) against purified water, lyophilized, and sterilized by gamma irradiation (3.41 Mrads, 20.5 hours) at the McMaster Nuclear Reactor. Copolymer stability during gamma irradiation was assessed by ^{1}H NMR. Retinal pigment epithelial cells (RPE-19) cells were cultured in a temperature-controlled CO_2 incubator (37°C, 5 % CO_2, 95 % air, 100 % humidity). Dulbecco's modified Eagle's medium without F12 was supplemented with fetal bovine serum (9% final) and penicillin-streptomycin (1% final). RPE-19 cells were seeded in 24 well polystyrene tissue culture plates with DMEM cell culture medium (50 000 cells $well^{-1}$). After allowing the cells to adhere to the bottom of the wells for 2 hours, the cell culture medium was replaced with 700 µL of test media. Test media for the intact copolymers consisted of 700 µL of DMEM medium followed by the addition of 50 µL of 20 wt.% copolymer solution in media injected into a cell culture insert (8 µm pore size). The day 2 and day 14 hydrolyzed test media consisted of 50 µL of 20 wt.% copolymer in media added to 700 µL of DMEM medium. Control samples consisted of 750 µL of supplemented DMEM medium. For all tests performed an n of 6 was used. Samples were incubated and viability was assessed after 90 hours using an MTT assay. Live/dead cell counts were determined by a calcein AM/ethidium homodimer-1 assay. % viability and morbidity for test samples were determined based on the ratio of intensity compared to control wells.

3.3.Statistical Analysis

A one-factor analysis of variance (ANOVA) was used to analyze the copolymer LCST, water content, gelation equilibrium and RPE-19 viability using a 95% level of confidence. Tukey or Games-Howell post hoc testing was performed for equal and unequal variances respectively. Statistical analysis was performed using IBM SPSS Statistics V22.0 statistical software (IBM Corp, Armonk, NY, USA). All error bars represent standard deviation.

3.4. Results

3.5. Copolymer Characterization

Copolymers were synthesized by RAFT polymerization to produce varying pNAND compositions and molecular weights. Table 3-1 summarizes polymerization feed ratios, yields, copolymer compositions, and molecular weights of each pNAND copolymer. ^{1}H NMR data shows final compositions and molecular weights that are consistent with reactant feed ratios.

Table 3 - 1. Copolymer feed ratios, polymerization yields, final copolymer compositions, and copolymer molecular weight determined by NMR and GPC.

Copolymer Feed Ratio (NIPAAm:NAS:AAm:DBA:DDMAT)	% Yield	Composition[a]	MW (Da)[a]	MW (Da)[b]	PDI[b]
13/8-5 (74:5:13:8:2)	95.0	76.6:4.1:12.0:8.5	5484	2797	1.1
17/6-5 (72:5:17:6:2)	97.0	75.3:4.1:16.4:6.6	5387	2730	1.1
21/4-5 (70:5:21:4:2)	96.6	73.0:4.0:22.8:4.4	5600	2650	1.2
9/10-30 (76:5:9:10:0.375)	89.1	76.7:4.1:10.3:9.9	27764	13449	1.4
13/8-30 (74:5:13:8:0.375)	91.0	76.4:2.8:14.2:8.5	28875	12199	1.4
17/6-30 (72:5:17:6:0.375)	91.7	75.0:3.3:18.4:6.1	27401	11757	1.5

[a] Copolymer composition in mol. % and M_n determined by ^{1}H NMR.
[b] M_n and PDI obtained using gel permeation chromatography (GPC).

3.6. pNAND Lower Critical Solution Temperature

The LCST of pNAND copolymers, assessed by DSC, are shown in Figure 1a. All copolymers showed sub-physiological gelation temperatures required for in vivo applications. Upon injection of 20 wt.% copolymer solutions in PBS from a 30G needle into 37°C PBS, copolymers undergo rapid gelation (white strands in Figure 1b) followed by coalescence of the

copolymer strands to form a hydrogel scaffold (white solid in Figure 1c) that conforms to the bottom of the container. Both the 5 and 30 kDa copolymers were easily injected from 30G needles. UV transmittance verified this rapid gelation process and strongly supported DSC results (Figure S1). Interestingly, the copolymer LCST was found to be linearly dependent on the AAm/DBA ratio in the copolymer (Figure S2), and dependent on molecular weight.

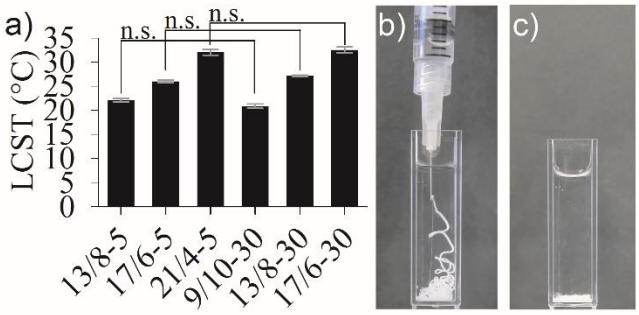

Figure 3 - 1. A) Copolymer LCST measured by DSC, B) rapid gelation following injection of 20 wt.% 13/8-30 from 30G needle into 37°C PBS, and C) 5 minutes post injection at 37°C. n.s. = not significant ($p \geq 0.05$). All other comparisons were significantly different (all had $p \leq 0.001$). The white copolymer ejected from the needle tip in B shows rapid gelation followed by fast coalescence of polymer strands to form a scaffold that conforms to the lowest point of the container in C.

3.7. Equilibrium Water Content and Gelation Equilibrium

The EWC and GE of the pNAND copolymers were assessed gravimetrically and both found to be dependent on their AAm/DBA ratio. Copolymers with higher AAm/DBA ratios are more hydrophilic, resulting in higher water contents. Figure 2a shows that the 30 kDa copolymers have a higher EWC than 5 kDa copolymers with the same LCST, although it is only significant for copolymers with an LCST of ~26 and 32°C ($p \leq 0.05$ and $p \leq 0.001$ respectively).

GE, shown in Figure 2b, is an important parameter in the drug release from pNAND materials because it measures the total percentage of copolymer that forms a drug releasing hydrogel scaffold upon gelation. Similar to EWC, copolymers with higher AAm/DBA ratios had lower gelation equilibria. Although copolymer MW was not found to influence GE (all had $p \geq 0.05$), composition was found to significantly influence GE (all had $p \leq 0.001$).

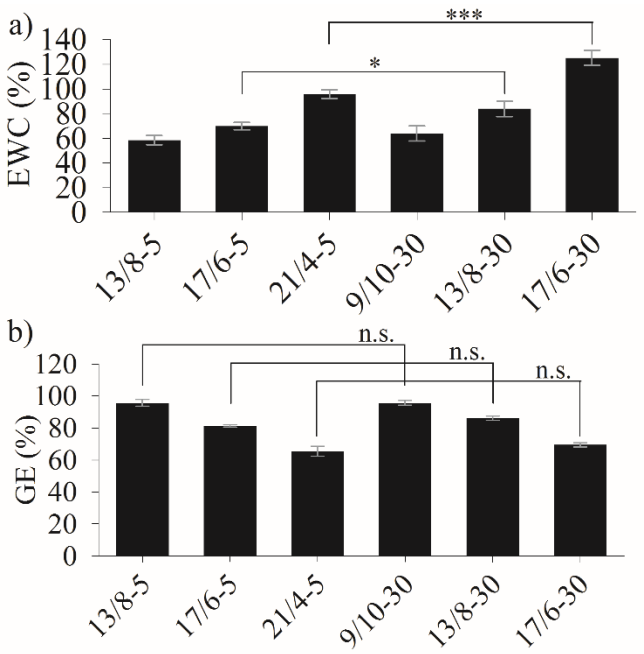

Figure 3 - 2. a) EWC of pNAND copolymers. All 30 kDa copolymers had significantly different EWC (all had p≤0.01) while only the 21/4-5 copolymer was significantly different from the other 5 kDa copolymers (p≤0.001). b) GE of pNAND copolymers. All copolymers with equal MW showed significant differences in GE (all had p≤0.001). * = p≤0.05, ***p≤0.001, n.s. = not significant (p≥0.05).

3.8. pNAND Accelerated Degradation Mechanism

FTIR and NMR spectroscopy were used to determine the copolymer structure during the degradation process (Figure 3). Intact 13/8-30 FTIR (Figure 4a) showed characteristic NIPAAm and AAm C=O stretching, N-H bending, and N-H stretching peaks of the amide group at 1652, 1540 cm^{-1}, and 3400 cm^{-1} respectively. Characteristic C-H bending from the NIPAAm isopropyl and DBA CH_3 group are seen at 1457, 1387, and 1367 cm^{-1}. DBA carbonyl stretching peaks belonging to the ring C=O and the copolymer backbone C=O can be seen at 1786 and 1740 cm^{-1} respectively. NAS exhibits an ester carbonyl peak as a shoulder at approximately 1810 cm^{-1}, and ring carbonyl peaks overlapping with the DBA peaks at 1786 and 1740 cm^{-1}.

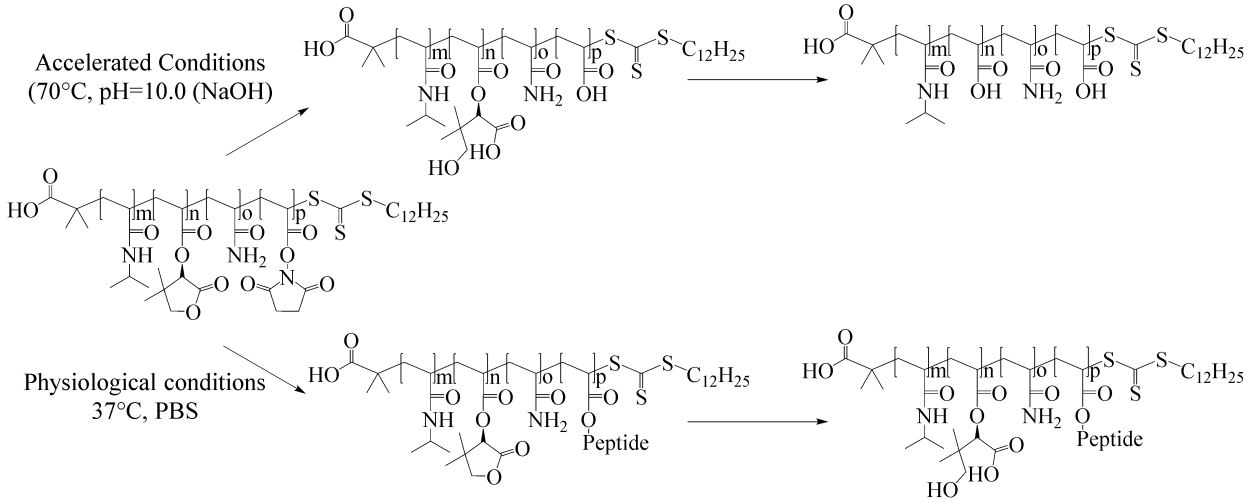

Figure 3 - 3. Degradation mechanism of the pNAND copolymers under accelerated conditions (top), and proposed degradation mechanism under physiological conditions (bottom). The physiological degradation schematic shows NAS coupling to a peptide, which is believed to protect it from full hydrolysis into poly(acrylic acid).

The accelerated hydrolysis process subjected pNAND copolymers to a pH of 10.0 and temperature of 70°C. The largest pH decreases of approximately 2 to 3.5 units were observed in the first three days followed by gradual reduction until stabilization was reached after 14 days. Partially degraded 13/8-30 after two days of degradation (Figure 4b) shows a reduction in NAS and DBA ring C=O stretching peaks at 1786 and 1740 cm^{-1}, and an increase in the broad acrylic acid (AA) O-H stretching peak at approximately 3300 cm^{-1} can be seen. Fully degraded 13/8-30 copolymer after 14 days of hydrolysis (Figure 4c) shows the complete disappearance of ring C=O stretching of DBA and NAS, and a shoulder at approximately 1710 cm^{-1} belonging to the C=O stretching of AA has appeared.

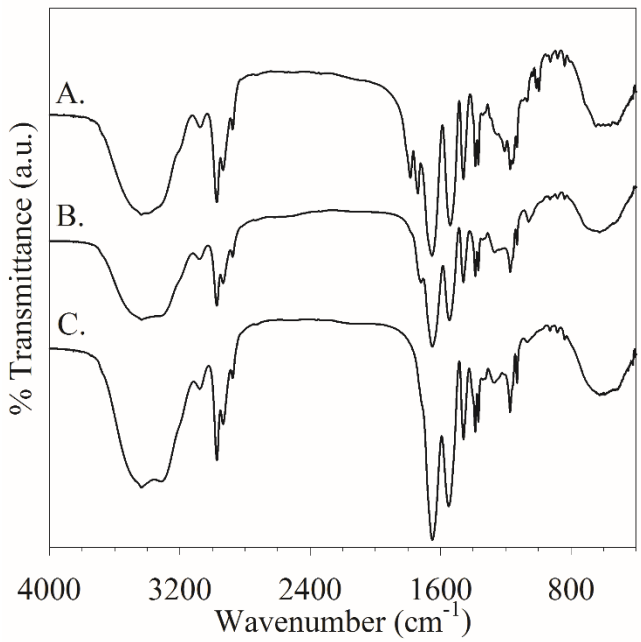

Figure 3 - 4. FT-IR spectra of A) intact, B) 2 day partial hydrolysis, and C) 14 day complete hydrolysis 13/8-30 copolymer. All copolymers showed similar FT-IR degradation spectra.

To further identify the proposed degradation mechanism determined by FTIR, ^{1}H NMR was performed on intact and degraded materials. The intact 13/8-30 copolymer spectrum (Figure 5a) shows a NIPAAm isopropyl CH peak at 3.7-4.0 ppm, DBA CH_2 and CH peaks at 4.0-4.3 and 5.4-5.7 ppm respectively, an NAS CH_2 peak at 2.7-3.0 ppm, and DDMAT CH_3 and CH_2 peaks at 0.83-0.87 and 1.22-1.25 ppm respectively. After 2 days of harsh degradation conditions (Figure 5b) the magnitude of DBA CH_2 and CH peaks have decreased and shifted upfield to 3.1-3.4 and 4.4-4.8 ppm respectively. It can also be seen that the CH_3 peak of the DBA undergoes an upfield shift to 0.75-0.95 ppm. The disappearance of the NAS peak from the spectra after 2 days is consistent with FTIR results, and is due to its high hydrolytic activity under harsh basic conditions, which quickly converts the NAS to AA. The fully degraded copolymer (Figure 5c) shows the absence of all DBA and NAS peaks, which suggests these have been completely removed to produce AA subunits. It should also be noted that characteristic CH_2 peaks of DDMAT remain intact throughout all stages of accelerated degradation.

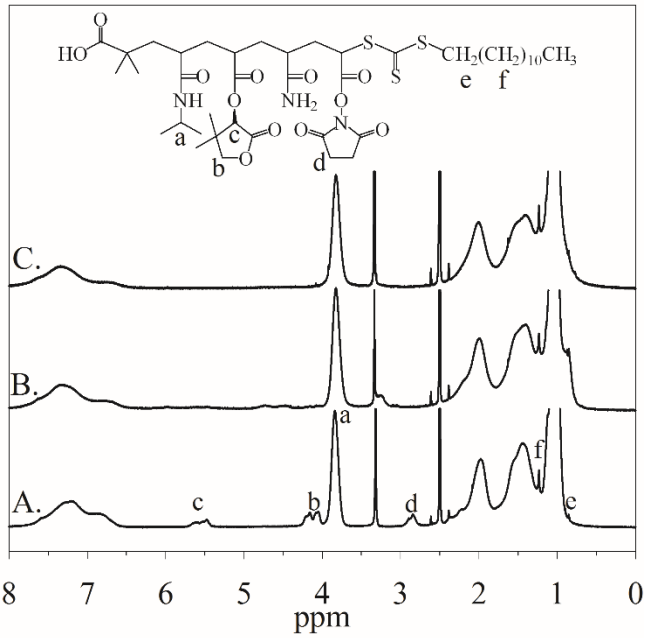

Figure 3 - 5. ^{1}H NMR [$(CD_3)_2SO$, 600 MHz] spectra of A) intact 13/8-30, B) 2 day partially degraded 13/8-30, and C) fully degraded 13/8-30. DMSO-d6 solvent for all NMR spectra. All copolymers showed similar ^{1}H NMR degradation spectra.

Following partial and complete degradation, no LCST was observed below 50°C compared to the intact copolymer (Figure 6), showing that DBA ring opening is sufficient to increase the LCST above physiological temperature for clearance from the body.

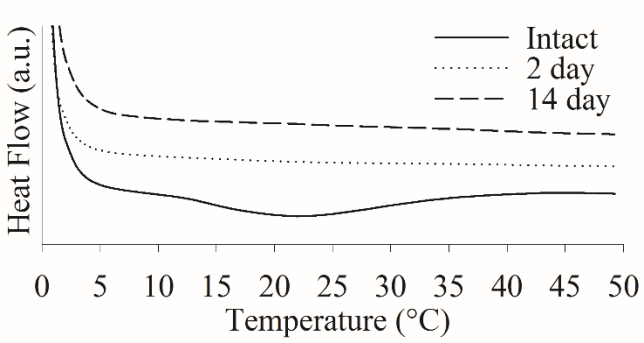

Figure 3 - 6. DSC spectra of intact, 2 day partially hydrolyzed, and completely hydrolyzed 13/8-5 copolymers after accelerated degradation.

3.9.Copolymer Degradation in heated PBS

In vitro copolymer degradation was assessed by incubating copolymer in PBS at 20 wt.%. After 10, 30, and 60 days of incubation at 37°C the supernatant containing hydrolyzed copolymer was discarded, and the remaining gel was used to determine % mass remaining. Depending on

molecular weight and composition, copolymers showed mass losses of approximately 4-12% over 120 days (Figure 7). Molecular weight was not shown to affect the degradation rate in this closed system (all time points had $p \geq 0.05$).

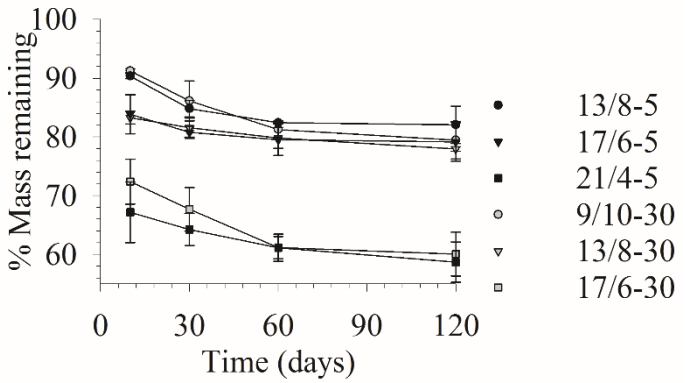

Figure 3 - 7. Copolymer degradation in PBS at 37°C assessed gravimetrically.

3.10. Dexamethasone Release

In this study 100 mg of each copolymer scaffold was dissolved in 0.5 mL of PBS containing 50 µg of Dex. Encapsulation efficiency (EE) is an important parameter for injectable drug delivery systems because it describes the % of loaded drug that becomes entrapped in the material after injection. Figure 8 shows that the EE of pNAND copolymers is related to both composition and molecular weight. Copolymers with LCSTs of approximately 22 and 26°C, but different MWs show significant differences in EE ($p \leq 0.01$ and $p \leq 0.05$ respectively). Copolymers with equal molecular weight but increasing AAm/DBA ratios showed decreasing EE.

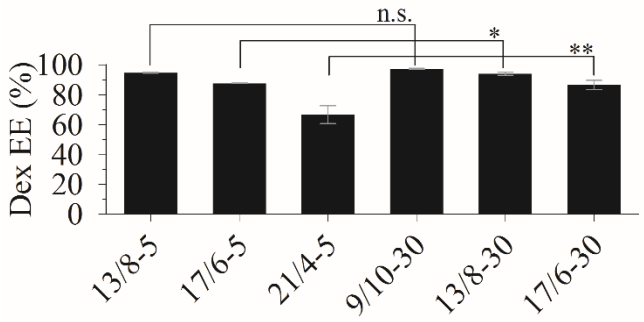

Figure 3 - 8. Copolymer burst release of Dex after gelation. Copolymers with equal molecular weight show a trend of decreasing EE with increasing AAm/DBA ratio. *= $p \leq 0.05$, **= $p \leq 0.01$.

Figure 9 shows the cumulative Dex release from various pNAND copolymer scaffolds. 21/4-5 and 17/6-5 copolymers achieved ~100% release after 5 and 20 days respectively; at these time points it was observed that the copolymer had completely re-dissolved. It can be seen that each copolymer undergoes a biphasic release profile; all characterized by an initial non-linear burst release, which stabilizes after approximately 2 days to provide a sustained release. After 2 days of release, the 17/6-5, 17/6-30, and 13/8-30 copolymers all show a zero-order release of 0.84, 0.51, and 0.48 µg day^{-1}. The 13/8-5 and 9/10-30 copolymers show a similar sustained release of Dex after the initial burst phase, but have slightly non-linear release profiles releasing an average of 0.25 and 0.31 µg day^{-1} respectively.

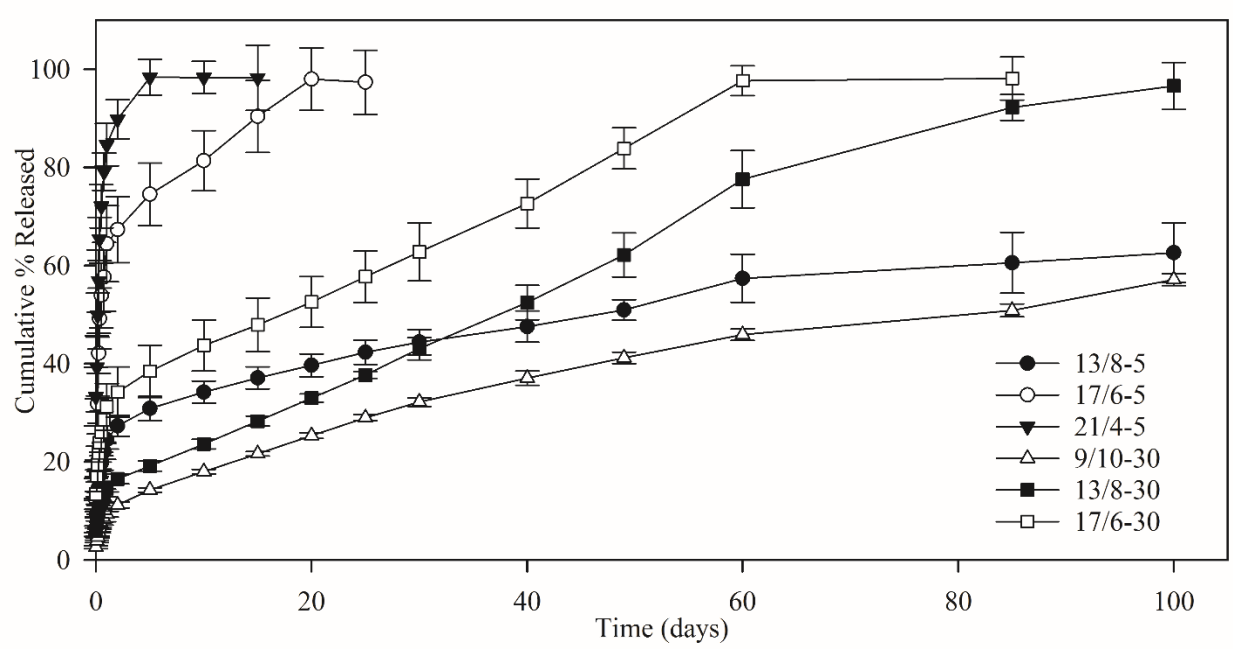

Figure 3 - 9. Dex cumulative % release curves from various pNAND copolymers in PBS at 37°C.

3.10.1. In Vitro Cell Viability

In vitro cell viability determined by the MTT and Calcein/Ethidium assays are shown in Figure 10a and 10b-d respectively. Copolymers did not show any change in structure after gamma sterilization determined by ^{1}H NMR (Figure S3). Both assays show high RPE viability for intact and degraded copolymers. Although insignificant (all had $p \geq 0.05$), it appears that the degraded copolymers have slightly lower viability than the intact copolymer.

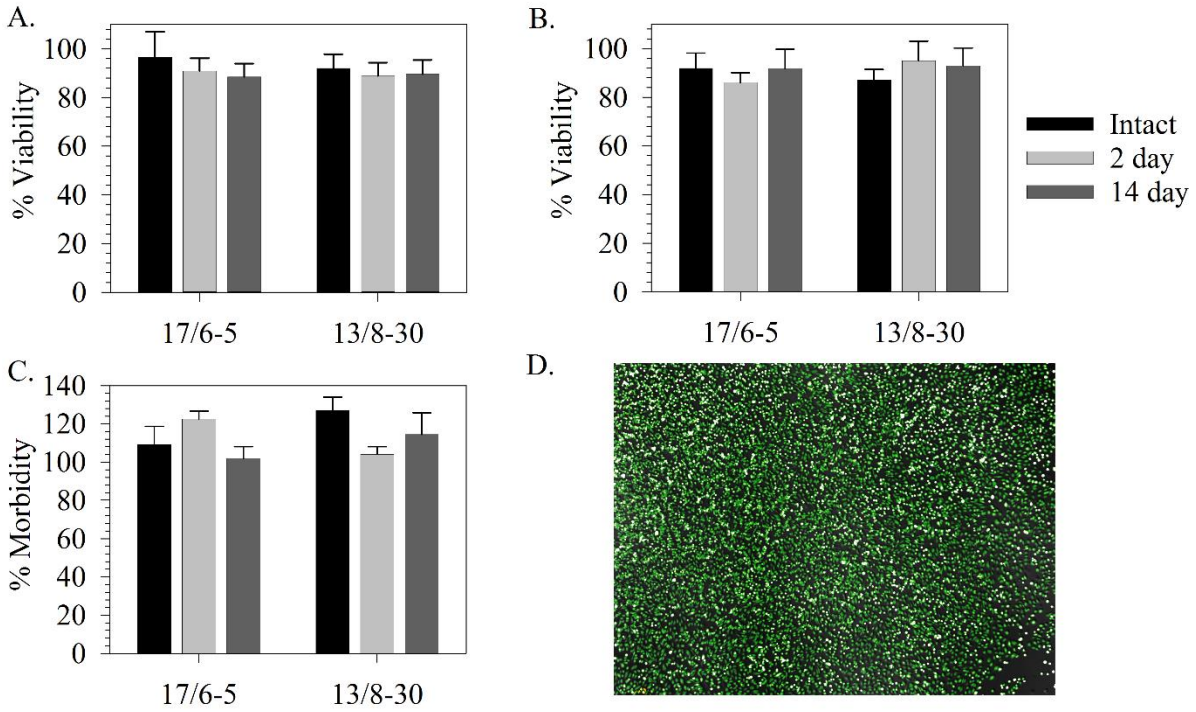

Figure 3 - 10. Cell viability results showing excellent RPE-19 cell viability. A) MTT assay, B) Calcein AM assay, C) Ethidium bromide assay, d) Live dead cell staining (live=green, dead=red).

3.11. Discussion

3.11.1. Copolymer Chemical and Physical Properties

Copolymer synthesis data (Table 1) showed the DDMAT RAFT agent's ability to tightly control copolymer composition and molecular weight in this system. Although GPC analysis determined molecular weights that are ~60% of theoretical values, this was due to calibration with PEG standards and does not affect analysis. GPC results showed a slight increase in PDI at higher

molecular weights, which can be expected in RAFT polymerization [33], but is still well controlled for the purpose of this study. Molecular weight is a vital property for resorbable polymers to ensure clearance from the kidney, which has a threshold of approximately 30-50 kDa for soluble polymers depending on size, shape, conformation, and flexibility [34].

The linear relationship between LCST and composition (Figure S1) provides a simple method to target an LCST for a particular drug delivery application. Molecular weight was also shown to significantly influence copolymer LCST (Figure 1). It was consistently found that that copolymers with a MW of 5 kDa had the same LCST as 30 kDa copolymers containing 4 mol. % less AAm and 2 mol. % greater DBA. Xia et al. also showed that increasing the molecular weight of pNIPAAm polymers resulted in an increase in LCST [28]. All copolymers were observed to undergo rapid gelation (Figure 1b), which is beneficial for drug entrapment because it hinders immediate drug diffusion out of the liquid copolymer phase. Although these materials are seen to be initially opaque (Figure 1b,1c), it was observed during drug release studies that both the 17/6-30 and 13/8-30 copolymers become visually transparent after approximately 20 and 25 days respectively. This is desirable to reduce vision obstruction caused by copolymer migration. This transition is likely due to hydrolysis that occurs in the DBA rich hydrophobic phases, which increases water content to produce a more homogenous hydrogel. The low initial transparency of these copolymers will not hinder vision because these scaffolds conform to the lowest point of their container after injection. This suggests that they will spread on the floor of the vitreous outside of the eye's visual axis.

Copolymer composition and molecular weight are important properties that have been shown to affect water content, drug entrapment efficiency, and release rates in other controlled

release systems [35]. The precise control over composition and molecular weight in this system provides a method for tuning final drug delivery properties from these hydrogels.

3.11.2. Degradation Mechanism

The copolymer degradation in PBS is thought to measure the DBA ring opening process because in this closed system losses due to gelation equilibrium are negligible between copolymers of the same LCST. Although copolymers with the same LCST did not have significantly different degradation in PBS at any time point (Figure 7), it is believed that the copolymers with higher water content would have a faster degradation due to increased accessibility of water to the DBA subunits for hydrolysis.

Under the accelerated conditions it was observed that NAS and DBA functional groups were completely hydrolyzed to form AA. The DDMAT functional groups were intact during all stages of accelerated hydrolysis (Figure 5), which suggests that these components will remain intact under physiological conditions. It is not believed that pNAND copolymers would undergo the same degree of hydrolysis under physiological conditions. As shown in Scheme 1, under physiological conditions DBA would undergo ring opening, but would not subsequently cleave to form AA. NAS conjugation to peptides or other biological moieties would form stable amide bonds preventing complete hydrolysis. However, NAS conjugation to biological molecules would alter the physical properties of the copolymer including LCST, water content, MW, and drug release kinetics, which would need to be further studied. It is not expected that DBA ring opening would produce harmful degradation products in vivo, but could alter the pH during the degradation process. DBA ring opening is believed reduce the hydrophobicity of the copolymer by introducing carboxylic acid and hydroxyl functional groups raising the LCST of the pNAND copolymer [30]. Once the LCST increases above physiological temperature the copolymer will re-dissolve whereby

it can be cleared from the vitreous and excreted from the body. Hyaluronic acid with molecular weights ranging from 18 kDa up to 500 kDa were shown to be readily cleared from the vitreous, which suggests that upon degradation of our 5-30 kDa pNAND copolymers clearance will occur [36].

3.11.3. Drug Delivery

The pNAND copolymer's AAm/DBA ratio and molecular weight were both shown to influence the EE (Figure 8). A lower AAm/DBA ratio increases the hydrophobicity of the copolymer, which affects EE in two ways: it increases the hydrophobic interactions between the copolymer and Dex and it increases the gelation equilibrium, which increases the amount of copolymer able to entrap Dex in a hydrogel scaffold. Higher molecular weight increases the EE by increasing copolymer entanglement, which hinders diffusion of Dex from the scaffold during the gelation process. Higher molecular weight and increased hydrophobicity have also been shown to increase drug entrapment in other controlled release copolymer systems [37]. Although in some cases a burst release may be undesirable, post-surgical IVI of 0.4 mg Dex has been shown to reduce inflammation and improve surgical outcomes of cataract surgery in eyes with and without glaucoma [38]**.** The initial burst release from these copolymer scaffolds could improve surgical outcomes by treating the initially aggressive post-surgical environment followed by a prolonged release of the therapeutic agent to provide ongoing treatment.

Drug release from non-degradable resorbable copolymer scaffolds occurs through two mechanisms: diffusion and dissolution of copolymers by disentanglement. Based on Fick's laws, diffusion controlled systems are often non-linear due to the variation in flux with time, while dissolution controlled systems can follow zero-order kinetics due to a constant rate of dissolution at the polymer front [37]. The 5 kDa copolymers had a faster Dex release rate than the 30 kDa

copolymers due to an increased rate of copolymer dissolution and faster diffusion caused by less entanglement of the copolymer chains [39]. Copolymers with the same molecular weight show slower Dex release as the AAm/DBA ratio is reduced. This is due to three factors: increased hydrophobic interactions between Dex and the copolymer, reduced EWC, and reduced GE, which determines how much copolymer will transition back into the solution phase during each sampling cycle. It is not expected that the gelation equilibrium will be reached during each sample cycle for the higher molecular weight copolymers due to increased chain entanglement, which slows the dissolution of copolymer from the interface [39]. Laurent et al. showed the vitreal turnover of hyaluronic acid to be 0.45 μg day^{-1} [36], which suggests that the rate of copolymer dissolution and subsequent release could be even slower in vivo. The 13/8-30 and 17/6-30 copolymers both show a zero order release profile while the 9/10-30 copolymer shows a first order release profile. Compared to the 13/8-30 and 17/6-30 copolymers, the lower LCST and EWC, and higher GE of the 9/10-30 copolymer reduces significant copolymer re-dissolution during each sampling cycle, which forces diffusion as the rate-limiting release mechanism.

3.11.4. RPE-19 Cell Viability

To model in vivo conditions, intact copolymers were injected into cell inserts rather than directly into the media, which simulates the indirect contact that pNAND copolymers would have with the posterior layers of the eye. This prevented any unrepresentative physical starvation of cells, but still allowed any dissolved copolymer or by-products to enter into solution through the large pores. Degraded samples were dissolved directly into the DMEM medium as these soluble copolymers are freely soluble to interact with cells in the posterior eye tissues.

The slight reduction in viability for degraded copolymer samples is thought to be due to slight changes in pH rather than toxicity. When the degraded copolymers were initially dissolved

in DMEM medium containing phenol red indicator the solution turned yellow indicating a pH shift below 6.8. Although this solution was diluted with DMEM medium the slightly sub-optimal pH may have inhibited growth in the presence of these copolymers. While the 5 and 30 kDa copolymers show good in vitro RPE-19 cell compatibility, future testing will examine the in vivo biocompatibility of these copolymers.

3.12. Conclusion

We report the well-controlled synthesis of NIPAAm, AAm, NAS, and DBA copolymers by RAFT polymerization with varying composition and molecular weight. These copolymers show highly tunable properties depending on composition and molecular weight that can be targeted to suit a particular drug delivery application. Increasing the AAm/DBA ratio showed increases in LCST, water content, and drug release rates, and showed decreased gelation equilibria and entrapment efficiency. Increased molecular weight showed increases in LCST, water content, and entrapment efficiency, and showed decreased drug release rates, but did not affect gelation equilibria. Degradation of these copolymers was shown to occur through hydrolytic ring opening of DBA, which increases the LCST above physiological temperatures allowing clearance from the body. Good biocompatibility in cell culture with RPE-19 cells shows potential for these materials to be used in vivo, although further testing is required. This study shows a highly controllable method to synthesize injectable, resorbable, thermoresponsive copolymers to provide minimally invasive sustained delivery of corticosteroids. These copolymers show multiple improvements over current commercially available sustained intravitreal therapies: They can be injected from a 30 gauge needle, which reduces the invasiveness of application, they settle to the lowest point in solution, which will prevent visual obstruction and reduce implant migration, and their ability to re-dissolve prevents the accumulation of devices in the vitreous and need for surgical removal.

Future studies will examine the use of the NAS monomer to immobilize biological molecules for delivery of cell therapy and biological molecules to the posterior segment.

3.13. Acknowledgments

The authors would like to thank the Natural Sciences and Engineering Research Council (NSERC), and the 20/20 NSERC Ophthalmic Materials Research Network for funding. We would also like to thank Dr. Nicholas Burke, Dr. Alex Adronov, Stephanie Kedzior, Robert Pasuta, and the staff at the McMaster Biointerfaces Institute for their expertise and equipment.

3.14. References

1. Thrimawithana TR, Young S, Bunt CR, Green C, Alany RG. Drug delivery to the posterior segment of the eye. *Drug Discov Today*. 2011;16(5-6):270-277.
2. Freddo TF. A contemporary concept of the blood-aqueous barrier. *Prog Retin Eye Res*. 2013;32:181-195.
3. Gaudana R, Ananthula HK, Parenky A, Mitra AK. Ocular drug delivery. *AAPS J*. 2010;12(3):348-360.
4. Gaudana R, Jwala J, Boddu SHS, Mitra AK. Recent perspectives in ocular drug delivery. *Pharm Res*. 2009;26(5):1197-1216.
5. Duvvuri S, Majumdar S, Mitra AK. Drug delivery to the retina: challenges and opportunities. *Expert Opin Biol Ther*. 2003;3(1):45-56.
6. Mishima S, Gasset A, Klyce SDJ, Baum JL. Determination of tear volume and tear flow. *Invest Ophthalmol*. 1966;5(3):264-276.
7. Shell JW. Pharmacokinetics of topically applied ophthalmic drugs. *Surv Ophthalmol*. 1982;26(4):207-218.
8. Robinson MR, Lee SS, Kim H, et al. A rabbit model for assessing the ocular barriers to the transscleral delivery of triamcinolone acetonide. *Exp Eye Res*. 2006;82(3):479-487.
9. Kim H, Robinson MR, Lizak MJ, et al. Controlled drug release from an ocular implant: an evaluation using dynamic three-dimensional magnetic resonance imaging. *Invest Ophthalmol Vis Sci*. 2004;45(8):2722-2731.
10. Ranta V-P, Mannermaa E, Lummepuro K, et al. Barrier analysis of periocular drug delivery to the posterior segment. *J Control Release*. 2010;148(1):42-48.
11. Peyman GA, Lad EM, Moshfeghi DM. Intravitreal injection of therapeutic agents. *Retina*. 2009;29(7):875-912.
12. Sampat KM, Garg SJ. Complications of intravitreal injections. *Curr Opin Ophthalmol*. 2010;21(3):178-183.
13. Musch DC, Martin DF, Gordon JF, Davis MD, Kuppermann BD. Treatment of Cytomegalovirus Retinitis with a Sustained-Release Ganciclovir Implant. *N Engl J Med*. 1997;337(2):83-90.

14. Jaffe GJ, Martin D, Callanan D, Pearson PA, Levy B, Comstock T. Fluocinolone Acetonide Implant (Retisert) for Noninfectious Posterior Uveitis: Thirty-Four–Week Results of a Multicenter Randomized Clinical Study. *Ophthalmology*. 2006;113(6):1020-1027.
15. Taban M, Lowder CY, Kaiser PK. Outcome of fluocinolone acetonide implant (Retisert™) reimplantation for chronic noninfectious posterior uveitis. 2007;28(9):2-6.
16. Naveed Yasin M, Svirskis D, Seyfoddin A, Rupenthal ID. Implants for drug delivery to the posterior segment of the eye: A focus on stimuli-responsive and tunable release systems. *J Control Release*. 2014;196:208-221.
17. Chan A, Leung L-S, Blumenkranz MS. Critical appraisal of the clinical utility of the dexamethasone intravitreal implant (Ozurdex(®)) for the treatment of macular edema related to branch retinal vein occlusion or central retinal vein occlusion. *Clin Ophthalmol*. 2011;5:1043-1049.
18. Kuno N, Fujii S. Biodegradable intraocular therapies for retinal disorders: progress to date. *Drugs Aging*. 2010;27(2):117-134.
19. Kane FE, Burdan J, Cutino A, Green KE. Iluvien: a new sustained delivery technology for posterior eye disease. *Expert Opin Drug Deliv*. 2008;5(9):1039-1046.
20. De Stefano VS, Abechain JJK, de Almeida LFS, et al. Experimental investigation of needles, syringes and techniques for intravitreal injections. *Clin Experiment Ophthalmol*. 2011;39(3):236-242.
21. Sanabria MR, Montero J a, Losada MV, et al. Ocular pain after intravitreal injection. *Curr Eye Res*. 2013;38(2):278-282.
22. Hubschman J-P, Coffee RE, Bourges J-L, Yu F, Schwartz SD. Experimental model of intravitreal injection techniques. *Retina*. 2010;30(1):167-173.
23. The Eye Diseases Prevalence Research Group. The prevalence of diabetic retinopathy among adults in the united states. *Arch Ophthalmol*. 2004;122(4):552-563.
24. Comer GM, Ciulla T a. Current and future pharmacological intervention for diabetic retinopathy. *Expert Opin Emerg Drugs*. 2005;10(2):441-455.
25. Chung H, Hwang JJ, Koh JY, Kim J-G, Yoon YH. Triamcinolone acetonide-mediated oxidative injury in retinal cell culture: comparison with dexamethasone. *Invest Ophthalmol Vis Sci*. 2007;48(12):5742-5749.
26. Sharma A, Pirouzmanesh A, Patil J, et al. Evaluation of the toxicity of triamcinolone acetonide and dexamethasone sodium phosphate on human lens epithelial cells (HLE B-3). *J Ocul Pharmacol Ther*. 2011;27(3):265-271.
27. Fitzpatrick SD, Jafar Mazumder M a, Muirhead B, Sheardown H. Development of injectable, resorbable drug-releasing copolymer scaffolds for minimally invasive sustained ophthalmic therapeutics. *Acta Biomater*. 2012;8(7):2517-2528.
28. Xia Y, Yin X, Burke NAD, Sto HDH, Stöver HDH. Thermal Response of Narrow-Disperse Poly(N-isopropylacrylamide) Prepared by Atom Transfer Radical Polymerization. *Macromolecules*. 2005;38(14):5937-5943.
29. Furyk S, Zhang Y, Ortiz-Acosta D, Cremer PS, Bergbreiter DE. Effects of end group polarity and molecular weight on the lower critical solution temperature of poly(N-isopropylacrylamide). *J Polym Sci Part A Polym Chem*. 2006;44(4):1492-1501.
30. Cui Z, Lee BH, Vernon BL. New hydrolysis-dependent thermosensitive polymer for an injectable degradable system. *Biomacromolecules*. 2007;8(4):1280-1286.

31. Mazumder M a J, Fitzpatrick SD, Muirhead B, Sheardown H. Cell-adhesive thermogelling PNIPAAm/hyaluronic acid cell delivery hydrogels for potential application as minimally invasive retinal therapeutics. *J Biomed Mater Res A*. 2012;100(7):1877-1887.
32. Chiefari J, Chong YKB (Bill), Ercole F, et al. Living Free-Radical Polymerization by Reversible Addition−Fragmentation Chain Transfer: The RAFT Process. *Macromolecules*. 1998;31(16):5559-5562.
33. Yang C, Cheng Y-L. RAFT synthesis of poly(N-isopropylacrylamide) and poly(methacrylic acid) homopolymers and block copolymers: Kinetics and characterization. *J Appl Polym Sci*. 2006;102(2):1191-1201.
34. Duncan R. The dawning era of polymer therapeutics. *Nat Rev Drug Discov*. 2003;2(5):347-360.
35. Makadia HK, Siegel SJ. Poly Lactic-co-Glycolic Acid (PLGA) as Biodegradable Controlled Drug Delivery Carrier. *Polymers (Basel)*. 2011;3(3):1377-1397.
36. Laurent UB, Fraser JR. Turnover of hyaluronate in the aqueous humour and vitreous body of the rabbit. *Exp Eye Res*. 1983;36(4):493-503.
37. Mittal G, Sahana DK, Bhardwaj V, Ravi Kumar MN V. Estradiol loaded PLGA nanoparticles for oral administration: effect of polymer molecular weight and copolymer composition on release behavior in vitro and in vivo. *J Control Release*. 2007;119(1):77-85.
38. Ophthalmology C, Chang DTW, Herceg MC, et al. Intracameral dexamethasone reduces inflammation on the first postoperative day after cataract surgery in eyes with and without glaucoma. *Clin Ophthalmol*. 2009;3:345-355.
39. Narasimhan B, Peppas N a. Disentanglement and reptation during dissolution of rubbery polymers. *J Polym Sci Part B Polym Phys*. 1996;34(5):947-961.

3.15. Supplementary Figures

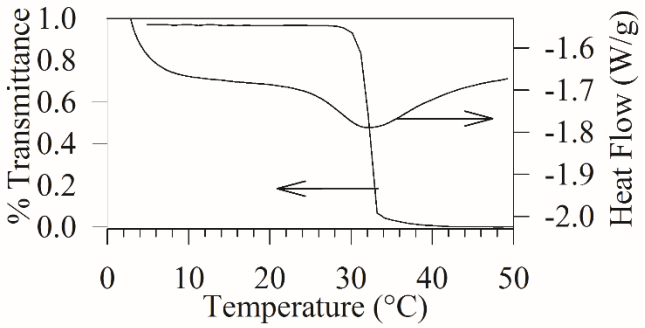

Figure 3S - 1. Lower critical solution temperature determined by UV transmittance and differential scanning calorimetry. Both methods show a similar LCST.

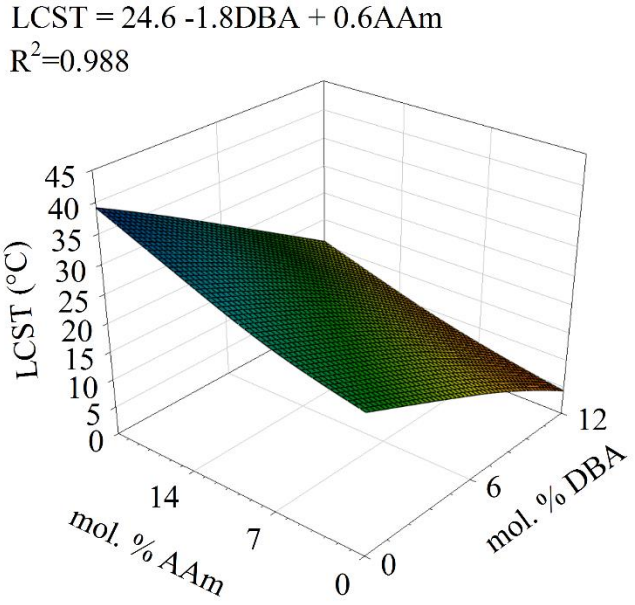

Figure 3S - 2. Lower critical solution temperature model. 5 kDA pNAND copolymers with mol. % AAm and DBA ranging from 0-21 and 0-12% respectively (unpublished data). Equation determined using a multiple linear regression.

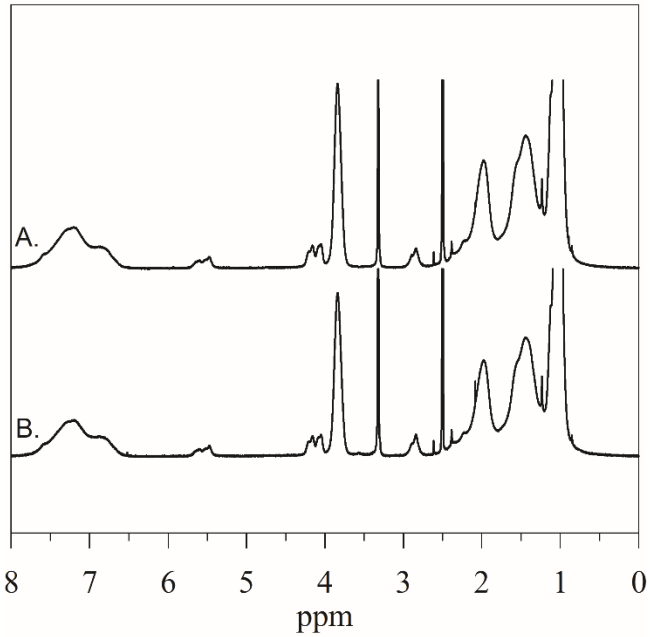

Figure 3S - 3. ^{1}H NMR showing A) Intact 13/8-30, and B) 13/8-30 after gamma sterilization of 3.41 Mrad for 20.5 hours. No changes in copolymer structure are noted after gamma sterilization based on ^{1}H NMR.

4. CHAPTER 4: Phenylboronic acid based micelles for sustained mucoadhesive drug delivery to the ocular surface

Authors: Graeme Prosperi-Porta, Stephanie Kedzior, and Heather Sheardown
Publication Information: Manuscript in preparation

Objectives: To develop mucoadhesive nanoparticles capable of increasing the bioavailability of ophthalmic therapeutics to the front of the eye through interaction with the ocular mucins. By increasing the bioavailability of drugs on the ocular surface, improved therapeutic effects and reduced drug applications can be achieved.

Main Scientific Contributions:

- Developed a well-controlled method to synthesize poly(L-lactide)-b-poly(methacrylic acid-co-phenylboronic acid) copolymers that are capable of assembly into micelle structures.
- Determined the size and structure of the micelles using a combination of NanoSight, TEM, Zeta potential, and mucin adsorption.
- High drug entrapment, greatly increased drug solubility, and mucoadhesive properties show potential to improve drug delivery.
- In vitro biocompatibility assays showed low cell cytotoxicity, but reduced proliferation when incubated with micelles.

Abstract

Topical drug delivery to the front of the eye is extremely inefficient due to effective natural clearance mechanisms of the eye such as precorneal tear turnover, and the impermeability of ocular tissues. This causes low ocular drug bioavailability requiring large, frequent doses resulting in systemic exposure and side effects. Mucoadhesive drug delivery systems have the potential to improve topical drug delivery by increasing bioavailability. We report the synthesis and characterization of a series of poly(L-lactide)-b-poly(methacrylic acid-co-phenylboronic acid) block copolymer micelles for use as mucoadhesive drug delivery vehicles. Micelle size, drug release rates, and mucoadhesion were shown to depend on phenylboronic acid content. These micelles show the potential to significantly improve the bioavailability of topically applied ophthalmic drugs.

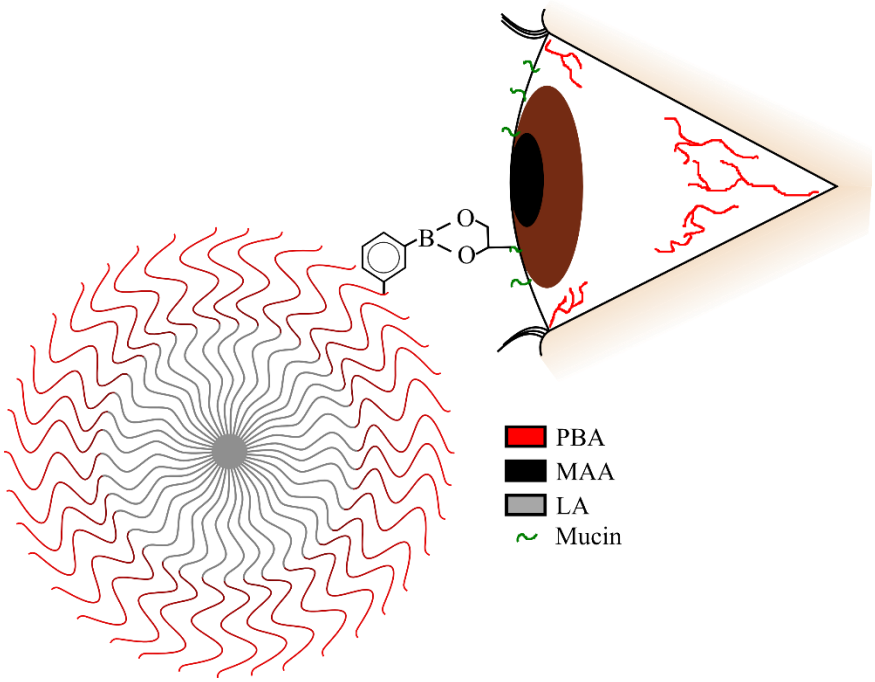

Keywords: Nanoparticles; Block Copolymer; Micelle; Mucoadhesive; Drug Delivery/Release

4.1.Introduction

The most common method to treat anterior segment diseases of the eye is by topical drop administration due to its low cost, ease of application, and non-invasiveness. Unfortunately, numerous barriers prevent efficient delivery of therapeutics to the anterior segment resulting in less than 5 % of the administered dose reaching the anterior tissues [1]. Static barriers including tight junctions of the conjunctiva, the hydrophobic corneal epithelium and hydrophilic corneal stroma, and dynamic barriers including the rapid tear turnover, and the vasculature and lymphatics of the conjunctiva all contribute to the highly impenetrable anterior surface [1,2]. Precorneal clearance mechanisms such as blinking, rapid tear turnover, and lacrimal drainage are additional barriers even before reaching the anterior tissues that must be overcome. Upon instillation of an eye drop, the maximal 30 μL that can be held in the cul-de-sac is restored to its normal 7 uL tear volume within 2 to 3 minutes resulting in the rapid drainage of 80 % or more drug through the nasolacrimal duct for systemic absorption and potential side effects [1,3].

The tear film itself is composed of an outer lipid layer, a middle aqueous layer containing secreted mucin, and an inner mucin layer immobilized on the glycocalyx covering the corneal and conjunctival epithelium [4,5]. The inner immobilized mucin layer is thought to act as yet another protective barrier against the diffusion of macromolecules, microbes, and hydrophobic molecules due to its hydrophilic nature [4]. Rose bengal, an anionic dye has been shown to stain corneal epithelium more readily with less mucin showing that mucin has an effect on drug delivery [6].

One method that has been explored to improve drug transport into the ocular tissues has been to utilize mucoadhesive polymers that increase the bioavailability of drug in the immobilized mucin layer. There are many well-known natural mucoadhesive polymers including chitosan [7,8], cellulose derivatives [9,10], thiomers [11,12], and many others, but these materials generally lack

the versatility for nanoparticle design to achieve desirable release characteristics. Phenylboronic acid (PBA) is a synthetic molecule that has been extensively used in glucose sensing and insulin delivery systems due to its ability to form high affinity complexes with 1,2-cis-diols [13]. This affinity between boronic acids and diols has also been utilized in other mucoadhesive drug delivery systems such as vaginal delivery of interferon [14], nasal delivery of insulin [15,16], and ocular delivery of cyclosporine A (CycA) [17].

Dry eye disease (DED) is one of the most frequent ocular illnesses in the United States with approximately 4.3% of men and 7.8% of women over the age of 50 showing dry eye symptoms [18,19]. Based on the Salisbury eye study, the prevalence of DED in elderly Americans aged 65-84 increases to over 14% [20,21]. DED is a multifactorial disease that can be caused by any combination of insufficient tear production and evaporative loss resulting in ocular burning, stinging, foreign body sensation, visual disturbance, inflammation, and potential damage to the ocular surface [22]. Cyclosporine A, commercially available as Restasis® (0.05% CycA ophthalmic emulsion) for the treatment of DED, is a non-water soluble cyclic peptide [23]. CycA is an immunosuppressive agent that has been shown to improve DED by reducing lymphocyte activation, which reduces the production of inflammatory substances that can lead to tissue damage [24,25], and by increasing the number of goblet cells, which are responsible for the secretion of lubricious mucin [26].

We have developed a series of mucoadhesive block copolymer micelles based on phenylboronic acid using reversible addition-fragmentation chain-transfer polymerization (RAFT) capable of targeted delivery of CycA to the ocular mucosa. The synthesis, chemical, and biological characterization of these micelles for mucoadhesive drug delivery to the anterior segment will be discussed herein.

4.2.Materials and Methods

4.2.1. Materials

Unless otherwise stated, all materials were purchased from Sigma Aldrich (Oakville, ON, Canada) and used as received. 3-acrylamidophenylboronic acid was purified by recrystallization in water. Azobisisobutyronitrile (AIBN) was purified by recrystallization in methanol. 1,4-dioxane, tetrahydrofuran, diethyl ether, N,N-dimethylformamide, and acetonitrile were purchased from Caledon Laboratories (Caledon, ON) and used as received. DMSO-d6 was purchased from Cambridge Isotope Laboratories Inc. (Andover, MA, USA) and used as received. Purified water with a resistivity of 18.2 MΩ cm was prepared using a Milli-pore Barnstead water purification system (Graham, NC, USA). Phosphate buffered saline (PBS) was purchased from BioShop (Burlington, ON, Canada). Cellulose dialysis membranes with molecular weight cut-off (MWCO) values of 3.5 and 50 kDa were purchased from Spectrum Laboratories Inc. (Rancho Dominguez, CA, USA). 3-[4,5-dimethylthiazol-2-yl]-2,5-diphenyl-tetrazolium bromide (MTT), calcein AM, and ethidium bromide were purchased from Life Technologies (Carlsbad, CA, USA) and were used as received.

4.2.2. pLA-b-p(MAA-PBA) copolymer synthesis and characterization

pLA-b-p(MAA-PBA) (LMP) copolymers were synthesized by RAFT polymerization. In a typical reaction procedure (80:20:1.4:0.2 molar feed ratio of MAA:PBA:pLA:AIBN), methacrylic acid (MAA; 192.9 mg, 2.24 mmol), PBA (107.1 mg, 0.56 mmol), poly(L-lactide) 4-cyano-4-[(dodecylsulfanylthiocarbonyl)sulfanyl]pentoate (pLA-CDP; 200.0 mg, 0.04 mmol), AIBN (1.10 mg, 0.01 mmol) were dissolved in 5 mL of 90:10 1,4-dioxane:water to form a 10 % solution. The solution was degassed by performing three freeze-pump-thaw cycles followed by replacement of the atmosphere with dry nitrogen. The flask was then heated to 70°C for 24 hours under constant

stirring. This copolymer, denoted LMP-20 (20 wt. % PBA in the poly(MAA-co-PBA) block) was isolated by precipitation into 10 times excess of cold anhydrous diethyl ether and further purified by repeated precipitation into diethyl ether from tetrahydrofuran. The copolymer was dried in a vacuum oven at 50°C for 24 hours until constant weight had been achieved.

LMP copolymer composition and molecular weight were determined using ^{1}H NMR (Bruker AV 600) in DMSO-d6.

LMP polymerization kinetics were studied to determine the distribution of PBA within MAA-PBA block and controlled nature of polymerization. Polymerization was performed as previously stated although at specified time points a nitrogen purged airtight needle was used to remove 50 μL samples for proton nuclear magnetic resonance (^{1}H NMR; Bruker AV 600) in DMSO-d6.

4.2.3. Micelle Formation and Characterization

Micelles were formed by the precipitation method. 20 mg of LMP copolymer was dissolved in 2 mL acetone. The copolymer solution was added drop-wise to 6 mL of purified water under constant stirring. The acetone/water solutions were then allowed to stir uncovered at room temperature for 48 hours to evaporate the acetone before further characterization.

Micelle size was determined using a NanoSight LM10 single nanoparticle tracking instrument (Malvern Instruments Ltd.). Micelle solutions in purified water were diluted to $5x10^{-2}$ mg mL^{-1} before measurement in pH 7.4 PBS. Micelle stability was assessed using Zeta potential (ZetaPlus Analyzer, Brookhaven) in pH 7.4 PBS with 10 mM NaCl. Zeta potential was measured for 1 mg mL^{-1} LMP.

The critical micelle concentration was determined using the pyrene fluorescent probe method. A predetermined amount of pyrene was dissolved in acetone and added to 2 mL vials and

allowed to evaporate. Micelle solutions ranging from 10 mg mL^{-1} to 10^{-5} mg mL^{-1} were added and incubated for 24 hours at room temperature resulting in final pyrene concentrations of $6.0x10^{-7}$ mol L^{-1}. Fluorescence was measured using a TECAN M1000 Pro plate reader (Männedorf, Switzerland). The excitation spectrum was measured after an excitation wavelength of 340 nm. The CMC was determined by plotting the intensity ratio of peaks at 373 nm to those at 383 nm against the logarithm of concentration. The emission and excitation bandwidths for all measurements was 5 nm.

4.2.4. Mucoadhesion by Surface Plasmon Resonance

Mucoadhesion was determined using Surface Plasmon Resonance (SPR; SPR Navi^{TM} 200, BioNavis). Briefly, SPR102-AU gold sensors were cleaned using piranha (3:1 94% sulfuric acid: hydrogen peroxide), rinsed extensively with purified water and dried under a stream of nitrogen. These sensors were then incubated in 100 µL of 100 µg mL^{-1} bovine submaxillary gland mucin for 24 hours at 20°C and then rinsed with purified water to remove unbound mucin. SPR measurements were conducted by flowing simulated tear fluid (STF; 23.1 mM KCl, 20.0 mM $NaHCO_3$, 1 mM $CaCl_2$•$2H_2O$, 113.5 mM NaCl; pH 7.4) for 10 minutes to achieve a stable baseline. The solution was then changed to a 1 mg mL^{-1} solution of chitosan or LMP micelles for 50 minutes. At this point, the solution was changed back to simulated tear fluid to assess mucoadhesion stability. All measurements were conducted at a flowrate of 50 µL min^{-1}, a temperature of 22°C, and a fixed angle scan of 65.4°.

4.2.5. Cyclosporine A Release

CycA release from micelles was determined using high performance liquid chromatography (HPLC). Briefly, a 20 mg of the LMP copolymer was dissolved in 2 mL of acetone containing 1.5 mg mL^{-1} CycA. This solution was added drop-wise to 6 mL of purified

water. The solution was left under stirring for 24 hours to evaporate the acetone. 0.5 mL was removed and filtered with Nanosep 10K Omega centrifugal units (10 kDa MWCO, Pall Corporation) to separate micelles from free CycA. The filtrate was collected to determine entrapment efficiency (EE). 5 mL of non-centrifuged sample was then added to 50 kDa MWCO dialysis tubes and placed in 15 mL of STF. At specified time points, 2.5 mL samples were removed and replaced with fresh pre-warmed STF. These samples were analyzed using a Waters HPLC consisting of a 2707 autosampler, 2489 UV spectrophotometer, 1525 binary HPLC pump, and Breeze 2 software (Build 2154). A 0.7 mL min^{-1} isocratic flow rate of 80:20 acetonitrile:0.1% trifluoroacetic acid in purified water as the mobile phase, a 60°C column temperature, a 20 μL sample injection volume, and a 210 nm detection wavelength were used. Sample concentrations were determined based on a standard calibration curve of CycA in the mobile phase.

4.2.6. Cell Culture

For cell culture, all copolymers were extensively dialyzed in 2:1 acetone:water solutions against 3.5 kDa MWCO dialysis tubing to prevent micelle formation followed by the transition to purified water and then were freeze dried. 50 mg of copolymer was then dissolved in 1 mL of acetone and added dropwise under constant stirring to 2.5 mL of sterile water. The acetone was allowed to evaporate for 48 hours under constant stirring whereby concentrated PBS and penicillin/streptomycin were added to final concentrations of 0.1 M and 1 % (v/v) respectively. Human corneal epithelial cells (HCECs) were cultured in keratinocyte serum-free media (KSFM) supplemented with bovine pituitary extract (BPE, 0.05 mg mL^{-1}) and epidermal growth factor (EGF, 0.005 mg mL^{1}). HCECs were seeded in 96 well plates at densities of 5,000 cells $well^{-1}$ and incubated in a temperature controlled CO_2 incubator (37°C, 5 % CO_2, 95 % air, 100 % humidity). After 24 hours of growth the media was replaced with 150 μL of KSFM and either 50μL of PBS,

50μL of 20 mg mL^{-1} LMP micelles, or 50μL of 4 mg mL^{-1} micelles for final LMP micelle concentration of 0, 5, and 1 mg mL^{-1}. The plates were incubated at 37°C at which point cell viability was assessed using an MTT assay, and live/dead cell counts were determined by a calcein AM (CalAM)/ethidium homodimer-1 (EthD-1) assay after 24 and 72 hours. % viability and % morbidity were determined based on the ratio of the absorbance (MTT) or fluorescence (CalAM/EthD-1) in samples containing micelles compared to control cells. All studies were performed with an n=6.

4.2.7. Statistical Analysis

A one-factor analysis of variance (ANOVA) was used to analyze the micelle size, Zeta potential, and HCEC viability using $\alpha = 0.05$ with Tukey post hoc. Statistical analysis was performed using IBM SPSS Statistics V22.0 statistical software (IBM Corp, Armonk, NY, USA). All error bars represent standard deviation.

4.3. Results and Discussion

4.3.1. Copolymer Characterization

Figure 4-1 shows the reaction scheme for polymer synthesis. ^{1}H NMR was used to determine the molar composition and the number average molecular weight of the LMP copolymers. According to Table 4-1, final compositions were determined to be consistent with feed ratios, and molecular weight was similar to the theoretical molecular weight based on reactant ratios.

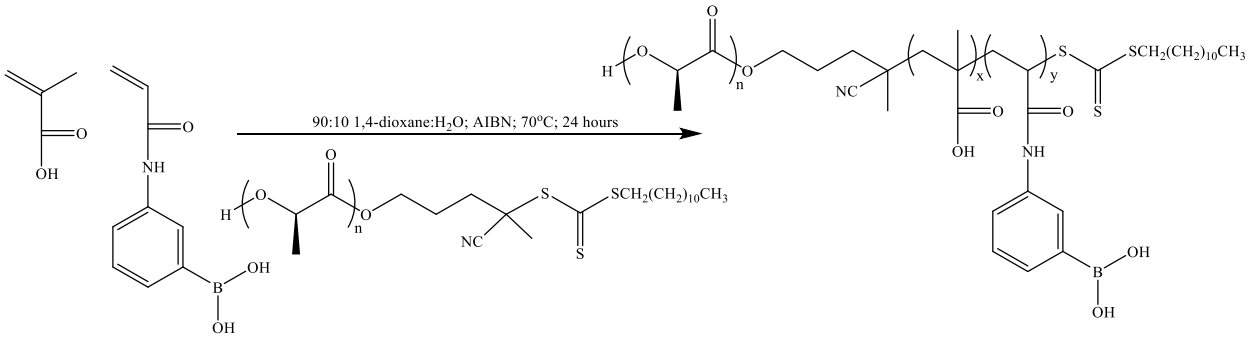

Figure 4 - 1. LMP reaction mechanism.

Table 4 - 1. LMP block copolymer polymerization data.

	Molar Feed Ratio (pLA-CDP:MAA:PBA)	**MAA[a] Conversion**	**PBA[a] Conversion**	**Final Composition[a]** (pLA:pMAA:pPBA)	**Mn[a] (Da)**
pLA-CDP	-	-	-	100:0:0	4711
LMP-0	44.3:55.7:0	0.80	-	49.8:50.2:0	10388
LMP-5	45.8:51.5:2.7	0.88	0.65	49.4:49.6:1.9	10741
LMP-10	47.2:47.5:5.3	0.87	0.66	51.3:46.7:3.8	10554
LMP-20	49.8:40.2:10.0	0.89	0.68	53.9:41.7:7.4	10459
LMP-30	52.1:33.5:14.4	0.84	0.65	58.1:35.2:10.4	10007

[a] Composition in mol. %, conversion, and molecular weight determined by ^{1}H NMR.

Due to the amphiphillic properties of the LMP copolymer as well as the affinity of unprotected phenylboronic acid, gel permeation chromatography did not give representative results. For this reason a kinetic study was performed to better understand the polymerization process and the distribution of phenylboronic acid in the hydrophilic block, shown in Figure 4-1. This kinetic study did not show a zero order relationship between conversion and time, which is expected for well controlled RAFT polymerization. Therefore, it is likely that the polydispersity will be higher than traditional RAFT polymerization. The kinetics also show that during the initial stages of polymerization, MAA reacts faster than the PBA, but after 12 hours they achieve a similar polymerization rate. This causes two results: the final copolymer composition has a higher MAA/PBA ratio then the feed ratio, and the distribution of PBA increases during the course of polymerization to produce a gradient within the poly(MAA-co-PBA) segment. The PBA gradient may be beneficial to mucoadhesion because more PBA will be located at the surface to interact with mucin.

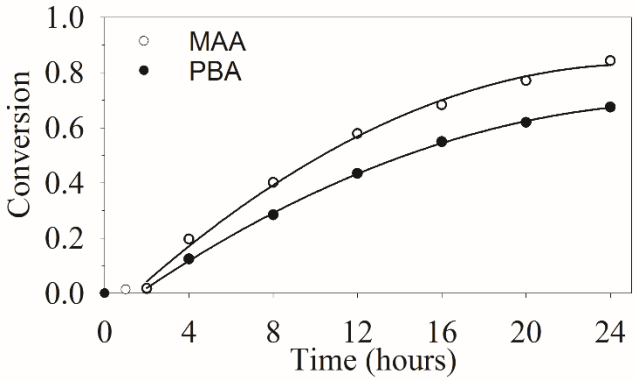

Figure 4 - 2. Polymerization kinetics of MAA and PBA in the LMP-10 copolymer synthesis.

4.3.2. Micelle Morphology

Using NanoSight and Zeta potential, the effect of PBA on micelle size and structure, depicted in Figure 4-2 was hypothesized. Due to MAA's pKa of ~4.6 and PBA's pKa of ~8.8, the majority of MAA groups should be negatively charged while most of the PBA groups should be uncharged in pH 7.4 PBS [27]. Based on micelle diameter, shown in Table 4-2 with a typical NanoSight spectrum shown in Figure 4-3, two trends can be seen.

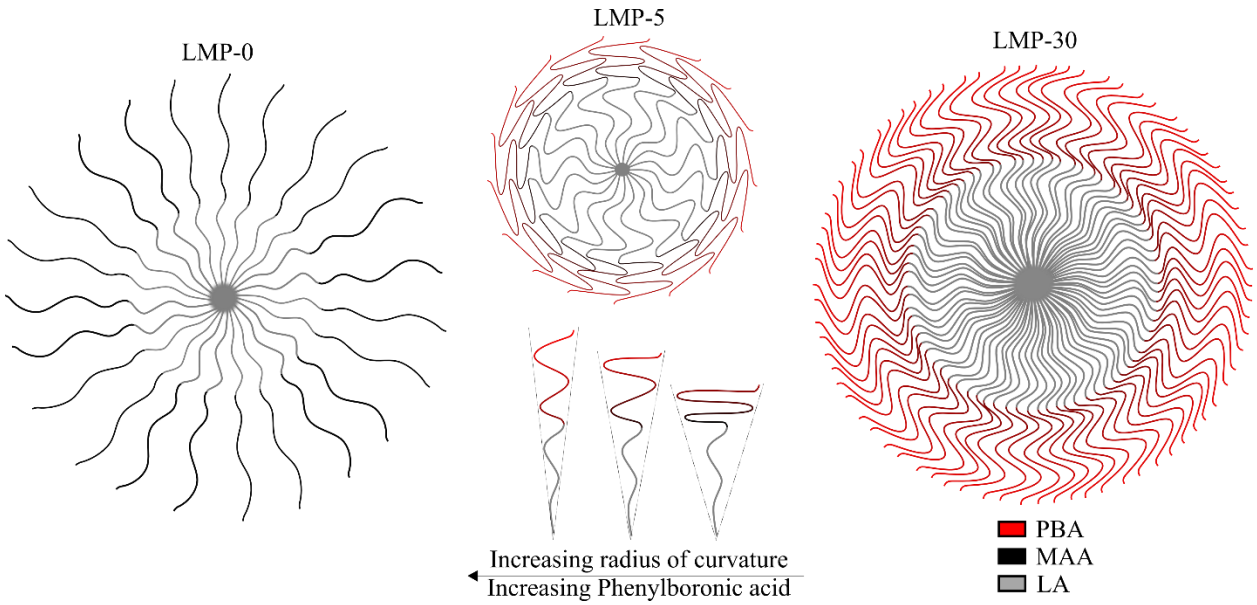

Figure 4 - 3. Proposed structural changes in LMP copolymer micelles

Table 4 - 2. Size determined using NanoSight of LMP block copolymer micelles. All reported measurements represent diameter ± SD in nm.

	PBS (pH 7.4)	CycA loaded (PBS pH 7.4)
LMP-0	124	129
LMP-5	108	113
LMP-10	114	117
LMP-20	130	180
LMP-30	282	252

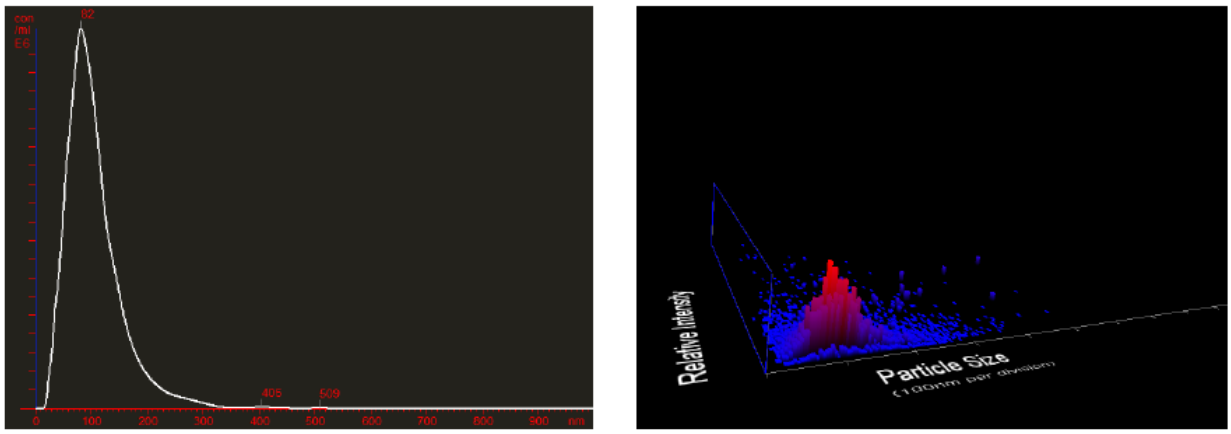

Figure 4 - 4. NanoSight spectrum of LMP-5 particles showing a mono-distributed size profile.

Firstly, as the ratio of PBA/MAA increases in LMP micelles containing PBA, the diameter increases. Secondly, the LMP-0 micelles are larger than LMP micelles containing minimal amounts of PBA. These results can be explained by the presence of two competing forces: intermolecular interactions between negatively charged MAA and water, and inter- and intra-molecular hydrophobic interactions induced by the PBA. The negatively charged MAA groups on the LMP-0 copolymer do two things: they electrostatically repel each other, and they form electronic interactions with water molecules. These effects form a large hydrated outer shell, which contributes to the large diameter. Similarly, Arimura et al. found that poly(lactide)-b-poly(aspartic acid) micelle size was increased as aspartic acid was depronated due to increased interaction with water [28]. The addition of a small amount of PBA into the outer shell causes the expulsion of some of these water molecules, which causes the outer shell to become less hydrated and smaller.

However, as the fraction of PBA is increased further, water expulsion occurs allowing for increased hydrophobic interactions between polymer chains leading to closer packing. Also, the large bulky phenyl ring creates intramolecular steric hindrance within the poly(MAA-co-PBA) polymer chain, creating a more rigid polymer unable to bend and fold into a bulky structure. The increased rigidity allows the hydrophillic poly(MAA-co-PBA) polymers to pack closer together resulting in a larger effective radius of curvature, which increases micelle diameter.

Zeta potential, shown in Figure 4-3, had similar trends to the micelle size. LMP micelles containing PBA showed that micelles became more negatively charged as PBA composition was increased. Although initially it seems counterintuitive that increasing the composition of neutral PBA would result in more negatively charged micelles, the change can be explained by charge density rather than total charge. As previously discussed, the LMP polymers with higher PBA compositions pack more closely together due to hydrophobic interactions and steric hindrance. The increased packing results in the greater surface charge measured by zeta potential.

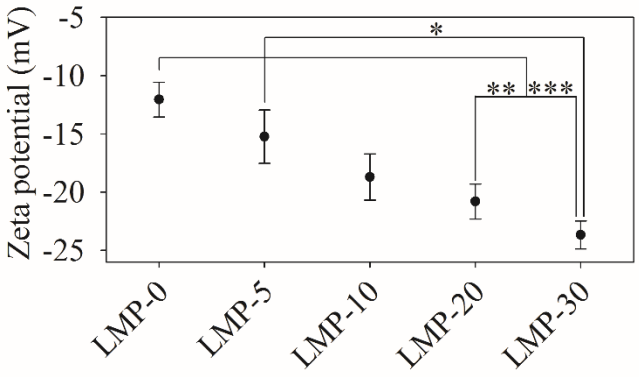

Figure 4 - 5. Zeta potential of LMP micelles at pH 7.4. Measurement was performed at 1 wt. % micelles.*p≤0.05, **p≤0.01, ***p≤0.001. All other comparisons were not significantly different (p≥0.05).

Characteristic micelle properties were confirmed by CMC and TEM. TEM characterization, shown in Figure 4-4, show circular morphology indicative of spherical micelles. All LMP micelles show diameters of less than 100 nm in their dry state.

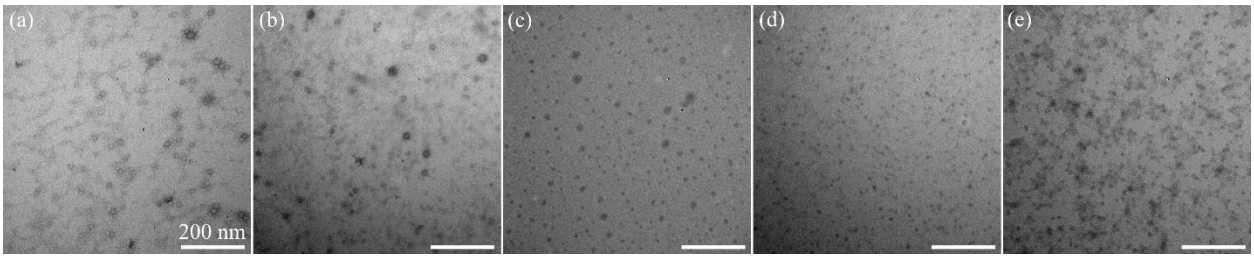

Figure 4 - 6. Transmission Electron micrograph of LMP copolymers. Scale bar represents 200 nm. (a) LMP-0, (b) LMP-5, (c) LMP-10, (d) LMP-20, (e) LMP-30. All copolymer micelles show a round morphology indicative of spherical micelles.

CMC was used to characterize the concentration at which micelles begin to form from free block copolymers in solution. The CMC, shown in Figure 4-5, was determined for LMP-0, 5, 10, 20, and 30 copolymers to be 73.0, 47.8, 40.6, 41.0, and 32.5 mg L^{-1} respectively. The slight decreasing trend in CMC with increasing PBA composition can be explained by block copolymer solubility and micelle stability differences. Increasing the PBA composition makes the poly(MAA-co-PBA) block less water soluble, which reduces the driving force for it to enter into solution. Additionally, the hydrophobic interactions between PBA in the outer shell increase the micelle stability by slightly locking it into place preventing the release of block copolymer into solution. Xue et al. developed poly(D,L-lactide)-b-poly(acrylic acid) micelles of similar molecular weight, which were determined to have a CMC of ~80 ml L^{-1} [29]. This slightly

increased CMC is likely due to the use of somewhat more hydrophilic acrylic acid compared to methacrylic acid, but these values are still very similar.

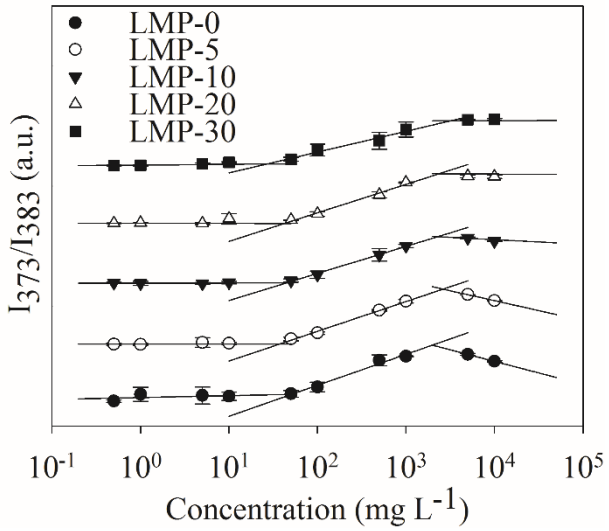

Figure 4 - 7. Critical micelle concentration for LMP copolymers in PBS (pH 7.4) determined from the ratio of fluorescent intensity at 373 nm to 383 nm after excitation at 340 nm.

4.3.3. Cyclosporine A Release

CycA was entrapped within the LMP micelles by dissolving both components in acetone followed by the drop-wise addition into purified water at a ratio of 20 mg copolymer to 3 mg CycA. Upon evaporation of the acetone under constant stirring for 24 hours, the drug loaded micelles were filtered to determine the % entrapment efficiency (EE). Figure 4-6A shows the EEs for LMP copolymers as well as a control CycA formulation. All LMP micelles showed EEs greater than 99.8% while the CycA formulation had significantly smaller EE of 98.7 %, which represents the maximum solubility of CycA in water. This shows that LMP micelles are very are efficient at entrapping CycA, which may reduce the initial undesirable burst release upon application. These LMP copolymers also showed significantly higher entrapment than similar pLA-b-Dextran-g-PBA micelles developed by Liu et al., which only achieved an 11.9% EE [17]. This low entrapment is likely because of the use of DMSO to form the micelles, which cannot be removed by prior to drug release studies helping to dissolve a large portion of the

CycA in solution. Figure 4-6B shows the visual transparency of CycA loaded LMP micelles. It can be seen that LMP-0/5/10 micelles are nearly transparent while the LMP-20 and LMP-30 loaded micelles form opaque suspensions. This is likely due to the distribution of CycA in the micelle, which is represented in Figure 4-7. In the LMP-20/30 micelles contain a significant amount of hydrophobic PBA in the outer hydrophilic shell, which increases the distribution of CycA throughout both the core and shell of the micelle causing changes in the micelle's refractive index. The LMP-0/5/10 micelles however have most of the CycA loaded within their hydrophobic poly(lactide) core and minimal loaded in the outer hydrophilic shell resulting in minimal refractive index changes. These hydrophobic distributions within the micelle also show an effect on the drug release characteristics of these micelles.

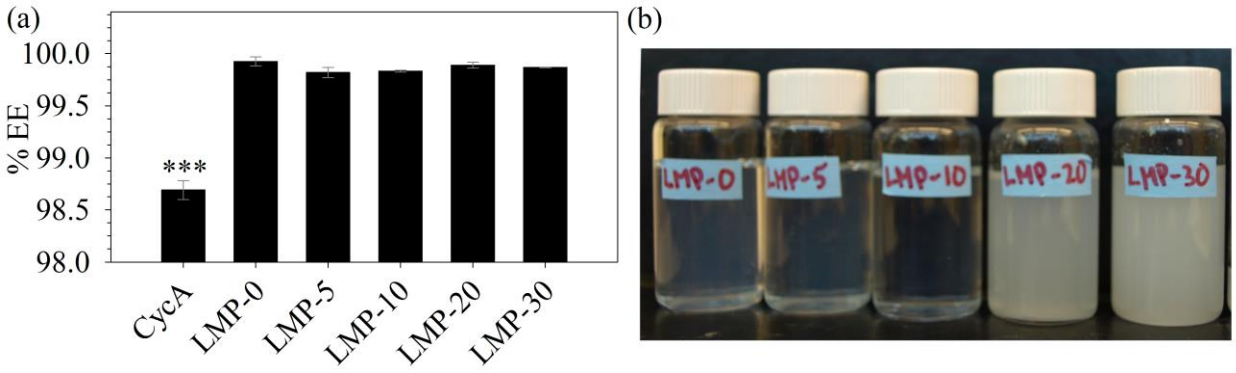

Figure 4 - 8. (a) Entrapment efficiencies of LMP copolymers and CycA control.*p<0.001 compared to all LMP copolymers. All other comparisons were not significant p>0.05. (b) CycA loaded LMP micelles. LMP0/5/10 all showed near visually transparency while the LMP-20/30 micelles showed transparent, but stable suspensions.**

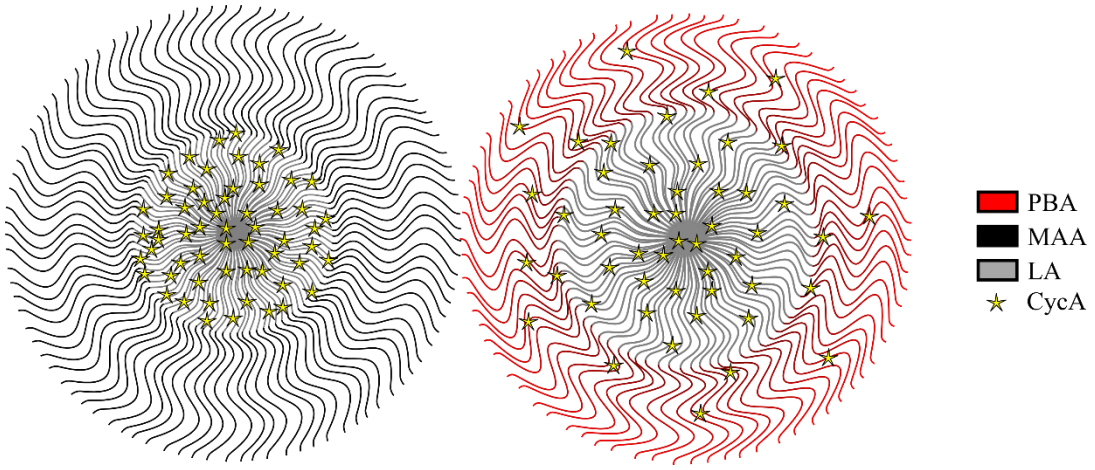

Figure 4 - 9. Proposed CycA loading distribution in LMP copolymers with varying amounts of PBA.

Interestingly, all LMP copolymers showed increased release compared to CycA in STF, shown in Figure 4-8. This increased release is likely due to free block copolymer diffusion across the 50 kDa MWCO dialysis membrane carrying with it CycA in the hydrophobic poly(lactide) block, which is more indicative of in vivo conditions where there would be no barriers to individual block copolymer diffusion. All LMP copolymers showed a two phase release profile characterized by an initial burst phase lasting approximately 24 hours resulting in between 35 to 45% released followed by a non-linear release of between 74 to 80% after 14 days depending on composition. During the initial burst release, the release rate was higher for micelles with lower PBA composition. This can be attributed to the higher CycA loading within the micelle core and the smaller micelle diameter, which results in a larger concentration gradient and shorter diffusion distance causing faster release compared to high PBA micelles, which are larger and have CycA distributed throughout the micelle core and shell. After the initial burst release, the concentration gradient is reduced, which allows the CycA diffusivity across the outer shell to dominate the release characteristics. Micelles with higher PBA composition will have more hydrophobic outer shells, which would increase the diffusivity of CycA from the micelle causing faster release compared to micelles with lower PBA. Compared

to the poly(lactide)-b-dextran-g-PBA micelles developed by Liu et al. who achieved a 100% release after approximately 5 days, our release is significantly slower, but again this is likely due to the use of DMSO, which increases the dissolution and release of CycA from these micelles at an increased rate [17]. The removal of organic solvent prior to drug release in our system shows more realistic drug release profiles.

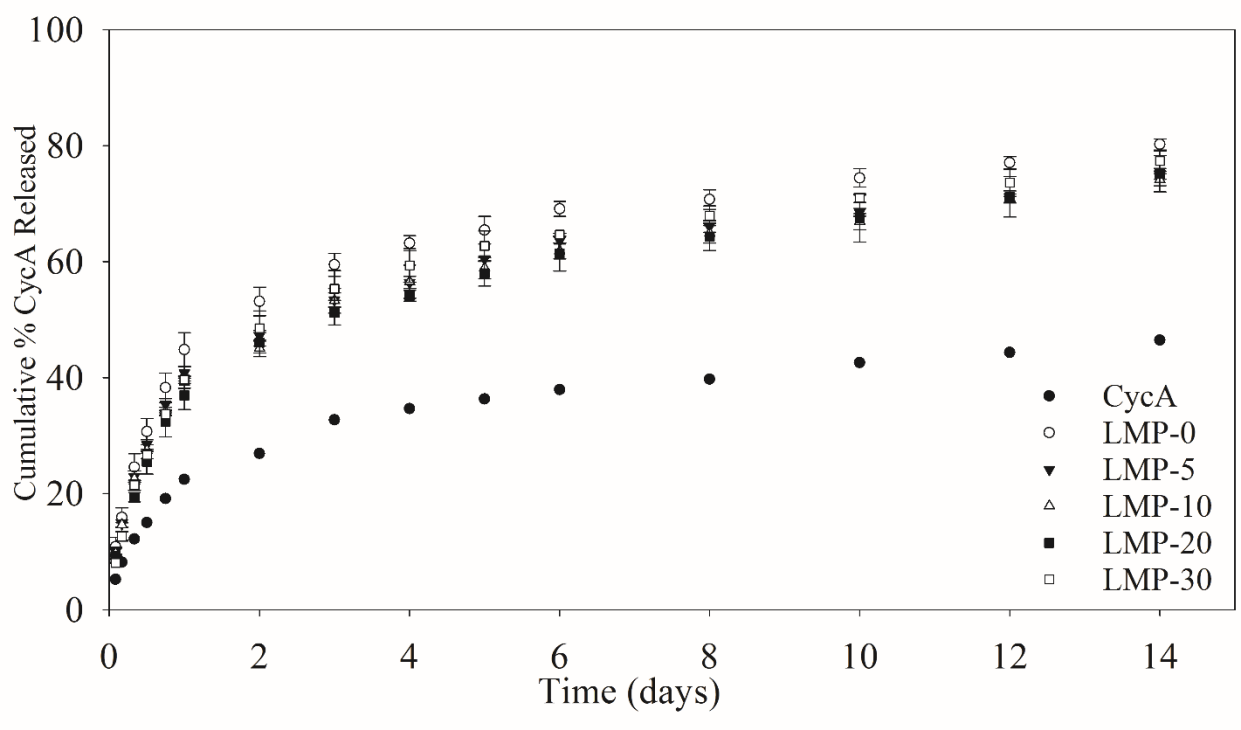

Figure 4 - 10. Cumulative CycA release from LMP micelles.

4.3.4. Mucoadhesion

Mucoadhesion of LMP copolymers was studied using SPR with chitosan as a positive control for mucoadhesive comparison. Figure 4-9 shows the single angle SPR sensorgram for chitosan and the LMP copolymers. It can be immediately seen from this figure that mucoadhesion of the LMP micelles increases with increasing PBA content, but appears to reach a ceiling whereby additional PBA does not greatly increase mucoadhesion. This ceiling effect is likely due to saturation of the mucin monolayer whereby no additional LMP polymers are able to adhere to the surface, which is representative of in vivo conditions. This suggests that higher PBA compositions,

which are not transparent, may not be beneficial to in vivo applications. The LMP-10/20/30 micelles all reached a significantly higher relative intensity compared to the chitosan and the LMP-0/5 micelles, which represents greater mucoadhesion. The LMP-0 micelles show the lowest mucoadhesion, which was expected. As with the chitosan, they also showed a greater reduction in relative intensity after the washing step compared to the PBA containing micelles. This reduction represents the stability of the adsorbed layer [30]. This is likely due to the stronger bonding between PBA and sialic acid diols compared to the LMP-0 micelles which forms hydrogen bonds and chitosan which forms electrostatic and hydrogen bonds. Springsteen et al. found that approximately 50% of PBA groups formed tetrahedral boronate ester bonds when incubated with glucose at pH 7.4, which explains how these PBA micelles achieved high mucoadhesion at physiological pH [31]. PBA containing LMP micelles show significant in vitro mucoadhesion, which has the potential to improve bioavailability of topically applied drugs.

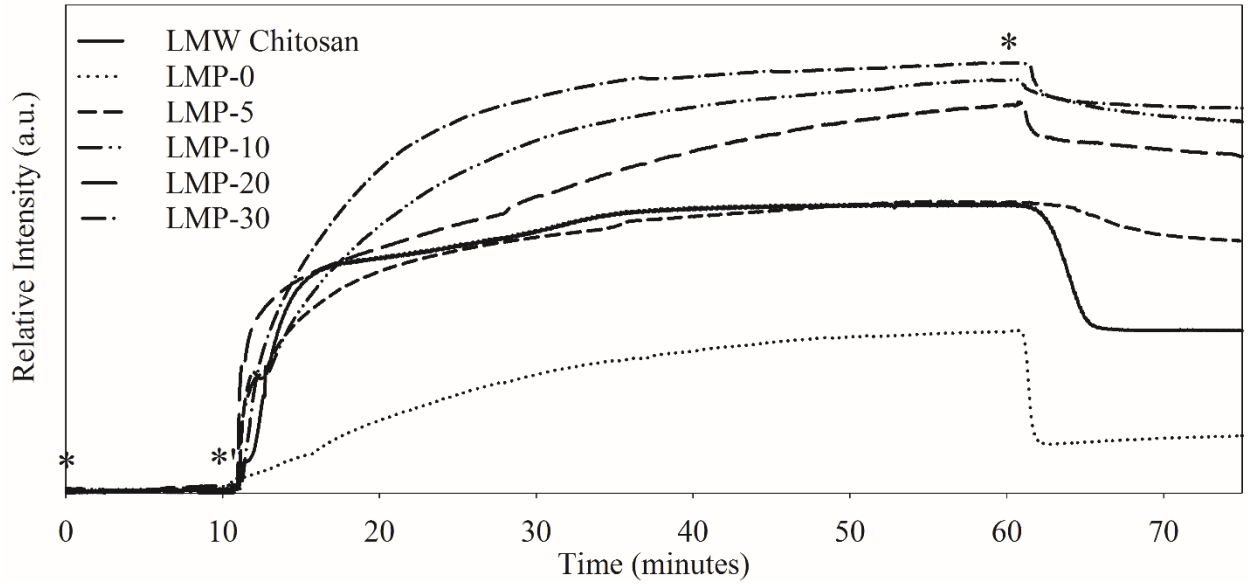

Figure 4 - 11. SPR sensorgram of LMP micelles. STF and LMP represents the flow of simulated tear fluid and LMP micelles respectively.

4.3.5. HCEC Viability

To test in vitro cell viability, LMP micelles were incubated with HCECs at concentrations of 1 mg mL^{-1} and 5 mg mL^{-1} for 24 and 72 hours. At each time point, cell metabolic activity was determined using an MTT assay, and live/dead cell counts were determined using CalAM/EthD-1 assays respectively. It can been seen, from the MTT assay results, (Figure 4-10A) that cell metabolism is reduced compared to controls. It also shows a trend that after 72 hours the metabolism of HCECs incubated with 1 mg mL^{-1} micelles is significantly higher than those incubated with 5 mg mL^{-1} micelles. The viability, determined from fluorescent CalAM staining, (Figure 4-10B) showed that viability was higher after 72 hours compared to 24 hour samples. This suggests that micelles are not cytotoxic, but rather inhibit growth. CalAM fluorescence also showed that viability was higher for 1 mg mL^{-1} micelles compared to the 5 mg mL^{-1} micelles. The EthD-1 assay (Figure 4-10C) showed less than three times morbidity for all micelles compared to controls, which suggests that LMP micelles are not significantly cytotoxic. The EthD-1 assay also showed a trend that % morbidity was significantly lower after 72 hours compared to 24 hours, which may be due to control cells reaching confluence which initiates cell death while the slower growing HCECs containing micelles had not. Interestingly, Figures 4-10D-M show morphological changes in HCEC growth. HCECs cultured with PBA containing micelles show dense clusters of cells rather than even spreading as seen in the micelles not containing PBA and the controls. The PBA micelles could be mediating cell-cell adhesion by interacting with cell surface mucins, which prevents them from spreading on the plate [32]. It is not believed that inhibition of cell growth seen with these LMP micelles will significantly affect corneal cells in vivo for two reasons: the concentration of LMP micelles on the corneal surface will be lower than those tested due to the rapid tear turnover upon topical administration of eye drops, and the anterior layer of corneal cells

is not actively dividing so the reduced in vitro proliferation may not translate to in vivo conditions [33]. The cell viability results show that these PBA containing micelles are not significantly cytotoxic, but do inhibit HCEC growth and cause cell clustering instead of spreading across the plate.

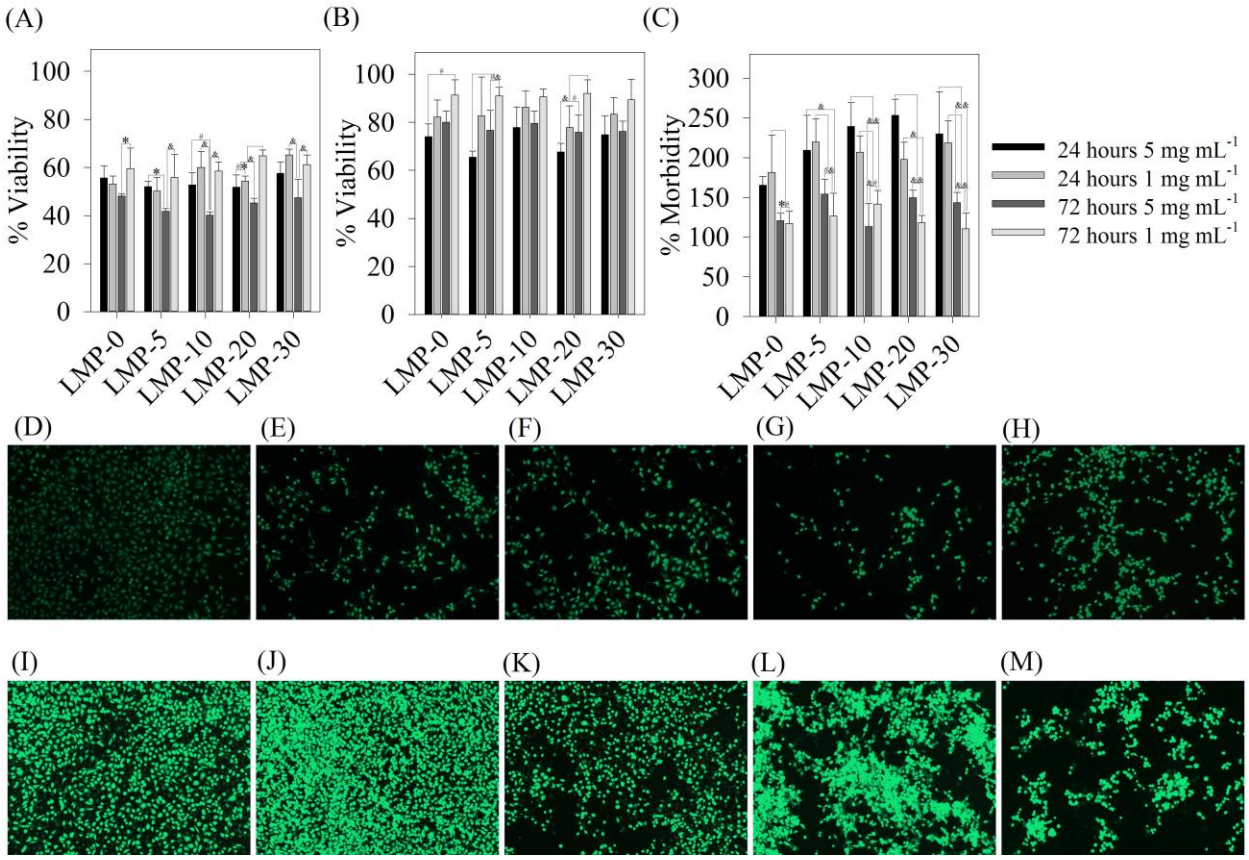

Figure 4 - 12. HCEC Viability by A) MTT assay, B) CalAM, C) EthD-1, D) Control 24 hours, E) LMP-0 24 hour 1 mg mL^{-1}, F) LMP-0 24 hour 5 mg mL^{-1} G) LMP-30 24 hour 1 mg mL^{-1}, H) LMP-30 24 hour 5 mg mL^{-1}, I) control 72 hours, J) LMP-0 72 hour 1 mg mL^{-1}, K) LMP-0 72 hour 5 mg mL^{-1}, L) LMP-30 72 hour 1 mg mL^{-1}, M) LMP-30 72 hour 5 mg mL^{-1}. Green=live cells and red=dead cells. *=p≤0.05, #=p≤0.01, &=p≤0.001.

4.4.Conclusions

Mucoadhesive micelles offer significant potential to increase the bioavailability of topically applied ophthalmic drugs. This would help to decrease the dosage, frequency of dose, and off-target systemic toxicity that are commonly associated with topical drops. We have synthesized a series of poly(L-lactide)-b-poly(methacrylic acid-co-phenylboronic acid) copolymer micelles with varying amounts of phenylboronic acid by reversible addition-fragmentation chain-transfer polymerization. These micelles have shown improved mucoadhesion compared to commonly known mucoadhesive chitosan with the ability to improve the delivery of cyclosporine A. Cell viability showed changes to cell proliferation and morphology, but did not show significant cytotoxicity suggesting the safe translation to in vivo conditions. This simple method to synthesize mucoadhesive micelles offers significant potential to improve the bioavailability of topically applied drugs to treat anterior segment eye diseases.

4.5. Acknowledgments

The authors would like to thank the Natural Sciences and Engineering Research Council (NSERC), and the 20/20 NSERC Ophthalmic Materials Research Network for funding. We would also like to thank Lina Liu and Marion Jamard for their help with TEM, Dr. Emily Cranston for SPR use, Dr Robert Pelton for ZetaPlus use, and Dr. Todd Hoare, and the McMaster Biointerfaces Institute for their equipment use and expertise.

4.6. References

[1] J.W. Shell, Pharmacokinetics of topically applied ophthalmic drugs, Surv. Ophthalmol. 26 (1982) 207–218.

[2] K. Cholkar, S.P. Patel, A.D. Vadlapudi, A.K. Mitra, Novel Strategies for Anterior Segment Ocular Drug Delivery, J. Ocul. Pharmacol. Ther. 29 (2013) 106–123.

[3] S. Mishima, A. Gasset, S.D.J. Klyce, J.L. Baum, Determination of tear volume and tear flow., Invest. Ophthalmol. 5 (1966) 264–276.

[4] M. Ruponen, A. Urtti, Undefined role of mucus as a barrier in ocular drug delivery, Eur. J. Pharm. Biopharm. (2015) In press.

[5] H.J. Davidson, V.J. Kuonen, The tear film and ocular mucins, Vet. Ophthalmol. 7 (2004) 71–77.

[6] P. Argüeso, A. Tisdale, S. Spurr-Michaud, M. Sumiyoshi, I.K. Gipson, Mucin characteristics of human corneal-limbal epithelial cells that exclude the rose bengal anionic dye, Investig. Ophthalmol. Vis. Sci. 47 (2006) 113–119.

[7] C.-M. Lehr, J.A. Bouwstra, E.H. Schacht, H.E. Junginger, In vitro evaluation of mucoadhesive properties of chitosan and some other natural polymers, Int. J. Pharm. 78 (1992) 43–48.

[8] I. a Sogias, A.C. Williams, V. V Khutoryanskiy, Why is chitosan mucoadhesive?, Biomacromolecules. 9 (2008) 1837–42.

[9] D.S. Jones, A.D. Woolfson, A.F. Brown, Textural, viscoelastic and mucoadhesive properties of pharmaceutical gels composed of cellulose polymers, Int. J. Pharm. 151 (1997) 223–233.

[10] D. Pal, A. Nayak, Development, Optimization, and Anti-diabetic Activity of Gliclazide-Loaded Alginate–Methyl Cellulose Mucoadhesive Microcapsules, AAPS PharmSciTech. 12 (2011) 1431–1441.

[11] A. Bernkop-Schnürch, Thiomers: A new generation of mucoadhesive polymers, Adv. Drug Deliv. Rev. 57 (2005) 1569–1582.

[12] M. Roldo, M. Hornof, P. Caliceti, A. Bernkop-Schnürch, Mucoadhesive thiolated chitosans as platforms for oral controlled drug delivery: synthesis and in vitro evaluation, Eur. J. Pharm. Biopharm. 57 (2004) 115–121.

[13] G. Springsteen, B. Wang, A detailed examination of boronic acid-diol complexation, Tetrahedron. 58 (2002) 5291–5300.

[14] C. Li, Z. Liu, X. Yan, W. Lu, Y. Liu, Mucin-controlled drug release from mucoadhesive phenylboronic acid-rich nanoparticles, Int. J. Pharm. 479 (2015) 261–264.

[15] C. Cheng, X. Zhang, J. Xiang, Y. Wang, C. Zheng, Z. Lu, et al., Development of novel self-assembled poly(3-acrylamidophenylboronic acid)/poly(2-lactobionamidoethyl methacrylate) hybrid nanoparticles for improving nasal adsorption of insulin, Soft Matter. 8 (2012) 765.

[16] R. Jachowicz, A. Czech, Preparation and evaluation of piroxicam-HPMCAS solid dispersions for ocular use., Pharm. Dev. Technol. 13 (2008) 495–504.

[17] S. Liu, L. Jones, F.X. Gu, Development of mucoadhesive drug delivery system using phenylboronic acid functionalized poly(D,L-lactide)-b-dextran nanoparticles., Macromol. Biosci. 12 (2012) 1622–6.

[18] D.A. Schaumberg, R. Dana, J.E. Buring, D.A. Sullivan, a Sullivan, Prevalence of Dry Eye Disease among US Men: Estimates from the Physicians' Health Studies, Arch. Ophthalmol. 127 (2009) 763–768.
[19] D.A. Schaumberg, D.A. Sullivan, J.E. Buring, M.R. Dana, Prevalence of dry eye syndrome among US women, Am. J. Ophthalmol. 136 (2003) 318–326.
[20] O.D. Schein, B. Munoz, J.M. Tielsch, K. Bandeen-Roche, S. West, Prevalence of dry eye among the elderly., Am. J. Ophthalmol. 124 (1997) 723–728.
[21] O.D. Schein, M.C. Hochberg, B. Munoz, J.M. Tielsch, K. Bandeen-Roche, T. Provost, et al., Dry eye and dry mouth in the elderly: a population-based assessment., Arch. Intern. Med. 159 (1999) 1359–1363.
[22] J.L. Gayton, Etiology, prevalence, and treatment of dry eye disease, Clin. Ophthalmol. 3 (2009) 405–412.
[23] G.D. Kymionis, D.I. Bouzoukis, V.F. Diakonis, C. Siganos, Treatment of chronic dry eye: focus on cyclosporine, Clin. Ophthalmol. 2 (2008) 829–836.
[24] K.S. Kunert, A.S. Tisdale, M.E. Stern, J. a Smith, I.K. Gipson, Analysis of topical cyclosporine treatment of patients with dry eye syndrome: effect on conjunctival lymphocytes., Arch. Ophthalmol. 118 (2000) 1489–1496.
[25] M.E. Stern, J. Gao, T.A. Schwalb, M. Ngo, D.D. Tieu, C.-C. Chan, et al., Conjunctival T-cell subpopulations in Sjogren's and non-Sjogren's patients with dry eye., Invest. Ophthalmol. Vis. Sci. 43 (2002) 2609–2614.
[26] K.S. Kunert, A.S. Tisdale, I.K. Gipson, Goblet cell numbers and epithelial proliferation in the conjunctiva of patients with dry eye syndrome treated with cyclosporine., Arch. Ophthalmol. 120 (2002) 330–337.
[27] J. Yan, G. Springsteen, S. Deeter, B. Wang, The relationship among pK a, pH, and binding constants in the interactions between boronic acids and diols - It is not as simple as it appears, Tetrahedron. 60 (2004) 11205–11209.
[28] H. Arimura, Y. Ohya, T. Ouchi, Formation of core-shell type biodegradable polymeric micelles from amphiphilic poly(aspartic acid)-block-polylactide diblock copolymer, Biomacromolecules. 6 (2005) 720–725.
[29] Y.N. Xue, Z.Z. Huang, J.T. Zhang, M. Liu, M. Zhang, S.W. Huang, et al., Synthesis and self-assembly of amphiphilic poly(acrylic acid-b-dl-lactide) to form micelles for pH-responsive drug delivery, Polymer (Guildf). 50 (2009) 3706–3713.
[30] I. Bravo-Osuna, M. Noiray, E. Briand, a M. Woodward, P. Argüeso, I.T. Molina Martínez, et al., Interfacial interaction between transmembrane ocular mucins and adhesive polymers and dendrimers analyzed by surface plasmon resonance., Pharm. Res. 29 (2012) 2329–40.
[31] G. Springsteen, B. Wang, A detailed examination of boronic acid–diol complexation, Tetrahedron. 58 (2002) 5291–5300.
[32] T. Inatomi, S. Spurr-Michaud, a. S. Tisdale, I.K. Gipson, Human corneal and conjunctival epithelia express MUC1 mucin, Investig. Ophthalmol. Vis. Sci. 36 (1995) 1818–1827.
[33] G.J. Thassu, Deepak and Chader, Eye anatomy, physiology, and occular barriers: basic considerations for drug delivery, in: Ocul. Drug Deliv. Syst. Barriers Appl. Nanoparticulate Syst., CRC Press Taylor & Francis Group, 2013: pp. 17–40.

5. Chapter 5: Conclusions and Future Work

5.1. Tunable release of ophthalmic therapeutics from injectable, resorbable, thermoresponsive copolymer scaffolds

The development of injectable, resorbable, and thermoresponsive pNAND copolymer scaffolds has shown significant potential to provide sustained drug release over extended periods of time. By altering the composition and molecular weight of these pNAND copolymers we were able to effectively tune the physical properties such as LCST and water content, and we were able to adjust the entrapment of dexamethasone and subsequent release profile. Depending on composition and molecular weight these materials could be chosen to release 100% of dexamethasone after 5 days up to approximately 60% after 100 days. These results show the potential for these materials to be further developed as drug delivery depots for intravitreal injection. To do this there are two projects that could be pursued. The first is studying the release of other ophthalmic therapeutics to further understand the release mechanism from these hydrogels and possibly extend the versatility of these copolymers. These could include more hydrophilic drugs or biological anti-VEGFs such as Ranibizumab for the treatment of wet AMD. Another study that would progress the development of these materials is to use them in the treatment of an animal model with a posterior segment diseases such as diabetic retinopathy. This would test the material's in vivo efficacy of improving treatment outcomes in a relevant disease model. Due to these materials' injectability through a 30G needle, there is significant potential for the development of injectable cell therapies. We are also exploring the use of these materials as injectable cell scaffolds that can be used to deliver cells to posterior tissues. This would greatly reduce the invasiveness of cell delivery while providing an environment for cells to attach and proliferate. The ability to regenerate damaged tissue in the back of the eye by an injection of cells could provide a method to treat degenerative diseases in a minimally invasive fashion.

5.2. Phenylboronic acid based micelles for sustained mucoadhesive drug delivery to the ocular surface

The LMP nanoparticle micelles show the potential to improve topical drug delivery by increasing the bioavailability of hydrophobic drugs on the ocular surface and improving the loading and release kinetics. The two most important characteristics of these particles must be studied further to determine if these materials have clinical relevance: drug permeation studies and in vivo ocular bioavailability. Ex vivo permeation studies could be performed to understand the effect of the block copolymers on the permeation rate of drug across the cornea, conjunctiva, and sclera. Ocular bioavailability could be performed by measuring the concentration of a molecular probe delivered using the LMP micelles in the anterior tissues and ocular surface. This would determine if the micelles successfully interact with the mucin surface to improve drug delivery across anterior ocular tissues. Finally, by applying these micelles containing cyclosporine A to an animal dry eye disease model the clinical relevance of these particles could be studied. The synthesis and in vitro characterization of these LMP micelles shows that these materials have the potential to improve topical drug delivery, but further biological characterization is needed to fully develop these materials.